DEA Photonics, Image and Cybernetics
University Louis Pasteur (Strasbourg I)

End of studies project dissertation

Second harmonic generation and iodine spectroscopy for the frequency stabilization of an Nd:YAG Laser emitting at 1.319µm

Nicolas Schuhler
Promotion 2003

Keywords: second harmonic generation, laser frequency stabilization, metrology, iodine spectroscopy

Internship carried out at

European Southern Observatory
VLT Interferometry group
Karl Schwarzschildstrasse 2
D-85748 Garching beï München

from 01.03.03 to 31.08.03

ENSPS supervisor :
Dr Pierre Pfeiffer

ESO supervisor :
Dr Samuel Lévêque

Change Record

Issue / Rev.	Date	Section / Page. affected	Reason/Remarks
1.0	25 August 2003	all	First Issue

Abstract

The Phase Referenced Imaging and Micro-arcsecond Astrometry (PRIMA) facility is a forthcoming instrument for the European Southern Observatory (ESO) Very Large Telescope Interferometer (VLTI). PRIMA is based on the simultaneous coherent observation of two celestial objects in which the two interferometric signals are tied together by an internal metrology system. In order to fulfill the goal of 10 micro-arcsecond astrometry, the PRIMA metrology system, based on superheterodyne laser interferometry, must reach an accuracy of 5nm.

To reach this objective, an Nd:YAG laser emitting at 1.319µm, must be stabilized to a $d\nu/\nu=10^{-8}$ level. The stabilization scheme based on the work of Arie [7] requires the generation of the second harmonic to use an iodine transition at 659.5nm as a frequency reference. The Pound-Drever-Hall method is used to derive a convenient error signal.

In this report it is showed that Second Harmonic Generation (SHG) with Periodically Poled KTP (PPKTP) can provide enough power in the second harmonic beam. SHG sensitivity to variation of the temperature of the crystal, of the fundamental wavelength or of the angular alignment is also studied and is proved not to be critical. Based on these results an optical configuration fulfilling at the same time the requirements for the Infrared power and Second Harmonic power is proposed.

The frequency tuning of the selected Nd:YAG is characterized and the results of iodine spectroscopy show the availability of convenient transitions in the frequency tuning range of the laser. Finally the specifications of the required iodine cell are deduced from the previous results.

Résumé

PRIMA (Phase Referenced Imaging and Micro-arcsecond Astrometry) est un futur instrument du VLTI (Very Large Telescope Interferometer) de l'ESO (European Southern Observatory). PRIMA est basé sur l'observation cohérente et simultanée de deux objets de la voûte célèste dont les signaux interférométriques sont liés par un système de métrologie interne. Pour que l'instrument atteigne une précision de 10 micro seconde d'arc en mode astrométrique le système de métrologie de PRIMA, basé sur l'interférométrie superhétérodyne, doit atteindre une précision de 5nm sur un temps de mesure de 30 minutes.

Afin de remplir cet objectif, la source laser du système de métrologie doit être stabilisée en fréquence à un niveau de $d\nu/\nu=10^{-8}$. La méthode de stabilisation choisie pour le laser Nd:YAG à 1.319µm s'appuie sur le travail d'Arie qui nécessite le doublage en fréquence du faisceau laser pour pouvoir utiliser une transition de l'iode à 659.5nm comme référence de fréquence. La méthode de Pound-Drever-Hall est utilisée pour générer le signal d'erreur.

Dans ce rapport il est montré que le doublage en fréquence avec un crystal de KTP à polarisation périodiquement inversée PPKTP peut fournir un faisceau de puissance suffisante à 659.5nm. En outre la sensibilité du doublage en fréquence aux variations de température, de longueur d'onde du faisceau fondamental et de l'angle d'incidence est étudiée et ne se révèle pas critique. S'appuyant sur ces résultats une configuration optique satisfaisant les besoins en puissance aussi bien du faisceau infrarouge que du faisceau visible est proposée.

L'accordabilité en fréquence du laser Nd:YAG Lightwave 125 est caractérisée. Les spectres de l'iode obtenus expérimentalement confirment la présence de transitions utilisables comme références de fréquence dans l'intervalle d'accordabilité du laser. Enfin, les caractéristiques de la cellule d'iode qui sera utilisée pour la stabilisation du laser du système de métrologie de PRIMA sont déduites du déroulement et des résultats obtenus pour la spectroscopie.

Acknowledgements

I would like to thank my supervisor Dr Samuel Lévêque for his guidance and his help all through the 6 months.

I would like to thank also Dr Andreas Glindemann and everyone at VLTI group for their help and their welcome.

Table of contents

Abstract 2
Résumé 3
Acknoledgements 4
Table of contents 5
Table of figures 8
List of tables 10
Acronyms 11
Symbols 12
Introduction 13
1 Laser fequency stabilization 14
1.1 Frequency noise 14
1.2 State of the art 14
1.2.1 Generation of the error signal 15
1.2.2 Applying the error signal 16
1.3 Laser stabilization for PRIMA 16
2 Second Harmonic Generation (SHG) 18
2.1 Theoretical analysis 18
2.1.1 SHG basics 18
2.1.2 Phase-matching 19
2.1.2.1 Critical Phase-Matching (CPM) 20
2.1.2.2 Quasi Phase-Matching (QPM) 21
2.1.3 Expected conversion efficiency 21
2.1.3.1 Critical phase-matching 21
2.1.3.2 Quasi phase-matching 22
2.1.3.3 Summary of the expected conversion efficiency 23
2.1.4 Temperature, angle and wavelength tolerances for QPM 24
2.1.4.1 Temperature tuning 24
2.1.4.2 Angular dependence 25
2.1.4.3 Wavelength dependence 27
2.2 Experimental results using bulk PPKTP 27
2.2.1 Experimental set-up 27
2.2.1.1 Optical set-up 27
2.2.1.2 Periodically Poled KTP (PPKTP) crystal 28
2.2.1.3 Oven and temperature controller 29
2.2.2 Measured conversion efficiency 30

2.2.3 Parameters affecting the conversion efficiency 31
2.2.3.1 Temperature of the crystal 31
2.2.3.2 Power of the fundamental beam 32
2.2.3.3 Angular orientation of the crystal 34
2.2.3.4 Wavelength of the fundamental beam 34
2.2.3.5 Number of longitudinal modes in the fundamental beam 35
2.2.4 Optical quality of the output beam 41
2.2.4.1 Intensity spatial distribution and wavefront error 41
2.2.4.2 Polarization state of the IR beam after SHG 43
2.3 Experimental results using a PPKTP waveguide 43
2.3.1 Experimental set-up 44
2.3.1.1 Optical set-up 44
2.3.1.2 PPKTP waveguide 45
2.3.1.3 Oven and temperature controller 46
2.3.2 Coupling efficiency 46
2.3.3 Tuning and tolerances 46
2.3.4 Optical quality of the IR Output beam 47
2.4 Conclusion on the second harmonic generation 47
3 Characterization of the iodine transitions around 659.5nm .. 51
3.1 Frequency tuning of the Lihgtwave Model 125 51
3.1.1 Experimental set-up for the test of frequency tunability 51
3.1.1.1 Set-up 51
3.1.1.2 Burleigh WA-1500 Wavemeter 52
3.1.2 Frequency tuning by changing the temperature of the laser's . 52
3.1.3 Frequency tuning with a piezo element 53
3.1.4 Summary of the frequency tuning parameters of the Lightwave 125 54
3.2 Iodine spectroscopy for the laser stabilization 55
3.2.1 Exprerimental set-up for iodine spectroscopy 55
3.2.2 Iodine spectroscopy 58
3.2.3 Temperature dependence of linedepth of the transitions 62
3.3 Conclusion on the iodine spectroscopy 65
Conclusion 67

Appendix A : The European Southern Observatory, ESO 69
Appendix B : The Very Large Telescope Interferometer (VLTI) and

PRIMA 72
Appendix C : KTP Physical properties 78
Appendix D : LN Physical properties 79
Appendix E : Set-up and wiring for the oven and the temperature controller 80
Appendix F : Burleigh WA-1500 Wavemeter 83
Appendix G : Characteristics of the Dichroic mirror 85
Appendix H : Iodine cells 86

Table of figures

Figure 1 : Spontaneous emission origin of the frequency noise. 14
Figure 2 : Two possible optical configurations for the laser frequency stabilization. 17
Figure 3 : Basic principle of Second Harmonic Generation. 18
Figure 4 : Growth of the intensity of the SH beam with the length of propagation in the nonlinear medium.. 20
Figure 5 : Temperature dependence of the SH conversion efficiency for a PPKTP crystal. 25
Figure 6 : Schematic view of a PPKTP bulk crystal.. 26
Figure 7 : Angular dependence of the efficiency for a PPKTP crystal. 26
Figure 8 : Wavelength dependence of the efficiency for a PPKTP crystal.......................... 27
Figure 9 : Second Harmonic Generation with bulk PPKTP set-up.................................... 28
Figure 10 : Schematic view of a PPKTP bulk crystal and of the incident electric field vector. 29
Figure 11 : Conversion efficiency as a function of the temperature for a PPKTP crystal.... 32
Figure 12 : SH power and conversion efficiency as a function of fundamental power. 33
Figure 13 : Measured wavelength dependence of SHG for a given set of parameters. 34
Figure 14 : Increase of the Second Harmonic power during the mode-hops....................... 36
Figure 15 : Different spectra measured for the SH beam.. 37
Figure 16 : Fabry-Perot modes of the spectrum analyzer. 38
Figure 17 : Relative power of the three SH modes as a function of the efficiency.............. 39
Figure 18 : .Wavefront error and intensity distribution of the red beam after the SHG. 42
Figure 19 : Polarization of the output IR beam after SHG.. 43
Figure 20 : Optical set-up for SHG with PPKTP waveguide... 45
Figure 21 : Waveguide chip layout. 46
Figure 22 : IR spot after SHG with PPKTP waveguide.. 47
Figure 23 : Power of SH as a function of the incident IR power. 48
Figure 24 : Block diagram of the Light Source System of the PRIMA Metrology. 49
Figure 25 : Two possible hardware configurations for PRIMA laser stabilization. 50
Figure 26 : Experimental set-up for the characterization of the frequency tuning of the Lightwave no 125.. 52
Figure 27 : Emitted wavelength of the laser as a function of the target and measured temperatures of the resonator.. 54
Figure 28 : Set up for the iodine spectroscopy.. 57
Figure 29 : Set-up for iodine spectroscopy. 59
Figure 30 : Iodine spectrum in the area of interest (cell temperature 150ºC). 60
Figure 31 : Iiodine spectrum in the "Arie" area obtained at cell temperature of 150 ºC and taking into account the wavelength dependence of the SHG... 61
Figure 32 : Transmission spectrum of I2 for three different temperatures of the cell. 63
Figure 33 : Normalized absorption as a function of the pressure for a 13cm long cell. 64
Figure 34 : Expected absorption for P(48)6-6 in an iodine cell with a pressure of 3.5Torr as a function of the cell length.. 65
Figure 35 : Geographical establishements. 70
Figure 36 : Internal structure of ESO.. 71
Figure 37 : The Very Large Telescope Interferometer and its first generation instruments. 72
Figure 38 : General principle of PRIMA. 74
Figure 39 : PRIMA Metrology system... 77
Figure 40 : Rearpanel of a CN77XXX controller. 81

Figure 41 : Wiring for a 2wires pt100/RTD. 81
Figure 42 : Burleigh WA-1500 wavemeter optical schematic. 83
Figure 43 : Polarization after the dichroic mirror of an linearly polarized incident beam at 1.319µm. 85
Figure 44 : Partial pressure of iodine (Torr) as a function of the cold finger temperature (ºC). 87

List of tables

Table 1 : Summary of the expected conversion efficiency for KTP 23
Table 2 : Summary of the expected conversion efficiency for $LiNbO_3$............................... 23
Table 3 : Specification of the bulk PPKTP 29
Table 4 : HC Photonics oven (OV03) specifications. 29
Table 5 : Power distribution over the different longitudinal modes in the fundamental beam and in the SH beam. 45
Table 6 : “slow input” tuning (temperature tuning) measured characteristics for the Lightwave 125 55
Table 7 : “fast input” (piezo tuning) characteristics given for the Lightwave 125. 55
Table 8 : Characteristics of the three main transitions at a temperature of 150ºC (~2.81 Torr). 62
Table 9 : Absorption depth of the three transitions at 50,100 and 150 ºC. 63
Table 10 : Specifications of the iodine cell 66
Table 11 : Physical properties of KTP. 78
Table 12 : Physical properties of LN ($LiNbO_3$). 79
Table 13 : Cable connector configuration for the HC Photonics OV03 oven...................... 80
Table 14 : Hardware menu configuration in Micro-infinity (configuration 1.1) for setting-up the comunication between the PC and the CN77352-C4 controller. 81
Table 15 : CN77352-C4 configuration for setting up the communication between the PC and the controller. 82

Acronyms

- ESO : European Southern Observatory
- VLT : Very Large Telescope
- VLTI : Very Large Telescope Inteferometer
- PRIMA : Phase Referenced Imaging and Microarcsecond Astrometry
- UT : Unit Telescope
- AT : Auxiliary Telescope
- DL : Delay Lines
- DDL : Differential Delay Lines
- FSU : Fringe Sensor Unit
- OPD : Optical Path Difference
- FP : Fabry-Pérot interferometer
- AOM : Acousto-optic Modulator
- EOM : Electo-optic Modulator
- IMT : Institut de Micro-Technologie de Neuchâtel
- SHG : Second Harmonic Generation
- SH : Second Harmonic
- IR : Infrared
- KTP : Potassium Titanyl Phosphate
- LN : Lithium Niobate
- PPKTP : Periodically Poled Potassium Titanyl Phosphate
- PPLN : Periodically Poled Lithium Niobate
- CPM : Critical Phase-Matching
- QPM : Quasi-Phase-Matching
- NPRO : Non Planar Ring Oscillator
- NA : Numerical Aperture

Symbols

ν_F : frequency of the fundamental wave

ν_{SH} : frequency of the second harmonic wave

η : second harmonic conversion efficiency

P_{SH} : power of the second harmonic

P_F : power of the fundamental wave

n_{SH} : refractive index of the second harmonic

n_F : refractive index of the fundamental harmonic

λ_F : wavelength of the fundamental wave

λ_{SH} : wavelength of the second harmonic wave

A : cross sectionnal area of the beam

d_{eff} : effective nonlinear coefficient

k : wave number

Λ : period of the variations of the second harmonic power with the length of propagation

$\Lambda_0/2$: theoretical poling period

n_o^{ω} : refractive index for an ordinary wave of frequency ω

n_e^{ω} : refractive index for an extraordinary wave of frequency ω

Lc : crystal length

E : electric field

P : polarisation of the medium

$\chi_{lmn}^{(2)}$: element of the second order suceptibility tensor

d_{ij} : element of the nonlinear coefficients matrix for non absorbing crystal

$h(\sigma,\xi)$: Boyd-Kleinmann parameter

$\Delta k'$: phase mismatch correction error in periodically poled structures

η_{QPM} : second harmonic conversion efficiency for quasi-phase-matching

η_{CPM} : second harmonic conversion efficiency for critical-phase-matching

d_{QPM} : effective nonlinear coefficient for quasi-phase-matching

d_{CPM} : effective nonlinear coefficient for critical phase-matching

Introduction

The European Southern Observatory has been developing for the last 10 years the Very Large Telescope Interferometer on the top of the Cerro Paranal in Chile. The first interferometric fringes have been obtained in 2001 and were soon followed by scientific results. Despite these first success ESO keeps developping new instruments to improve the performances of the VLTI. Among the forthcoming instruments is the Phase Referenced Imaging and Micro-arcsecond Astrometry facility (PRIMA). It is based on the simultaneous coherent observation of two celestial objects in which the two interferometric signals are tied together by an internal metrology system. To reach the final goal of an accuracy better than 10 microarcseconds in the astrometric mode, the metrology system must measure an optical path difference with a resolution higher than 5nm over several hundreds meters.

This metrology system is based on superheterodyne interferometry and is developped in partnership with the Institute of Micro-Technology of Neuchâtel (IMT). As a consequence of the resolution requirements the laser source need to be stabilized to a $d\nu/\nu=10^{-8}$ level. The method chosen for the stabilization of the NPRO Nd:YAG laser emitting at 1.319µm used in the metrology system is based on the work of Arie [5][6][7] who has stabilized this type of laser before. This technique requires the generation of the second harmonic of the laser beam to use a transition of iodine at 659.5nm as a frequency reference. The second harmonic generation (SHG) is carried out with a nonlinear crystal such as potassium titanyl phosphate (KTP) or lithium niobate (LN). The red beam is then sent to a cell filled with iodine vapor and the frequency error signal is generated using Pound-Drever-Hall method. The measured frequency drift of the laser is corrected by changing the optical path length in the resonator of the laser.

My internship, carried out at ESO between the 1st March and the 31st August 2003 under the supervision of Dr Samuel Lévêque, took place in this context. Its aims were to study and characterize a part of the hardware requirements of the laser frequency stabilization system. More precisely, SHG with Periodically Poled KTP (PPKTP) had to be characterized theoretically and experimentally. In addition frequency tuning of the laser and iodine spectroscopy around 659.5nm had to be studied too.

This report describes the work done and the context in which it took place. In the first part the basics of laser frequency stabilization and the work of Arie are recalled (section 1). Section 2 presents the basics of second harmonic generation and a theoretical study of "critical and quasi" phase matching followed by experimental results obtained with periodically poled KTP. Based on these results two optical configurations for the laser stabilization are discussed. The following section (section 3) describes the experimental results obtained about the laser frequency tuning and the iodine spectroscopy at 659.5nm. Specifications for PRIMA laser frequency stabilization iodine cell are presented. More about the context of this work can be found in APPENDIX A (ESO) and APPENDIX B (VLTI and PRIMA).

1 Laser fequency stabilization

One of the main characteristics of interests of lasers is the monochromaticity of their output. Nevertheless noise intrudes to make the laser linewidth finite and drifting. The constant need for a better frequency stabilization brought by applications so different as spectroscopy, metrology or detection of gravitationnal waves has lead to the development of several methods. A review of the main techniques used for laser stabilization is given by Hamilton in [2]. Some of them which could be applied to the PRIMA Metrology System Laser will be summarized in the following part. The methods chosen for PRIMA will be described and explained in the next part.

1.1 Frequency noise

All the sources of frequency noise in a laser can be classified in two categories:

- fundamental noise: noise inherent to the lasing process such as the spontaneous emission noise;
- technical noise: noise due to the environment or pumping perturbations.

The fundamental limitations of frequency stability is given by the fundamental noise due to the spontaneous emission noise. In the lasing process the stimulated emission is the dominant process and is the key to the phase coherence of the emission. Nevertheless there are allways spontaneous emissions giving rise to uncorrelated photons of random phase. These photons change slightly the phase of the field as described in Figure 1. As the instantaneous frequency is the time derivate of the phase, variations of the phase will lead to variations of the frequency.

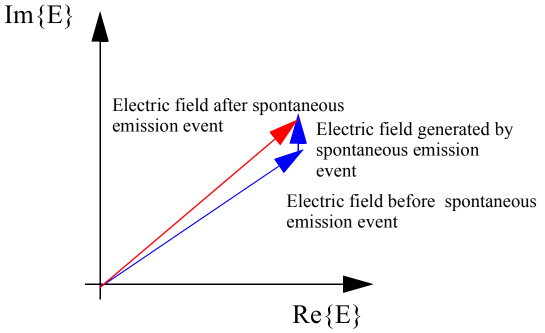

Figure 1 *Spontaneous emission origin of the frequency noise. A phasor diagram illustrating the random change in phase suffered by the laser light when spontaneous emission events occur in the gain medium.*

1.2 State of the art

The problem of frequency stabilization is carried out in two steps:

- generation of the error signal from a frequency reference;
- correction of the error.

1.2.1 Generation of the error signal

To achieve frequency stabilization a frequency reference is obviously needed. Fabry-Pérot interferometers and atom or molecular transitions are commonly used. The latter solution has the advantage of giving an absolute reference.

Once the frequency reference has been chosen one has to derive a suitable error signal from the reference. Such a signal will change of sign as the frequency goes through the desired frequency reference.

Saturated absorption([2])

The laser is directed through a cell filled with a gas. When the laser frequency is tuned little peaks appear in the output intensity. These peaks due to saturated absorption make ideal references for frequency stabilization. If the laser frequency is slightly dithered, for example with a piezo bonded on one of the mirror of the cavity and driven with an a.c signal, the frequency modulation causes an ouput power modulation whose phase depends on the slope of the saturation absorption peak. The slope is positive on one side of the peak and negative on the other side. Using a photodiode to monitor the ouput power and a lock-in amplifier one can derive a signal that indicates on which side of the transition the frequency is tuned.

Side-of-fringe locking([1],[2])

In this technique, the laser frequency is stabilized to a fixed point on the flank of the transition. The beam is splitted in two, one part goes through a cell filled with gas (frequency reference) to a photodiode and the other part goes to another photodiode. The two intensities coming from the photodiode should be carrefully balanced so their substraction gives the position of the frequency from the locking point. Unfortunately, to be efficient this technique requires a precise electronic set-up to balance properly the two intensities and a good control of the cell pressure (which modifies the absorption depth of the transition, hence the reference points is “moving” with the variations of pressure).

Pound-Drever-Hall method ([1],[2],[3],[4])

This technique, close to the Frequency Modulation spectroscopy used in atomic physics, first proposed for microwave oscillator has been extended to lasers. Phase modulation sidebands are generated by sending the beam in an EOM. The sidebands distance to the carrier should be greater than the transition linewidth. As the carrier is scanned through the transition its phase is shifted. On one side of the transition the phase shift is positive, on the other side the phase shift is negative. The sidebands are far enough from the transitions to avoid any phase shift. A beating will appear between the transmitted carrier and the sidebands due to the phase shift suffered by the carrier. If all the three optical frequencies were transmitted with the same phase shift the beat signal between the carrier and the first sideband would be in phase opposition with the beat signal between the carrier and the second sideband. As a consequence both signal would be cancelled. The phase of the beat signal in the transmitted light varies with respect to that of the signal that goes to the EOM. Using a homodyne detector one can detect the phase information and derive an error signal. Since the phase modulation frequencies can reach several tens of MHz, fluctuations of several MHz, which is beyond the usual technical noise frequency limit, can be detected.

1.2.2 Applying the error signal

After one has derived an error signal from a frequency reference one has to correct the error. Several means are available for this task.

One can use an AOM and/or an EOM to correct the frequency drift. The main limitation of the AOM comes from its slow speed of response. As a consequence, it is possible that between the detection of a short frequency variation and its correction the variation has already passed the AOM. On the contrary the EOM is not limited in its speed of response but it cannot produce a d.c frequency shift. Nonetheless the use of an AOM and an EOM in tandem as a frequency stabilization scheme has been proved to work.

Frequency stabilization can be directly achieved by changing the length of the cavity. In stabilized dye lasers one can find that the slow frequency control element is a glass plate inserted into the cavity and rotated about the Brewster's angle so as to vary the optical path length through it. The optical path length can also be changed by modifying the index of refraction of the resonator. This is achieved by changing the temperature of the crystal.

The cavity length can also be changed by the mean of a piezo element bonded on one of the cavity mirrors. This is usually used for high frequency correction.

1.3 Laser stabilization for PRIMA

As it has been presented before, the PRIMA Metrology System will use a NPRO Nd:YAG laser emitting at 1.319µm. The error signal will be derived from a molecular transition which has the advantage of being an absolute frequency. The choice of the molecular transition has been tackled by IMT in [1]. It has been showed that in the work conditions of the Paranal observatory no suitable transitions were available at 1.319µm. Nevertheless frequency stabilization of Nd:YAG lasers has already been carried out by Arie ([5],[6],[7]).Both for wavelength of 1.064µm and 1.319µm, he has first generated the second harmonic of the laser with a nonlinear crystal and has locked the laser frequency on an iodine transition. The Pound-Drever-Hall technique was used to derive the error signal.

From these conclusions two possible hardware configurations can be established (Figure 2). In the first configuration the full power of the laser is used for the SHG and the IR beam is recoupled into a polarization maintening monomode fiber after the dichroic mirror to be sent to the heterodyne assembly. Another possible solution is to use a first coupler after the laser to separate the IR beam in two: the first part would be used for the SHG and the second for the metrology. The choice between these two possibilities will be made depending on the power required at 659.5nm for the stabilization and on the power required at 1.319µm for the metrology.

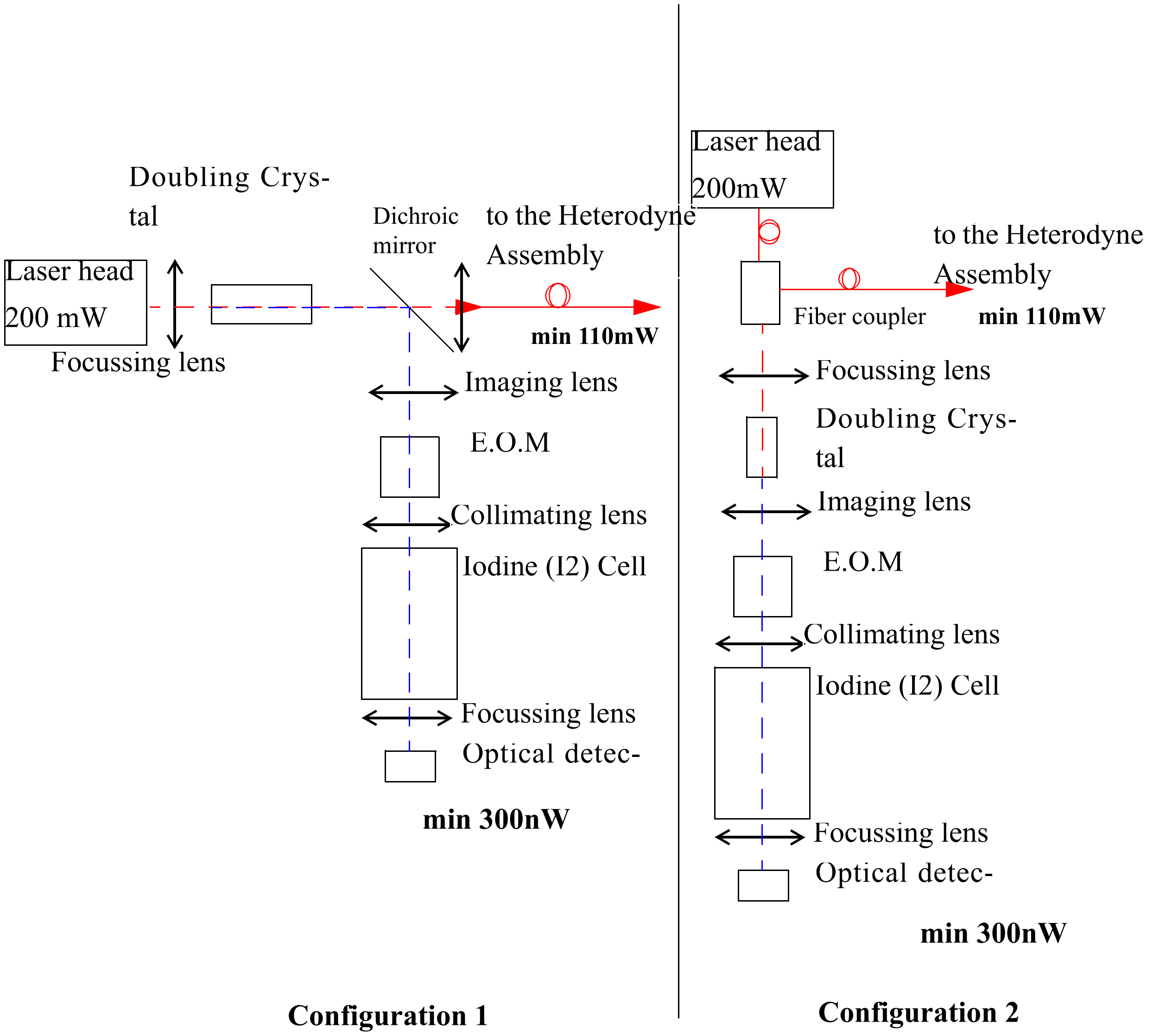

Figure 2 *Two possible optical configurations for the laser frequency stabilization. The dash lines represent the optical path..*

2 Second Harmonic Generation (SHG)

The previous part had presented possible frequency stabilization schemes for the PRIMA Metrology System. The stabilization method based on the work of Arie [7] requires the generation of the second harmonic of the laser beam. The SHG is achieved by the use of a nonlinear crystal which can be for example Potassium Titanyl Phosphate (KTP) or Lithium Niobate (LN).

The first section introduces the theory of Second Harmonic Generation (SHG) of a laser beam in the context of the PRIMA Laser Metrology System. The theoretical conversion efficiency is computed for the "*critical*" and "*quasi*" phase matching configurations using both the KTP and $LiNbO_3$ non linear crystals. In addition, the sensitivity of the conversion efficiency to the variation of temperature, angular alignment and wavelength is presented in the case of "quasi" phase matching.

Then experimental results are presented to evaluate the performance of "quasi" phase matching SHG of a 1319nm Nd-Yag laser using Periodically Poled KTP (bulk and waveguide).

Finally two hardware configurations for the SHG are proposed and discussed in the context of the frequency stabilization of the Nd-yag laser selected for the PRIMA laser Metrology System.

2.1 Theoretical analysis

2.1.1 SHG basics

The polarization induced in a medium by an electric field is usually described by a linear expression. Nevertheless it has been showed that by increasing the amplitude of the field nonlinear effects appear. One of the second-order nonlinear effects is the generation of a polarization oscillating at twice the frequency ν_F of the excitation field. This polarization emits a new wave of frequency $\nu_{SH}=2\nu_F$ which is spatially superimposed with the fundamental wave. This effect is called Second Harmonic Generation (SHG) [10][11].

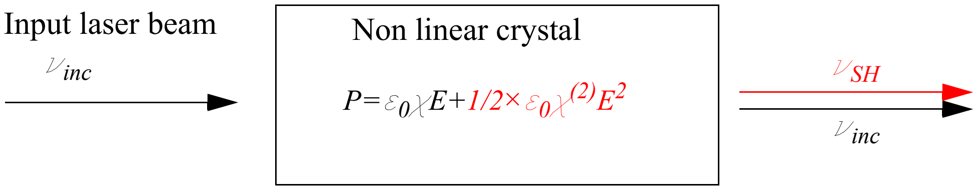

Figure 3 *Basic principle of Second Harmonic Generation. The incident electric field oscillating at a frequency* ν_{inc} *induces in the medium a polarization. If the field amplitude is large enough the polarization can oscillate at twice the frequency of the incident wave emitting a new wave at a frequency* $\nu_{SH}=2\nu_{inc}$*. This new wave spatially superimposed with the fundamental one is called Second Harmonic (SH).*

2.1.2 Phase-matching

If one assumes a low conversion rate, the conversion efficiency after a distance z in the nonlinear medium is given by [10]:

$$\eta(z) = \frac{P_{SH}(z)}{P_F} = \frac{8\pi^2}{n_{SH} n_F^2 \lambda_F^2 c \varepsilon_0} \cdot \frac{P_F}{A} d_{eff}^2 \left[\frac{\sin\left(\frac{\Delta k z}{2}\right)}{\frac{\Delta k}{2}} \right]^2 \tag{2.1-1}$$

with $\Delta k = |k_{SHG} - k_F|^2$ (k the wave number), P_F and P_{SH} the power of the fundamental and SH beam respectively, n_F and n_{SH} the refractive indexes at the fundamental and SH wavelength respectively, A the cross sectional area of the beam, d_{eff} a coefficient representing the nonlinearity of the crystal. Values for the KTP physical properties are given in APPENDIX C.

As a consequence the conversion efficiency is a function of the phase difference between the fundamental wave and the SH wave. Since the media used for SHG are usually dispersive the phase difference is not zero. Thus if one looks at the evolution of the SH wave intensity along the propagation axis, one sees it oscillating with a period Λ (Figure 4).

In order to get a significant efficiency one has to maintain the two waves in phase, i.e to create the conditions of “phase-matching”.

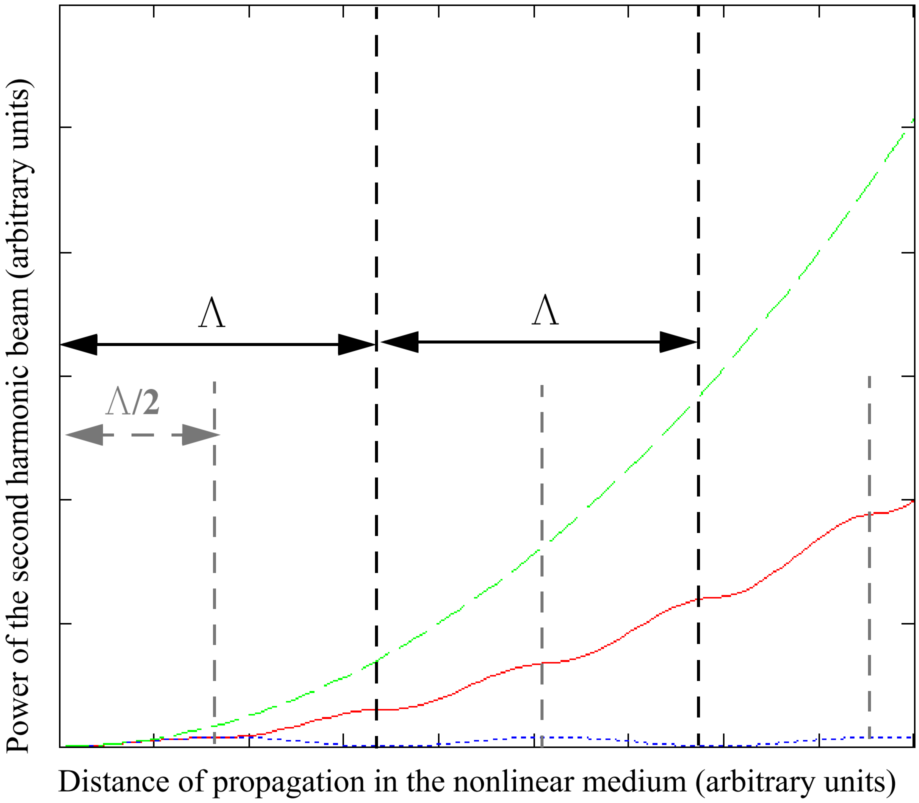

Figure 4 *Growth of the intensity of the SH beam with the length of propagation in the nonlinear medium with no phase matching (blue dots line), Critical Phase-Matching (green dashed line) and Quasi Phase-Matching (red line). For this graph the nonlinear coefficient is assumed to be the same for CPM and QPM which is usually not the case. Λ is the period of the conversion efficiency oscillation in case of SHG without phase matching (~34.44 µm for KTP at 30°C). For Quasi Phase Matching the period of poling is Λ/2 (~17.22 µm for PPKTP).*

2.1.2.1 Critical Phase-Matching (CPM)

The phase difference between the fundamental wave and the SH wave is due to the dispersion induced by the medium. If one can get equal refractive indexes for both waves the conversion efficiency will grow during all the propagation in the non-linear medium. This is called Critical Phase-Matching and it can be achieved in birefringent media in which the refractive index for a given wavelength is function of the temperature and of the polarization direction. A good choice of these two parameters allows to maintain a zero phase difference between the two waves [1][8][10][11]. Two types of CPM are usually employed:

Type I: In that case, the input and output waves are orthogonally polarized. The fundamental wave is an extraordinary wave with a refractive index $n_e^{\omega}(\Theta)$, and the second harmonic wave is an ordinary one with a refractive index $n_o^{2\omega}$. The phase matching condition is fulfilled by selecting an angle of incidence θ for which [8]

$$\frac{1}{(n_0^{2\omega})^2} = \frac{(\cos\theta)^2}{(n_0^{\omega})^2} + \frac{(\sin\theta)^2}{(n_e^{\omega})^2} \qquad (2.1\text{-}1)$$

Type II: In that case, the incoming polarization is at 45° of the crystal z-axis. We can therefore consider at the input an extraordinary and an ordinary wave with refractive indexes $n_e^{\omega}(\theta)$ and n_o^{ω}, respectively. The SH wave is either an extraordinary or ordinary wave. Assuming that the SH wave is an extraordinary ray with a refractive index $n_e^{\omega}(\theta)$, the phase-matching condition becomes [8]

$$n_e^{2\omega}(\theta) = \frac{1}{2}(n_e^{\omega}(\theta) + n_0^{\omega}) \qquad (2.1\text{-}2)$$

Nevertheless, in anisotropic media the poynting vector and the wave vector are not parallel. This effect, called birefringent walkoff, results in a finite distance of interaction between the waves which limitates again the conversion efficiency [8][10]. IMT has proposed a setup for the walkoff compensation in [8].

2.1.2.2 Quasi Phase-Matching (QPM) in Periodically Poled structures (PP)

In QPM the idea is to compensate periodically the phase mismatch by inverting the orientation of the nonlinear medium. This causes a shift of π of the SH wave phase. If the change of orientation is done when the phase mismatch is an odd multiple of π then the waves are again in phase and the energy keeps being transferred from the fundamental beam to the SH beam (Figure 4)

2.1.3 Expected conversion efficiency

2.1.3.1 Critical phase-matching

Loose focusing

In the loose focussing assumption the fundamental beam is not considered as a gaussian beam. This assumption holds as long as the beam is not too focused. Another usual assumption is that the power of the fundamental beam remains constant during the propagation which means that the absorption in the doubling crystal can be neglected and that the conversion efficiency is low. This last assumption is called “undepleted fundamental wave”. For perfect conventional phase matching with the assumptions of loose focusing and undepleted fundamental wave the efficiency of SH conversion is given by (Equation (2.1-1) with $\Delta k=0$, the phase matching is perfect, $\sin(\Delta kL/2))/(\Delta kL/2)=1$, [10])

$$\eta = \frac{P_{SH}}{P_F} = \frac{8\pi^2}{n_{SH} n_F^2 \lambda_F^2 c \varepsilon_0} \cdot \frac{P_F}{A} d_{eff}^2 L_C^2 \qquad (2.1\text{-}1)$$

where d_{eff} is function of the type of phase matching and of elements of the second order susceptibility tensor and Lc the length of the crystal.

For type II phase matching with KTP [8] showed that the angle of the incident polarization should be Θ=64°. The effective nonlinear coefficient d_{eff} is given by

$$d_{eff} = \chi^{(2)}_{223}\sin\theta \qquad (2.1\text{-}2)$$

The power of the SH generated with 50mW of power for the fundamental wave and a KTP crystal of 1 cm long should be *2.42µW* (with A chosen equal to the waist of a gaussian beam if confocal focusing[1] was carried out).

Nevertheless, in these conditions the walkoff angle is 34mrad which reduces the distance of interaction to approximately 1.5mm. The KTP crystal is only used efficiently on 1.5mm which leads to a SH power of *52nW*! [8]

With the same assumptions but for a $LiNbO_3$ crystal the power of SH obtained is 1.43µW with no birefringent walk off and 32.2nW if the walk off is not compensated.

Gaussian beam

If one assume an undepleted fundamental wave and a gaussian beam, the efficiency of conversion is [12]

$$\eta = \frac{P_{SH}}{P_F} = \frac{16\pi^2 d_{eff}^2}{\varepsilon_0 c n_F n_{SH}\lambda_F^3} P_F L_C h(\sigma, \xi) \qquad (2.1\text{-}3)$$

where $h(\sigma,\zeta)$ is function of the focusing and is maximum when the Rayleigh range of the beam is equal to 0.176 times the length of the crystal ($\sigma_{opt}=\Delta k z_r=0.56$, $\zeta_{opt}=L/2z_r=2.84$ with z_r the Rayleigh range of the fundamental beam). For perfect focusing with a 1cm long KTP crystal and an incident power of 50mW, *4.32µW* of red light at 659.5nm are expected.

With the same assumptions and parameters a $LiNbO_3$ crystal would provide 3.36µW of red light at 659.5nm.

2.1.3.2 Quasi phase-matching

Loose focusing

In the assumption of loose focusing and undepleted fundamental wave, Fejer [13] showed that the conversion efficiency is

$$\eta = \frac{8\pi^2}{\lambda_F^2 c\varepsilon_0 n_F^2 n_{SH}}\left(\frac{2d_{eff}}{\pi}\right)^2 L_C^2 \operatorname{sinc}^2\left(\frac{\Delta k' L_C}{2}\right)\frac{P_F}{A} \qquad (2.1\text{-}1)$$

where A is the cross sectional area, and with

$$\Delta k' = k_{SH} - 2k_F - \frac{2\pi}{\Lambda_0} \qquad (2.1\text{-}2)$$

---

[1] confocal focusing is achieved when the waist of the beam is in the middle of the crystal and when the length of the crystal is equal to twice the Rayleigh range of the beam.

$\Delta k'$ represents the error between the phase mismatch correction and the real phase mismatch, $\Lambda_0/2$ is the period of inversion of the nonlinear coefficient. If $\Lambda_0=\Lambda$ then $\Delta k=0$ and the phase mismatch is exactly compensated every $\Lambda/2$.

QPM gives usually access to nonlinear coefficients larger than those used in CPM. If $\Delta k'=0$ (perfect correction of the phase mismatch) for the same type of crystal and for the previous assumptions the gain in efficiency with a periodically poled crystal is [13]

$$\frac{\eta_{QPM}}{\eta_{CPM}} = \left(\frac{2d_{QPM}}{\pi d_{CPM}}\right)^2 \tag{2.1-3}$$

where d_{CPM} and d_{QPM} represent the effective nonlinear coefficient used in each process. In the case of type II phase matching with KTP, one has $d_{CPM}=4.49$pm/V [2] and $d_{QPM}=13.7$pm/V [3]. *With KTP, the QPM efficiency is approximately 3.6 times higher than CPM efficiency* . For 50mW of IR *8.6μW* of SH are expected.

For $LiNbO_3$ crystals, the gain of efficiency with QPM compared to CPM is approximately 33 times[4]! 50mW of IR would generate 112μW of red light at 659.5nm.

2.1.3.3 Summary of the expected conversion efficiency

Table 1 Summary of the expected conversion efficiency for KTP

Type of phase-matching	Focussing	η (P_F=50mW)	P_{SH} (P_F=50mW)	η (P_F=200mW)	P_{SH} (P_F=200mW)
CPM, Type II without birefringent walkoff compensation (KTP)	loose gaussian	1.04×10^{-6} 1.08×10^{-6}	52nW 54nW	4.16×10^{-6} 4.35×10^{-6}	0.832μW 0.871μW
CPM,Type II (KTP)	loose gaussian	4.84×10^{-5} 8.64×10^{-5}	2.42μW 4.32μW	1.94×10^{-4} 3.46×10^{-4}	38.72μW 69.12μW
QPM (KTP)	loose	1.72×10^{-5}	8.6μW	6.88×10^{-4}	137.6μW

Table 2 Summary of the expected conversion efficiency for $LiNbO_3$

Type of phase-matching	Focussing	η (P_F=50mW)	P_{SH} (P_F=50mW)	η (P_F=200mW)	P_{SH} (P_F=200mW)
CPM,Type II without birefringent walkoff compensation $LiNbO_3$	loose gaussian	6.44×10^{-7} 1.51×10^{-6}	32.2nW 75.6nW	2.57×10^{-6} 6.05×10^{-6}	0.515μW 1.21μW
CPM,Type II ($LiNbO_3$)	loose gaussian	2.86×10^{-5} 6.72×10^{-5}	1.43μW 3.36μW	1.14×10^{-4} 2.68×10^{-4}	22.9μW 53.76μW

---

[2] $d_{CPM}=\chi_{223}\times\sin(64°)$, $\chi_{223}^{(2)}=5.0$pm/V

[3] $d_{QPM}=\chi_{333}^{(2)}=13.7$pm/V

[4] $d_{CPM}(LiNbO_3)=d_{31}=5.0$pm/V, $d_{QPM}(LiNbO_3)=d_{33}=44$pm/V, [11]. Note: Arie in [7] gives a gain of $2d_{33}/\pi d_{31}=20$. The difference is due to a discrepancy in the value of the non linear coefficients

Table 2 Summary of the expected conversion efficiency for $LiNbO_3$

Type of phase-matching	Focussing	η (P_F=50mW)	P_{SH} (P_F=50mW)	η (P_F=200mW)	P_{SH} (P_F=200mW)
QPM ($LiNbO_3$)	loose	9.54×10^{-4}	47.7µW	3.8×10^{-3}	763.2µW

2.1.4 Temperature, angle and wavelength tolerances for QPM

Equation (2.1-1) shows that the conversion efficiency is depending on Δk' which is function of the temperature, the fundamental wavelength and the angle of incidence. Hence, the variations of these parameters can deteriorate or increase the conversion efficiency.

2.1.4.1 Temperature tuning

In QPM the phase-mismatch correction can be tuned with the temperature. The variations of temperature are responsible for thermal expansion and for the modification of the refractive index of the crystal.

$$\Delta k'(T) = k_2(T) - 2k_1(T) - \frac{2\pi}{\Lambda_0(T)} \qquad (2.1\text{-}1)$$

Using the thermal expansion coefficient and the refractive-index temperature derivatives of KTP, [13], it is possible to deduce, with the assumption of loose focusing and undepleted fundamental wave, the variation of efficiency around a central temperature T_0 for which the phase-mismatch correction is perfect (Figure 5)

$$\Delta k'(T_0) = 0 \qquad (2.1\text{-}2)$$

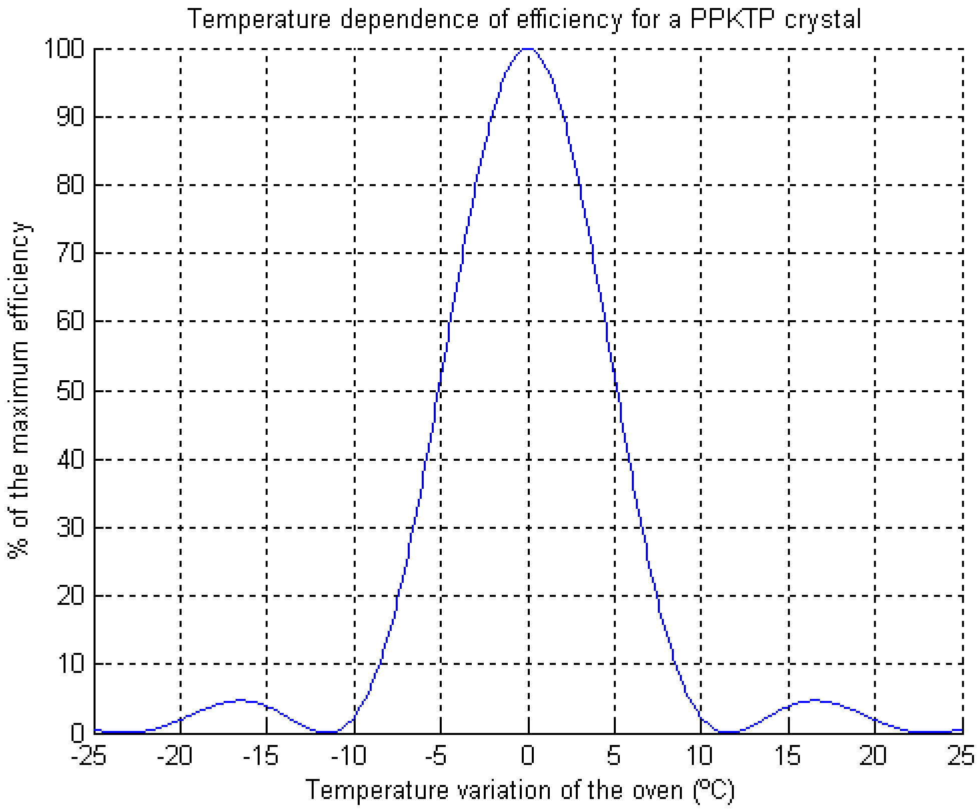

Figure 5 *Temperature dependence of the SH conversion efficiency for a PPKTP crystal. The percentage of the maximum efficiency is plotted as a function of the deviation of the crystal temperature from the central temperature T_0 for which the phase-mismatch correction is perfect. The bandwidth at 50% is 10*°C.

As it can be seen on Figure 5 the bandwidth at 50% of the efficiency is 10ºC. Since the stabilization of the temperature oven will be done with a precision of ±0.1ºC (see section 2.2.1.3) the temperature should not be a critical parameter.

2.1.4.2 Angular dependence

Assuming the propagation is done along the x-axis in the crystal with a direction of polarization parallel to the z-axis if the incident beam makes an angle α with the x-axis in the xOy plane the polarization remains unchanged but the period of poling seen by the beam is (Figure 6)

$$\frac{\Lambda_0(\alpha)}{2} = \frac{\Lambda_0}{2\cos\alpha} \tag{2.1-1}$$

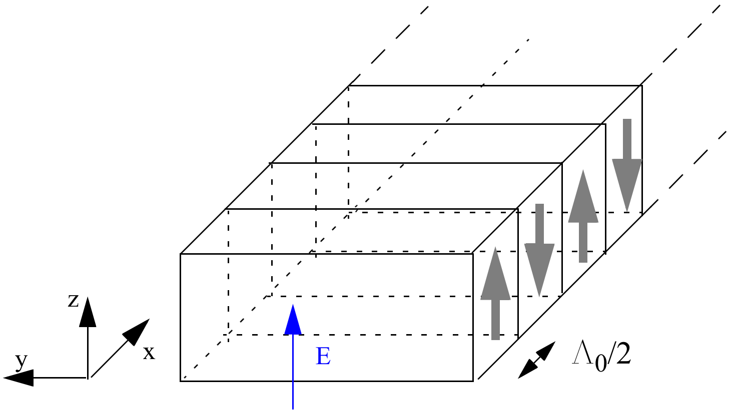

Figure 6 *Schematic view of a PPKTP bulk crystal. The direction of polarization should be parallel to the z axis to use the largest nonlinear coefficient* χ_{333}.

By replacing Λ_0 by $\Lambda_0(\alpha)$ it is possible to plot the angular dependence of the efficiency (Figure 7)

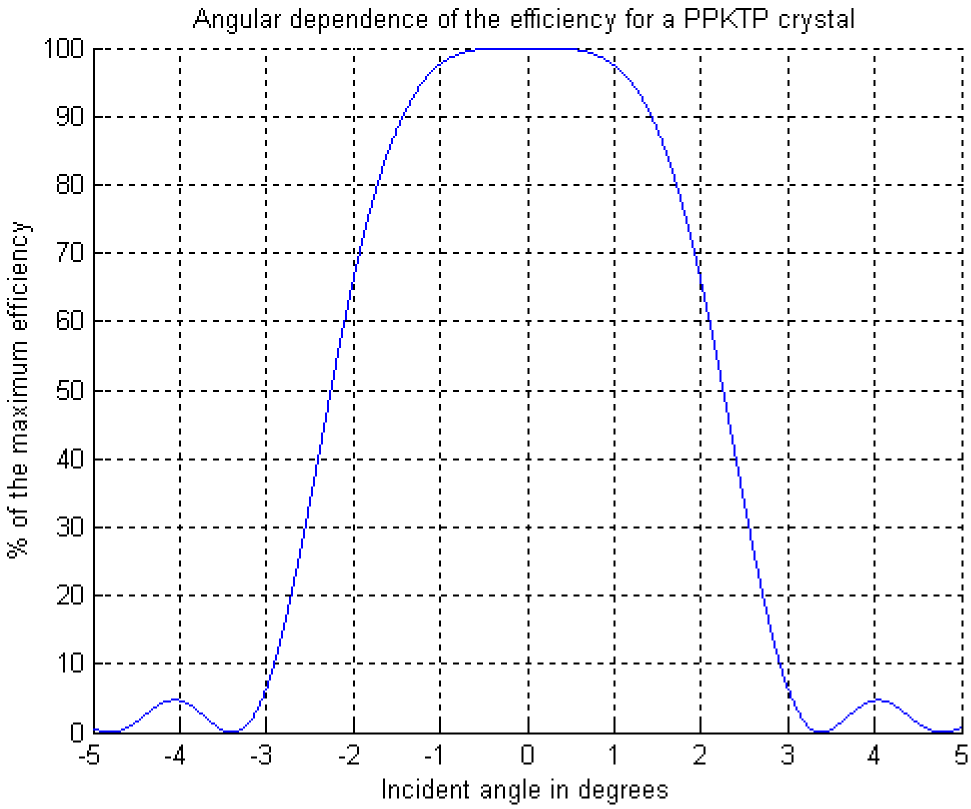

Figure 7 *Angular dependence of the efficiency for a PPKTP crystal with the assumption of loose focusing and undepleted fundamental wave. The bandwidth at 50% of the efficiency is 4.5°C.*

As long as the polarization remains unchanged the angular dependence doesn't seem critical.

2.1.4.3 Wavelength dependence

Δk' is function of the wavelength. For a given Λ_0 the variation of wavelength will cause a variation of Δk' and so a variation of the efficiency. In Figure 8 the variation of efficiency has been plotted for Λ_0 calculated for λ=1.139µm with the assumption of loose focusing and undepleted fundamental wave.

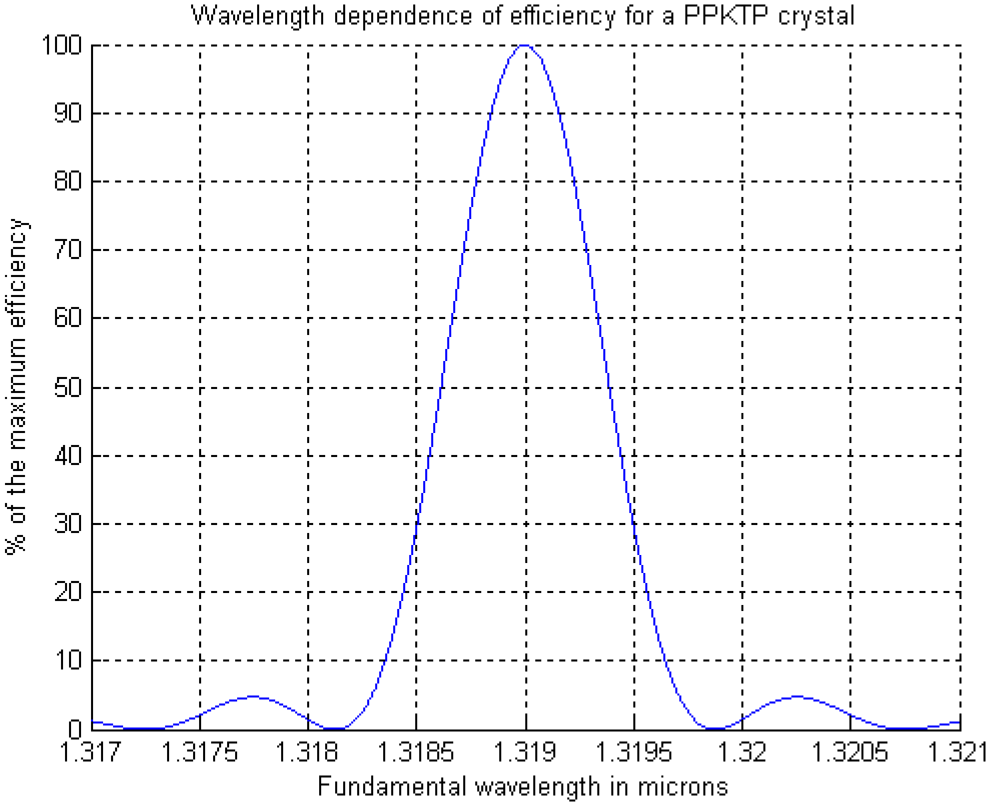

Figure 8 *Wavelength dependence of the efficiency for a PPKTP crystal with the assumption of loose focusing and undepleted fundamental wave for a crystal optimized for 1.319µm. The bandwidth at 50% is 750pm (172GHz).*

2.2 Experimental results using bulk PPKTP

2.2.1 Experimental set-up

2.2.1.1 Optical set-up

SHG has been tested and characterized using a 10x5x1mm^3 bulk PPKTP crystal. The fundamental IR beam is provided by a Lightwave Model-125 Nd-Yag laser emitting at 1.319µm (PRIMA Metrology System Laser). Its maximum power is 200mW. The laser is coupled to a monomode polarization maintaining fiber (9µm diameter core, NA=0.11) terminated by a FC-PC connector. The beam is focused with an OFR fiber port[5] on which is mounted an f=11mm lens. The direction of polarization of the fundamental beam is parallel to the z axis as on Figure 10 in order to use the largest nonlinear coefficients $\chi^{(2)}{}_{333}$. The crystal is hold inside an oven from HC Photonics, temperature controlled by a Newport Omega controller[6]. The fiber port and the oven are mounted on two different xyz translations stages to allow the best focusing (Figure 9). The oven position can also be controlled in Θz and Θy (see Figure 10).

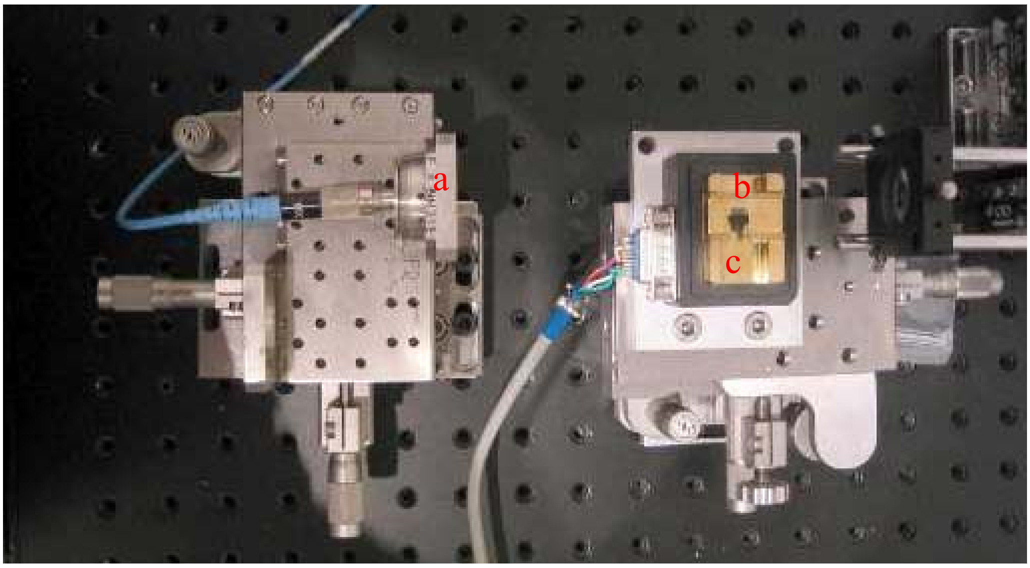

Figure 9 *Second Harmonic Generation with bulk PPKTP set-up. The fundamental bean is provided by a fiber-coupled NPRO Nd:YAG Laser*[1] *and is focused by a 11mm long focal length lens mounted on a fiber-port*[2]*(a). The crystal (b) is hold inside an oven*[3]*(c) controlled in temperature*[4] *(±0.1°C). On this picture the top of the oven has been removed so as to see the crystal.*

1. Lightwave model No. 125
2. OFR PAF-X-11-1319
3. HC Photonics
4. Newport omega CN-77352-C4

The power of the fundamental IR beam is measured after the f=11mm focussing lens using a Germanium detector. After the crystal, both IR and the SH beams are superimposed. However, the power of the SH (visible) is measured independently by a Silicon detector which is not sensitive to IR radiation. The conversion efficiency is simply given by the ratio between the IR and SH power.

2.2.1.2 Periodically Poled KTP (PPKTP) crystal

The characteristics of the PPKTP are summarized in Table 3 and the physical properties of KTP can be found in APPENDIX C.

---

[5] OFR PAF-X-11-1319

[6] Newport Omega CN-77352-C4

Table 3 Specification of the bulk PPKTP

Parameters	**Specifications**
Material	PPKTP
Application	SHG at λ=1319nm
Poled length	90%
Dimensions	1x5x10 mm^3
Anti-refection coatings	DBAR 1319/659.5 nm
Surface Quality - Scratch/Dig	Laser quality polishing- 10/5
Flatness	λ/10
Poling period	16.75 µm
Operating temperature	30-60 °C
Manufacturer/ Price	Raicol Crystals Ltd / 3950$

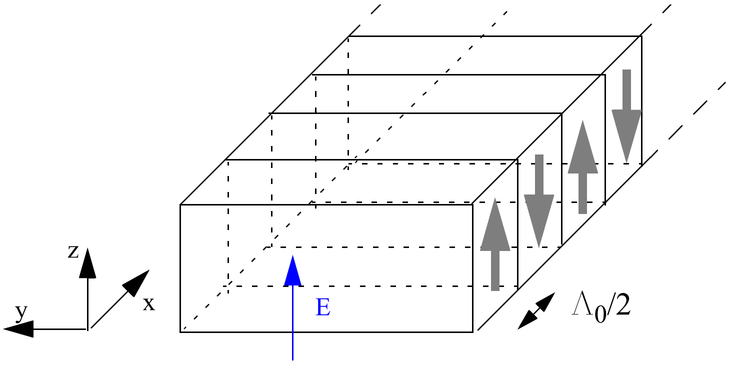

Figure 10 Schematic view of a PPKTP bulk crystal and of the incident electric field vector. The direction of polarization should be parallel to the z axis to use the largest nonlinear coefficient $\chi_{333}^{(2)}$.

2.2.1.3 Oven and temperature controller

As described in section 2.1.4.1 the conversion efficiency is a function of the temperature of the crystal therefore the PPKTP is hold in a temperature stabilized oven. We selected an oven from HC Photonics (Model series OV03, Figure 9). Its specifications are summarized in Table 4.

Table 4 HC Photonics oven (OV03) specifications.

Parameters	**Specifications**
Model series	OV03 series

Parameters	**Specifications**
Application	Heating of Periodically Poled Bulk chips and free space Waveguide chips
Outer housing material	Teflon
Inner base material	Brass
Sensor	pt100/RTD
Operating Range	Room temperature~250ºC
Warm up time (room temp to 250ºC)	~12mins
Power consumption	Input voltage 110V AC: current is 0.5A (Max) and the power is 55W(Max) Input voltage 220V AC: current is 1A (Max) and the power is 220W(Max)
Stability	±0.1°C or better (with a temperature controller)
Manufacturer/ Price	HC Photonics / 1000$

The temperature controller chosen for the regulation of the oven is a Newport Omega CN77352-C4. The controller can read the temperature from a pt100/RTD like the one used in the oven. The regulation can be done with an auto tunable PID used with an analogic output (0-10V P_{oven}=0.435W, 4-20mA P_{oven}=0.092W). Unfortunately this output does not furnish enough power to reach the required temperature. Indeed in order to heat the crystal to a temperature of 100 °C in a few minutes the voltage should be ~40V (7W). For the moment the controller is only used as a sensor and the power used by the oven is provided by a voltage generator (40V). Nevertheless a small electronic set-up will be implemented to amplify the analogic output so as to use the auto tunable PID. With the PID the temperature stability should be ±0.1°C which is largely enough compared to the temperature dependence of the conversion efficiency (see 2.1.4.1).

2.2.2 Measured conversion efficiency

The best measured conversion efficiency was $\eta=3.5\times10^{-4}$*, i.e 64µW of second harmonic for a maximum fundamental IR power of 180mW.* The reader can refer to Fig. 23 to see the measured SH power as a function of the fundamental input power.

By scaling the theoretical results given for QPM in Table 1[7], we should have obtained $(180mW/200mW)^2\times137.6\ \mu W = 111\ \mu W$, i.e a factor 1.7 more. We have obtained a lower efficiency experimentally most probably because the IR beam was not focused in an optimal way inside the crystal.

---

[7] Considering that the SH power is proportional to the square of the fundamental power. See experimental verification in section 2.2.3.2

2.2.3 Parameters affecting the conversion efficiency

As it has been showed in the theoretical analysis the conversion efficiency depends on several parameters such as the temperature, the power of the fundamental wave, the angle of incidence and the wavelength. Furthermore, the conversion efficiency also depends on the number of longitudinal modes in the fundamental beam, as demonstrated in [7]. The impact of these parameters on the conversion efficiency is detailed in the following sections.

2.2.3.1 Temperature of the crystal

In order to determine the optimal temperature for the PPKTP crystal, the SH power was measured and plotted for a large range of temperature. The best temperature was approximately 77.5°C whereas Raicol indicated that the working temperature of the PPKTP should be between 30-60°C. In fact, the measured temperature is not the crystal temperature but the temperature of the surrounding oven, which can explain this discrepancy.

Considering the poling period given by Raicol Crystals and the temperature dependent refractive indexes given in [14], it is also possible to compute the expected temperature for which conversion efficiency is maximum. This corresponds to T_0 such that $\Delta k'(T_0)=0$, i.e when the phase mismatch correction is perfect. For the 16.75µm poling period given by Raicol, we find T_0~120°C, which is more than a factor 1.5 larger than what was observed experimentally. This difference is either due to a different value of the poling period after the manufacturing process or a discrepancy in the refractive indexes.

Only an approximate value of the optimum temperature can be given because the efficiency is also function of the angle of incidence and of the wavelength. For a given set-up the oven temperature has been tuned so as to determine the variation of efficiency as a function of the temperature. On Figure 5 the experimental curve is compared to the curve of Figure 11 which has been translated such that their maxima are superimposed.

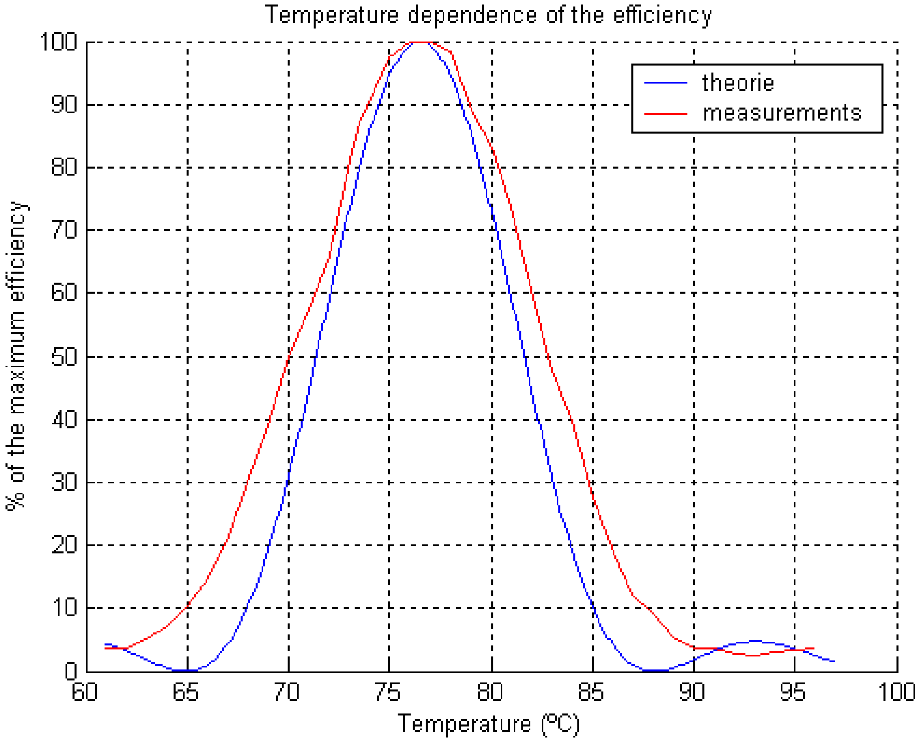

Figure 11 *Conversion efficiency as a function of the temperature for a PPKTP crystal. The experimental curve is plotted. in red. The blue theoretical curve has been plotted so as its maximum corresponds with the maximum of the experimental curve.*

The SH efficiency was measured when the crystal was cooling down from 96°C to 61°C. The voltage in the oven has been reduced so as to keep a constant cooling speed. One has to pay attention that the measured temperature is not the crystal temperature but the temperature of the surrounding oven. As these measurements were made without waiting for the crystal temperature being equal to the oven temperature the curve might be slightly translated along the horizontal axis. Nevertheless even if the experimental curve is wider its shape is similar to what expected by the theory. As the bandwidth at 50% and at 90% are 12.5°C and 5°C respectively the use of the previously described temperature controller will ensure that the conversion efficiency will not be reduced by temperature fluctuations (<0.1°C).

2.2.3.2 Power of the fundamental beam

The theory expects a square dependence of the SH power with the fundamental power. For a given set-up (oven temperature, focusing, angle), the SH power has been measured for different powers of the incident IR beam (Figure 12).

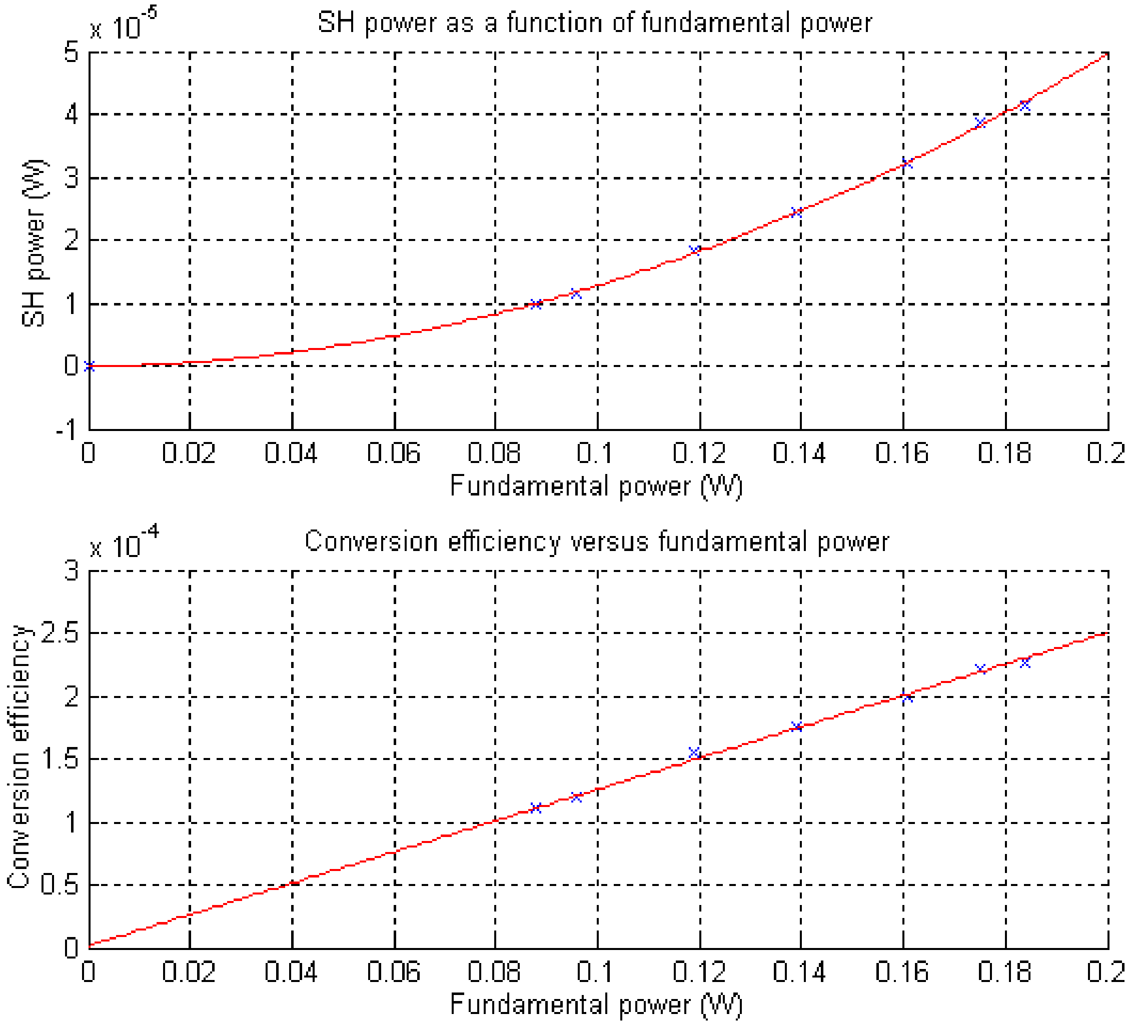

Figure 12 *SH power and conversion efficiency as a function of fundamental power.The measured points are the blue crosses. On the top figure the red curve has been obtained with a quadratic fit. On the bottom figure the red line is obtained with a linear fit. NOTE: The measured conversion efficiency is NOT the optimum efficiency for each indicated power of the fundamental beam. This graph is only intended to verify experimentally that the SH power is proportional to the square of the incident power (see Fig. 23 for the optimum conversion efficiency)*

The measurements fit well with the expected square dependence of the SH power with fundamental power.

2.2.3.3 Angular orientation of the crystal

The instruments necessary for the measurements of the angle dependence of the conversion efficiency were not available at the time of the experiment. Nevertheless the bandwidth at 50% is measured to be approximately 4° which is a little bit less than what was expected by the theory (2.1.4.2). The use of a simple translation stage will be enough to ensure that the angular dependence is not critical.

2.2.3.4 Wavelength of the fundamental beam

For a given set-up (focusing, temperature, angle) the wavelength emitted by the laser is tuned and the SH power is monitored (Figure 13). The wavelength has been tuned over the whole laser tunable range.

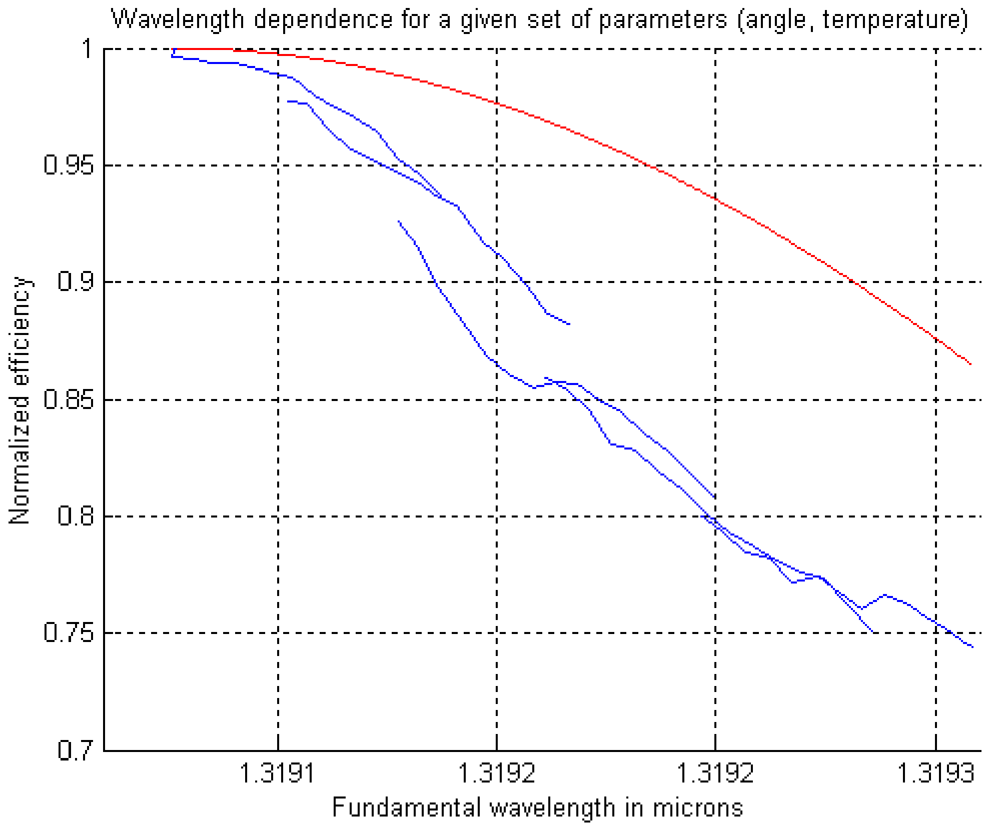

Figure 13 *Measured wavelength dependence of SHG for a given set of parameters (temperature, angle). The blue curve has been measured on the whole wavelength tunable range of the laser.The 'jumps' between the different parts of the curves correspond to the longitudinal mode hops of the laser. The red curve is the theoretical curve.*

On Figure 13, the experimental curve is plotted with the theoretical curve of Figure 8 translated so as their maximum correspond. If one compares the bandwidth at 80% of the experimental curve (assuming the left part can be obtained by symmetry) and the bandwidth part at 80% of the theoretical curve (Figure 8) one gets 82.7GHz and 87.2GHz respectively. Furthermore for the bandwidth at 90% one obtains approximately 50GHz and 51.7GHz for the measurements and the theory.

2.2.3.5 Number of longitudinal modes in the fundamental beam

During the study of the laser tuning characteristics, [9], the power of the SH harmonic was monitored while changing the wavelength of the laser by applying a voltage to the laser driver (Figure 14). One can notice periodical power increases of the SH beam.By comparing this curve to a curve representing the evolution of the wavelength with the voltage, it appears that these increases correspond to the mode hops of the laser. Considering that the power of the laser is stable during a mode hop, the increase of SH power is due to an increase of the conversion efficiency. This effect has already been described in [15].

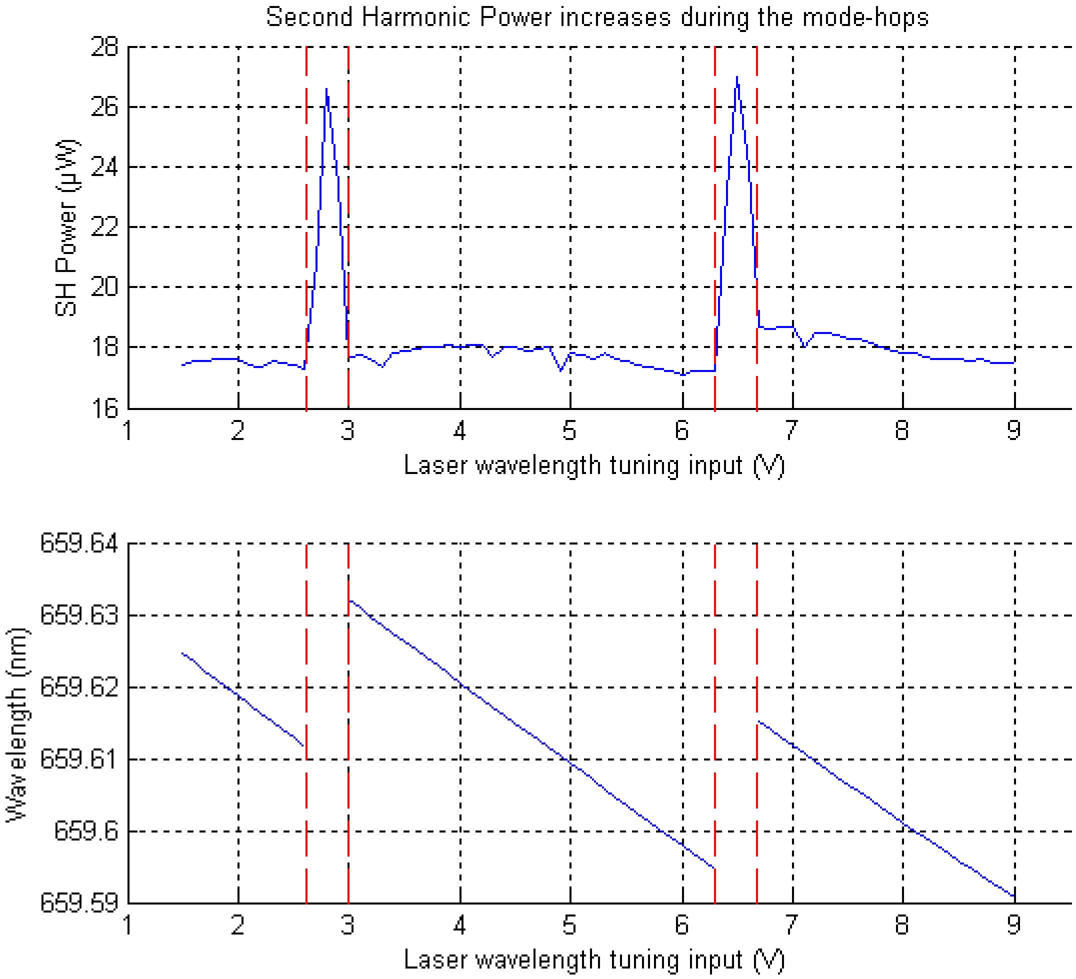

Figure 14 *Increase of the Second Harmonic power during the mode-hops. The upper graph shows the SH power while changing the laser wavelength. The lower graph shows the emitted wavelength as a function of the voltage. The curve is discontinuous because during the mode hops the wavelength is fluctuating too much to be monitored properly. The increases of power in the SH beam happen during the laser mode hops.*

The spectrum of the SH beam has been measured with a spectrum analyzer (Model 240, Spectrum Analyzer, Coherent) before and during a mode hop of the Nd-Yag laser. The results are presented in Figure 15. The first graph has been taken outside the mode hop area and only one SH mode can be seen. In the other graphs, the spectra of the SH beam is measured during a mode hop of the Nd-Yag laser and several SH modes appear with a maximum of three modes at the same time.

Let us consider a fundamental beam composed of two different longitudinal modes.

$$E(t) = E_1 \cdot e^{i\omega_1 t} + E_2 \cdot e^{i\omega_2 t} \qquad (2.2\text{-}1)$$

The nonlinear part of the polarization is given by

$$P_{\text{nonlinear}} = \frac{1}{2}\cdot\varepsilon_0\chi^{(2)}E^2 = \frac{1}{2}\varepsilon_0\chi^{(2)}\cdot\left(E_1^2\cdot e^{i2\omega_1 t} + E_1\cdot E_2\cdot e^{i(\omega_1+\omega_2)t} + E_2^2\cdot e^{i2\omega_2 t}\right) \qquad (2.2\text{-}2)$$

Three different electric fields appear at $2\omega_1$, $2\omega_2$ and $\omega_1+\omega_2$. In our case the fundamental beam seems to be composed of two longitudinal modes, if there are more they are weak enough to be neglected as they don't even appear on the spectrum.

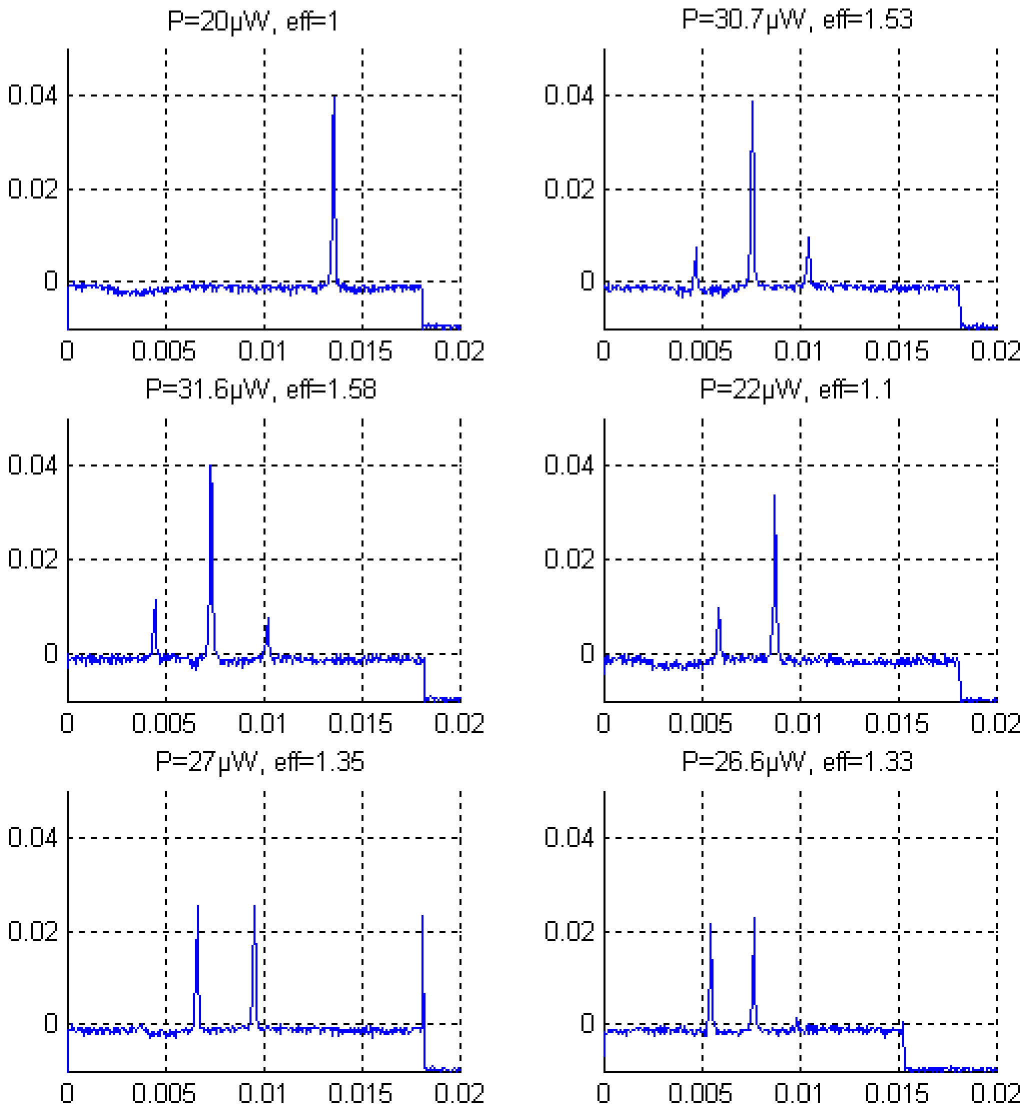

Figure 15 *Different spectra measured for the SH beam. The x axis is in ms (scanning of the piezo of the spectrum analyzer). For each spectrum the measured power of SH and the efficiency compared to the monomode efficiency is given.*

To deduce the separation between the two modes one uses the separation of two Fabry-Perot modes as a reference (Figure 16). The free spectral range given in the spectrum analyzer manual is 7.5 GHz. The average separation between the two modes of the fundamental beam is then calculated to be 1.16 GHz.

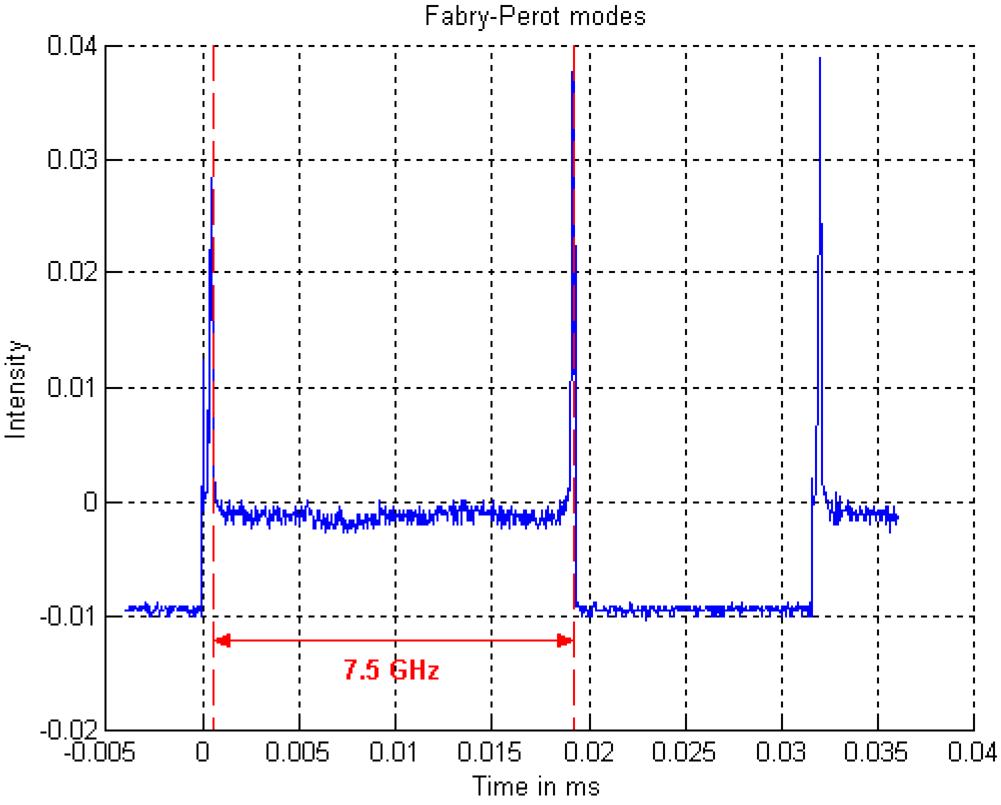

Figure 16 *Fabry-Perot modes of the spectrum analyzer. The free spectral range is 7.5 GHz and is used as the reference in the calculation of the separation between the two longitudinal modes of the fundamental beam.*

Assuming that the fundamental beam is composed of two longitudinal modes the energy distribution measured between the three SH modes can be compared to what is expected [15]. Indeed the efficiency is linked to the relative power of the two fundamental modes and should be maximum for two modes of same amplitude. Furthermore it is possible to deduce under certain assumptions[8] the relative power of the two fundamental modes from the efficiency and then the relative power of the three different modes observed in the SH beam. On Figure 17 the relative power of the three different SH modes is plotted versus the efficiency (it seems there are only two curves but as the process is symmetric the curve of the relative power of the modes $2f_1$ and $2f_2$ are superimposed). The experimental results show the relative power of the three different SH modes measured for different values of the efficiency.

---

[8] These assumptions are that the two longitudinal modes are uncorrelated and that the conversion efficiency is the same for both modes (the modes separation is small compared to the wavelength bandwidth of the conversion)

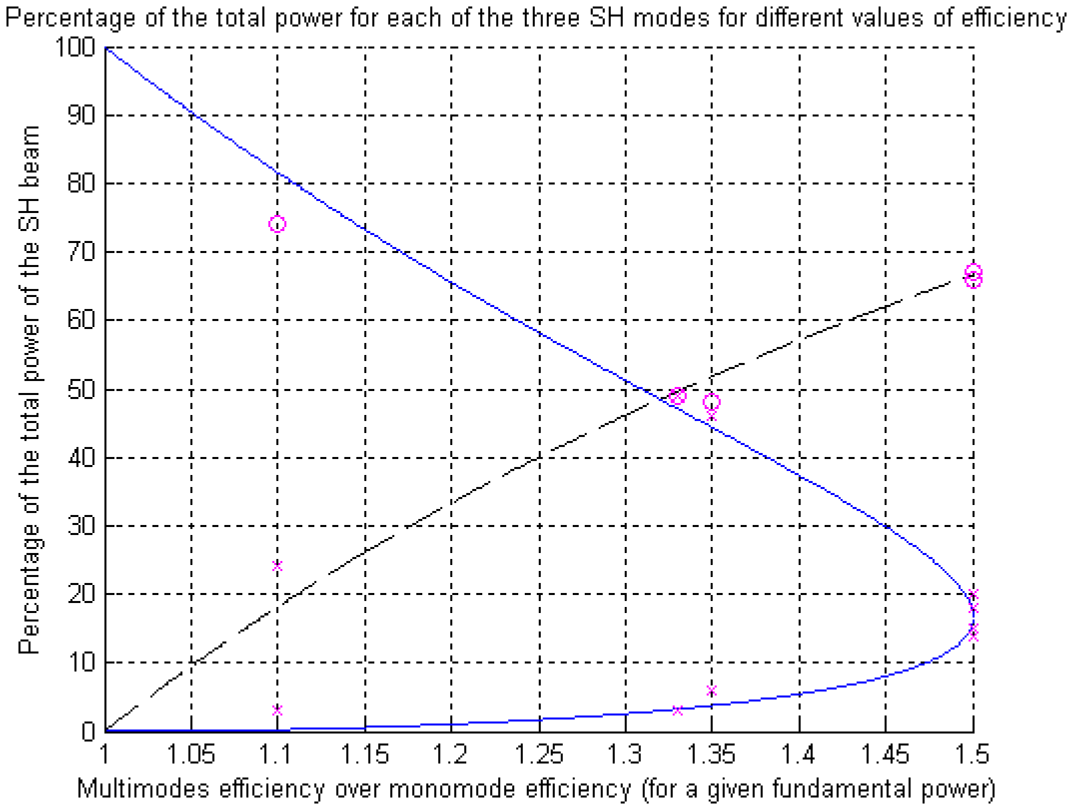

Figure 17 *Relative power of the three SH modes as a function of the efficiency.The blue curve represents the relative power of the modes at frequencies 2*f_1* and 2*f_2*. The black dashed curve is the relative power of the mode at frequency* f_1+f_2*. For a given efficiency the circle represents the measured relative power of the central peak (mode* f_1+f_2*) and the crosses the measured relative power of the modes 2*f_1* and 2*f_2*.*

The measured points are all along the curve except for the efficiency of 1.1. Nevertheless for this efficiency it is difficult to choose where is the third mode because it is faint and hidden by the noise. On the Figure 17 the third mode for this efficiency has been considered on the right of the two main peaks but it is possible that the mode was in fact on the other side which means that the circle and the upper cross should be inverted on the graph giving a result closer to what is expected. Finally, the model of a fundamental beam composed of two uncorrelated longitudinal modes whose separation is small compared to the wavelength bandwidth of the efficiency seems to correspond with our system during the mode hops.

Table 5 *Power distribution over the different longitudinal modes in the fundamental beam and in the SH beam. In the experimental setup the SH beam was splitted in two beams, one was directed to a spectrum analyzer to determine the distribution of power over the three modes and the second was directed to a power meter to calculate the efficiency. For a given IR configuration the theoretical SH beam is given along with an experimental result close to what is predicted by the theory.*

IR	SH (theory)	SH (observed)
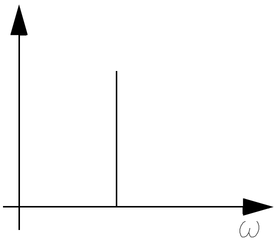 $p_{\omega 1}=100\%$ $p_{\omega 2}=0\%$	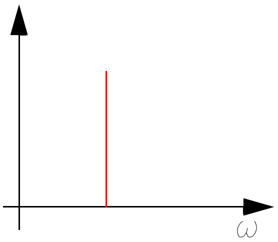 $p_{2\omega 1}=100\%$ efficiency=1	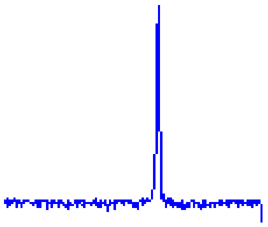 $p_{2\omega 1}=100\%$ efficiency=1
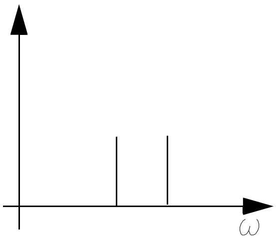 $p_{\omega 1}=50\%$ $p_{\omega 2}=50\%$	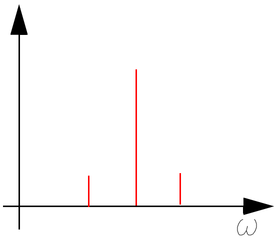 $p_{2\omega 1}=16.7\%$ $p_{\omega 1+\omega 2}=66.7\%$ $p_{2\omega 2}=16.7\%$ efficiency=1.5	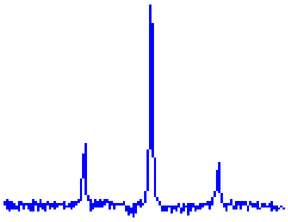 $p_{2\omega 1}=19.9\%$ $p_{\omega 1+\omega 2}=67.8\%$ $p_{2\omega 2}=13.1\%$ efficiency=1.58
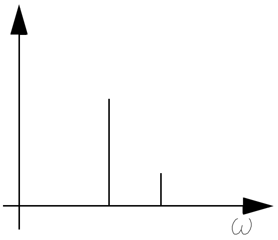 $p_{\omega 1}=80\%$ $p_{\omega 2}=20\%$	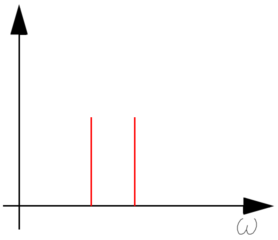 $p_{2\omega 1}=48.5\%$ $p_{\omega 1+\omega 2}=48.5\%$ $p_{2\omega 2}=3\%$ efficiency=1.32	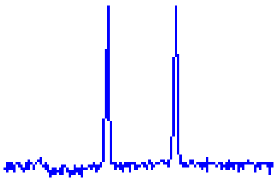 $p_{2\omega 1}=50\%$ $p_{\omega 1+\omega 2}=50\%$ $p_{2\omega 2}\sim 0\%$ efficiency=1.33

2.2.4 Optical quality of the output beam

As illustrated in Fig. 25, a possible configuration for the SHG of the PRIMA metrology laser consists in launching the full IR power into the doubling crystal to maximize the conversion efficiency. In this case, the fundamental and SH beams must be separated after the crystal by a dichroic mirror. Then the fundamental beam needs to be re-injected into a single-mode, polarization maintaining fiber to be further used by the PRIMA Metrology system.

Obviously, the optical quality of the IR beam after SHG will have an impact on the fiber coupling efficiency, and consequently on the amount of IR power available for the PRIMA Metrology.

2.2.4.1 Intensity spatial distribution and wavefront error

The wavefront error and the intensity distribution of the red SH beam (659.5nm) after the SHG have been measured with a HASO 50 wavefront sensor. It is assumed that the IR beam intensity distribution and wavefront error are identical for both the fundamental IR beam and the red SH.

The pupil size during the measurement was 6mm. The effect of tilt and defocus were removed. Figure 18 shows the wavefront error in radian on the upper graph and the intensity distribution in arbitrary units on the other graph. The optimum lens to focus a collimated beam of 6mm diameter into the SM-PM fiber (9µm core diameter, NA=0.11) has a focal length f=30mm. The coupling efficiency was simulated using this lens, the measured intensity distribution and the measured wavefront error as parameters. The result of the simulation shows that a coupling efficiency of approximately 60% should be reached.

The best coupling efficiency obtained is only 10%! Such a difference between the simulation and the experimental results might come from the optical quality of the focusing optics, from a non perfect matching of the beam size and of the NA and from the validity of the assumptions above (similar intensity distribution and wavefront error for both IR and SH beams).

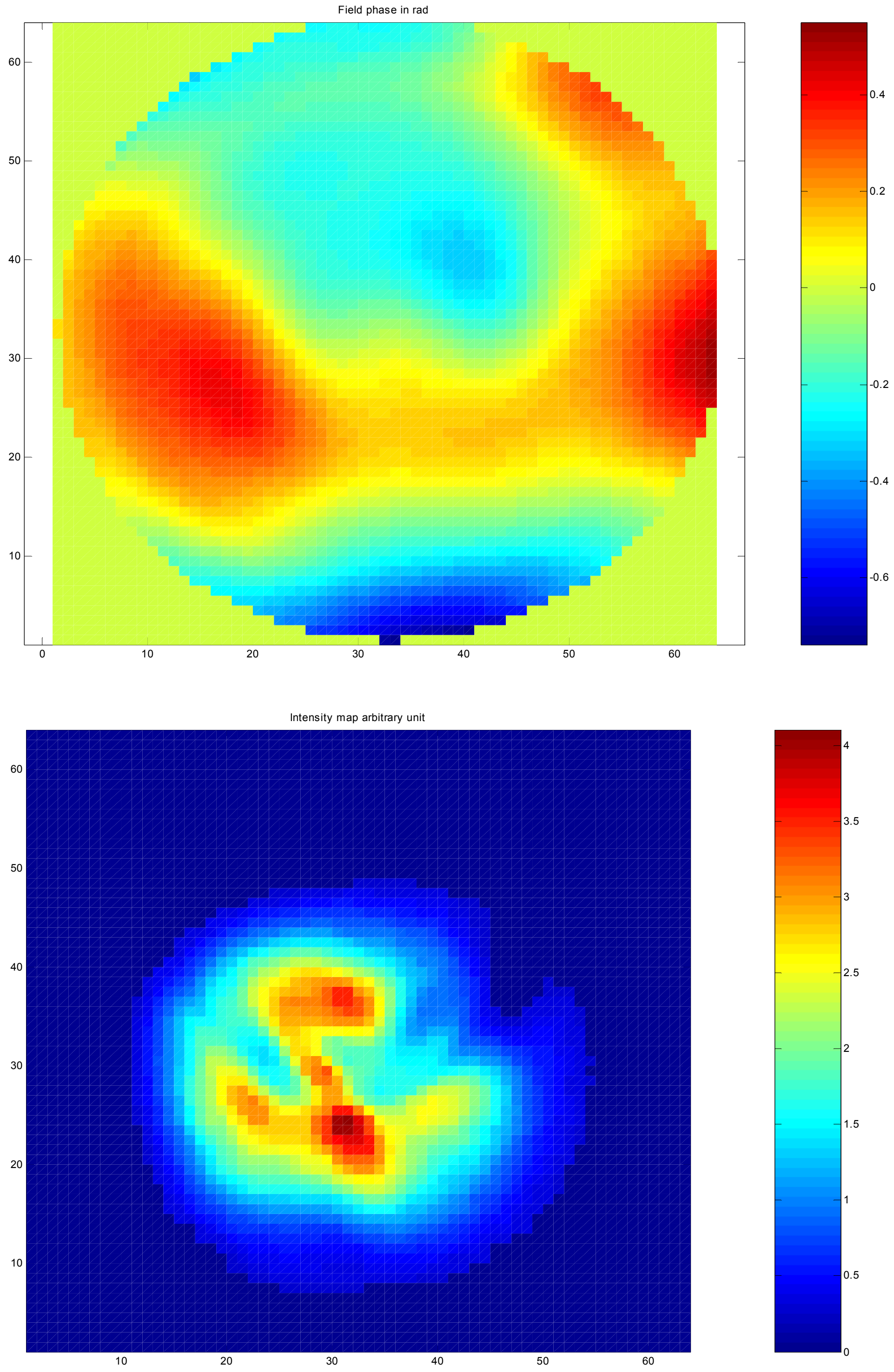

Figure 18 .Wavefront error and intensity distribution of the red beam after the SHG. The wavefront error is given radian whereas the intensity distribution is given in arbitrary units.

2.2.4.2 Polarization state of the IR beam after SHG

The Nd-Yag laser is linearly polarized with a specified extinction ratio at the output of its fibers of than less -20dB. We analysed the extinction ratio of the IR beam after propagation through the focusing lens, the PPKTP crystal and a dichroic mirror described in APPENDIX G. The measured extinction ratio was approximately -19dB.

This indicates that the crystal does not significantly affect the polarization state of the fundamental beam or at least maintain a polarization state compatible with the use of the IR beam in the PRIMA Metrology optical path.

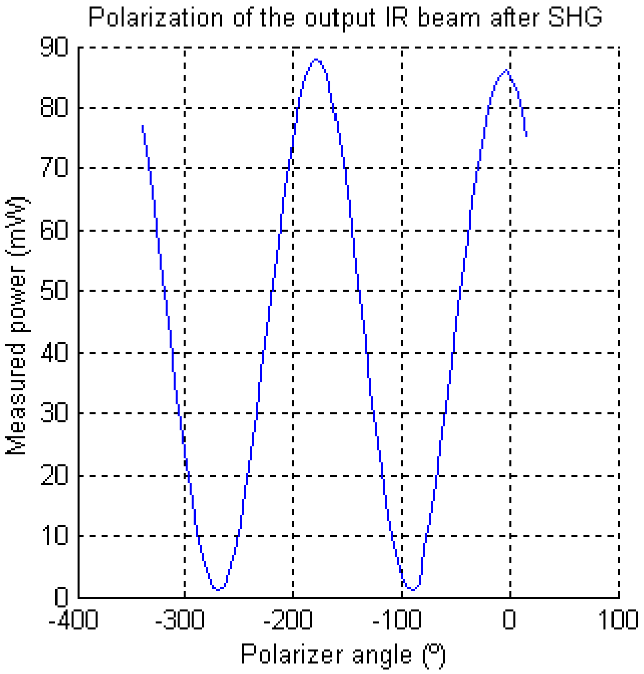

Figure 19 Polarization of the output IR beam after SHG.The extinction ratio is approximately -19dB for the whole system.

2.3 Experimental results using a PPKTP waveguide

The advantage of a waveguide doubling crystal is that the fundamental wave is confined into the waveguide structure, which allows to reach a theoretical conversion efficiency of about 10%/W/cm for PPKTP. This means that 4mW of SH could be obtained for a 200mW fundamental beam coupled into a 1cm waveguide PPKTP. This represents a gain of a factor 30 compared to the 137.6µW expected for bulk PPKTP, as shown in Table 1.

Manufacturing a waveguide doubling crystal requires to design a specific mask and the cost of a dedicated manufacturing run can reach up to 35000$. However, we obtained a PPKTP waveguide from Advr which was manufactured in parallel with another manufacturing batch. The cost of such a waveguide was reduced to 2500$.

2.3.1 Experimental set-up

2.3.1.1 Optical set-up

The main challenge in using a PPKTP waveguide is to obtain a good coupling efficiency. The fundamental beam must be focused on the waveguide such that its Numerical Aperture is smaller than the NA of the waveguide and simultaneously the diameter of the focused spot must be smaller than the cross-section of the waveguide. It is actually difficult to achieve at the same time both conditions considering that the cross-section of the waveguide that we used is only 4x4 μm^2 and its numerical aperture is approximately 0.2 (see details in section2.3.1.2). Indeed a small spot requires a focusing lens with a short focal length but such a lens will increase the N.A of the fundamental beam. In this case, the waveguide must be also physically located very close from the lens which makes the alignment more difficult.

The optical set-up consists of a fiber port with a f=11mm lens which collimates the IR Nd-Yag laser in a 2.1mm beam. This beam is then focused by a f=10mm lens in a ~15µm spot on the waveguide input. Nevertheless even with such a large spot coupling remains difficult because we cannot check visually if the position of the IR spot coincides with the waveguide input. As a consequence a visible beam emitted by a laser diode is superimposed with the IR one to ease the coupling process. The red beam is first coupled in a waveguide, no matter which one. A microscope is mounted on top of the chip to display the output face of the chip where a bright red spot should appear. The chip is then translated to couple the red beam into the desired waveguide. In the microscope one can see the red spot jumping from a waveguide to an other (it is sometimes necessary to correct the height of the chip to get the brightest spot). Once the red beam is coupled into the desired waveguide, one can turn the laser diode off and turn the Nd:YAG laser on. In principle, only a small correction is required to couple the IR beam and observe its SH at the output of the waveguide. However, the mechanical stability of the set-up is a critical aspect required to maintain a stable coupling efficiency

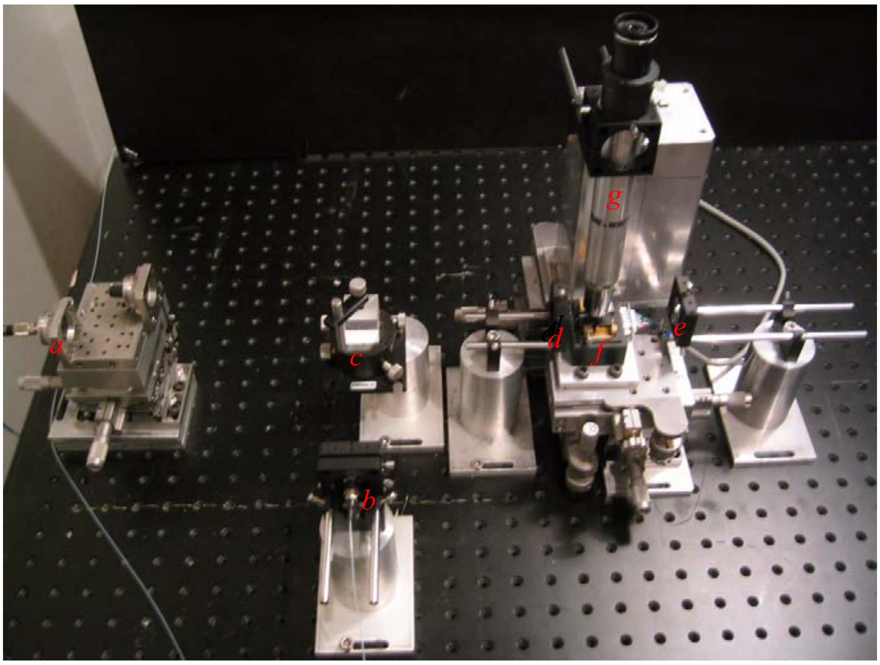

Figure 20 *Optical set-up for SHG with PPKTP waveguide. The IR beam is provided by a fiber coupled Nd:YAG laser (a) and the red probe beam by a fiber coupled laser diode (b). A cube beamsplitter (c) is used to superimposed both beams. The beams are then focused on the input face of the chip with a 10mm long focal length lens (d). A 60mm long focal length lens is used to focus the output beam on the photometer sensor (e). The chip containing the PPKTP waveguide is hold in an oven (f). A microscope is used to watch the waveguides and their output (g).*

2.3.1.2 PPKTP waveguide

The tests on SHG with PPKTP waveguide have been made on a chip from AdvR (specifications in Table 6). 12 groups of 3 to 9 waveguides are located on the chip. Almost all of them are designed for SHG but for different wavelengths. AdvR indicated us that two waveguides, group 9 waveguides 3 and 4, should provide SH at 80 °C and 35 °C respectively for a fundamental at 1.319μm. The layout of the chip is shown on Figure 21.

Table 6 *Specifications of the PPKTP waveguides chip*

Parameters	**Specifications**
Material	PPKTP
Application	SHG
Dimensions	1x3x10 mm^3
Waveguides for SHG @ 1.319μm	9.3 at ~80 °C 9.4 at ~35 °C
Poling period	16.1-16.7 μm

Parameters	Specifications
Waveguide dimensions	4x4 µm^2
Waveguide Numerical Aperture	~0.2
Manufacturer/ Price	AdvR/ 2500$

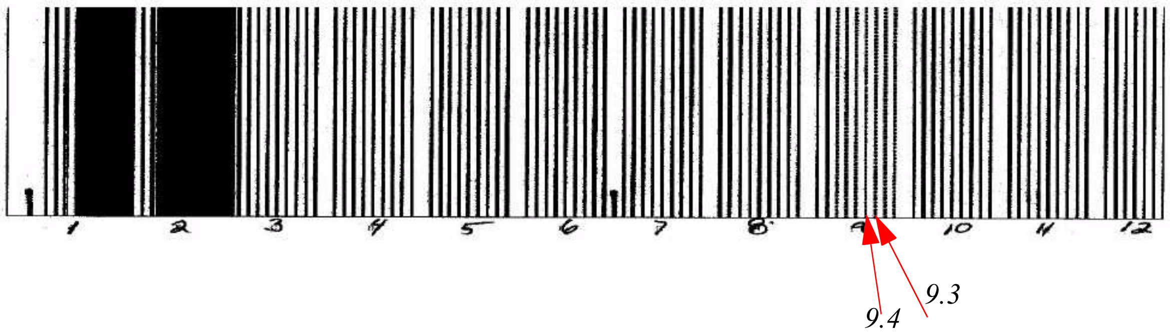

Figure 21 Waveguide chip layout. 12 groups of 3 to 9 waveguides are on the chip. AdvR indicated that waveguides 9.3 and 9.4 could provide SHG at 1319nm.

2.3.1.3 Oven and temperature controller

The system used is the same as for the bulk crystal (see 2.2.1.3).

2.3.2 Coupling efficiency

The best coupling efficiency achieved by AdvR was about 10%. In our case the efficiency could hardly be of the same order because the mechanical stability of the set-up was not good enough to possibly maintain a stable coupling efficiency.

2.3.3 Tuning and tolerances

Like in SHG with bulk crystal the conversion efficiency is function of different parameters. Unfortunately, the mechanical instability of the set-up did not allow to measure both the wavelength and the temperature dependence. As the coupling efficiency kept varying during the experiment because of the mechanical instability, it was impossible to deduce the contribution of the other parameters.

Considering that the matching of the NA is essential to obtain a good coupling efficiency, angle tuning cannot be practically implemented to optimize SHG.

As for bulk PPKTP (see section 2.2.3.5), we observed that the SH efficiency of the waveguide increased due to the number of longitudinal modes in the fundamental beam.

2.3.4 Optical quality of the IR Output beam

Figure 22 shows the intensity distribution of the IR spot at the output of the waveguide using the set-up described in 2.3.1.1. The beam quality is not better than what was obtained with the bulk PPKTP: The intensity spatial distribution is significantly uneven. Because of the mechanical instability of the set-up, the wavefront quality of the beams after SHG could not be measured. Nevertheless one can conclude that re-coupling the IR beam after SHG into a single mode fiber as illustrated in Fig. 25 should be very inefficient.

Figure 22 *IR spot after SHG with PPKTP waveguide.The spot was made visible on an IR viewing card. The picture has been taken 6cm after the chip and the spot is a bit smaller than 2cm. The faint details are not visible on this picture.*

2.4 Conclusion on the second harmonic generation

The absolute frequency stabilization of the laser of the PRIMA Metrology system is based on Second Harmonic Generation and frequency locking on an absorption line of iodine near 659.5 nm.

Second Harmonic Generation can be achieved using variety of nonlinear crystals (such as KTP or LiNbO3) where two types of phase matching can be implemented:

- Critical Phase Matching, CPM (also referred as birefringent phase matching)
- Quasi Phase Matching,QPM, obtained by manufacturing a Periodically Poled (PP) structure inside the crystal.

As detailed in the theoretical analysis of this part, QPM should provide a conversion efficiency of more than 3 times higher than CPM for KTP and more than 20 times higher than CPM for LiNbO3.

In addition, a Periodically Poled structure can be confined in a waveguide to further increase the conversion efficiency. However this manufacturing process remains in general expensive.

We also showed that the parameters affecting the conversion efficiency in QPM using PPKTP can be easily controlled.

Experimental results were presented to evaluate the performance of a bulk and a waveguide Periodically Poled KTP, for the second harmonic generation of a 1319nm Nd-Yag laser. Using bulk

PPKTP and a 200mW fundamental beam, 64µW could be converted at 659.5 nm. Figure 23 summarizes the theoretical and measured conversions obtained as function of the fundamental power.

Unfortunately, we could not obtain any useful conversion efficiency with our waveguide PPKTP, partially because the mechanical stability of the set-up was not good enough to possibly maintain a stable coupling efficiency of the fundamental beam in the waveguide. From a practical point of view the implementation of SHG with a waveguide is clearly more difficult than with a bulk crystal. It requires a precisely aligned and highly stable set-up as well as a tedious alignment procedure, both increasing the overall cost and maintenance constrains.

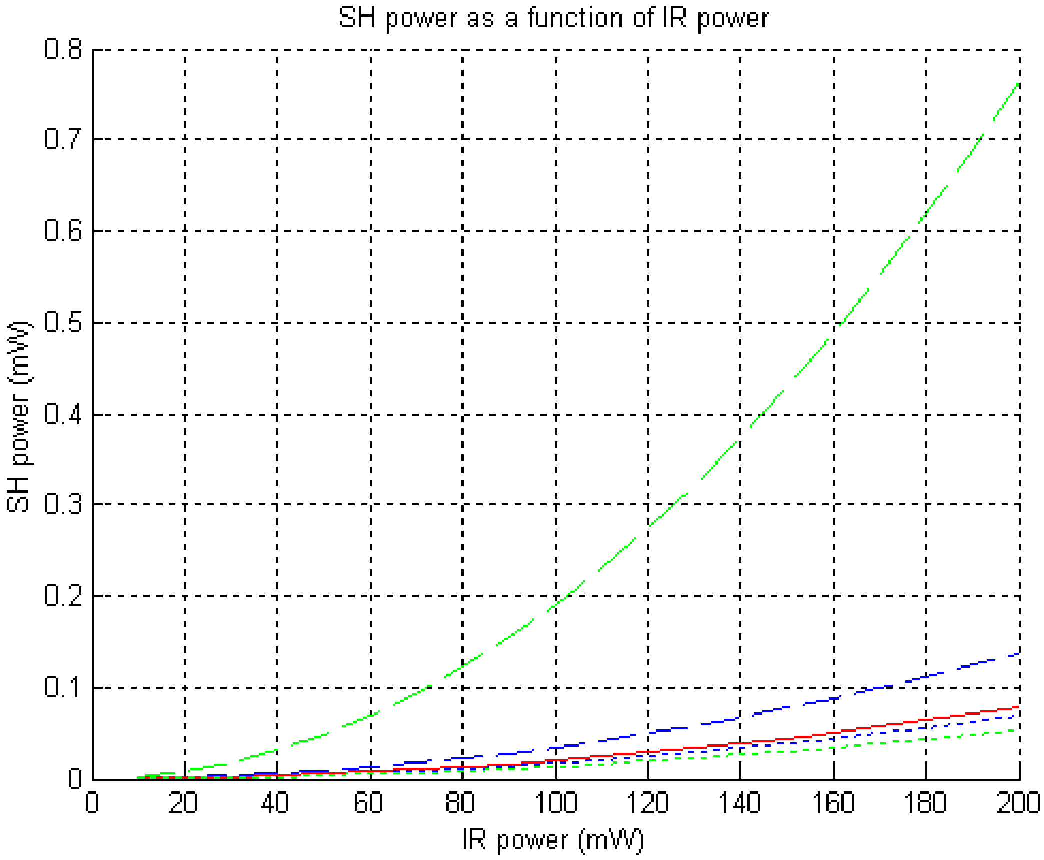

Figure 23 *Power of SH as a function of the incident IR power. The blue curves correspond to the theoretical conversion for KTP and the green curves for LiNbO3. CPM is plotted in dotted lines and QPM in dashed lines. The experimental results for PPKTP are plotted in red.*

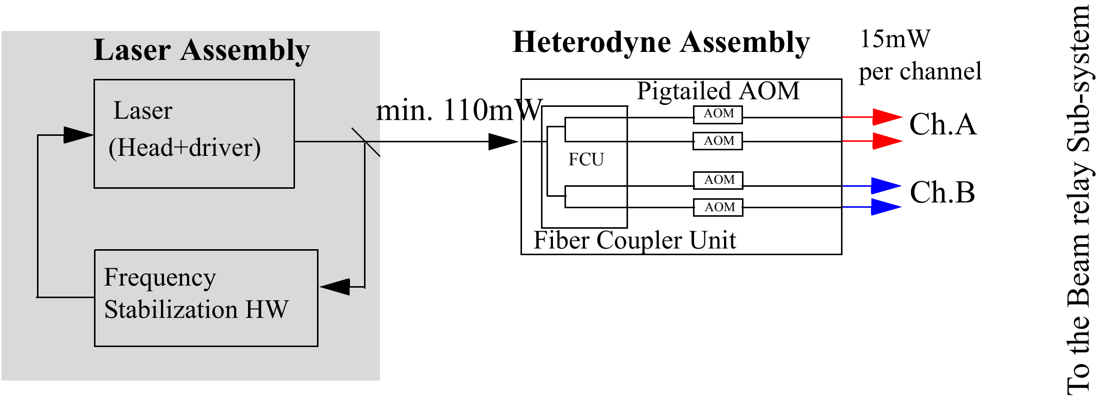

Figure 24 *Block diagram of the Light Source System of the PRIMA Metrology, including the Laser and Heterodyne Assemblies. A minimum of 110 mW at 1319 nm must output the laser assembly.*

The SHG is part of the frequency stabilization hardware which is a sub-system of the PRIMA metrology laser assembly, as shown in Figure 24. The laser assembly must be designed such that at least 110mW of the 1319nm Nd-Yag can be fed to the Heterodyne assembly. The baseline is to use the fiber pigtailed Nd-Yag laser, model 125 from lighwave, with an output power of 200mW.

Depending on the SH conversion efficiency, two types of optical configuration can be implemented as shown in Figure 25.

Configuration 1 consists in launching the full IR power into the doubling crystal to maximize the conversion efficiency. In this case, the fundamental and SH beams must be separated after the crystal by a dichroic mirror. Then the fundamental beam needs to be re-injected into a single-mode, polarization maintaining fiber to be forwarded to the Heterodyne assembly.

Configuration 2 consists in splitting a portion of the laser beam and redirect it towards the doubling crystal whereas the rest of the laser beam is directly transmitted towards the Heterodyne assembly. In this case, the conversion efficiency will be lower but the overall set-up is simpler, easier to align and can be better maintained.

The selection between these configurations depends on the initial laser power available (baseline 200mW), the IR power required at the input of the Fiber Coupler Unit (110mW) as well as SH power required for frequency stabilization (minimum 300nW as shown in [1]).

In configuration 1, 64µW can be converted into a 659.5 nm beam, based on the measured SHG with PPKTP. Considering the transmission factors shown in Figure 25, 29µW would reach the detector which is significantly larger than the required 300nW. However, at least 55% of the fundamental beam must be re-injected into a fiber such that 110 mW reaches the Heterodyne assembly. Although, the optical quality of the beam after SHG should be compatible with this value (see section 2.2.4.1), we only obtained 10% experimentaly. Even if we replace the laser head by the most powerful of its serie (350 mW), we would still not have enough IR power for the Heterodyne assembly.

In configuration 2, we first ensure that enough IR power reaches the heterodyne assembly. A 75/25 fiber coupler provides 150mW towards the Heterodyne assembly, whereas 50mW are available for SHG. From this 50mW fundamental beam, 4 µW should be converted into a 659.5nm beam, and finally 1.7µW should reach the detector. This represent more than 5 times what is required. In addition the conversion efficiency can still be increased either by changing the ratio of the fiber coupler or by using $PPLiNbO_3$ instead of PPKTP.

Therefore configuration 2 should be used as a baseline for the design of the frequency stabilisation of the PRIMA metrology laser.

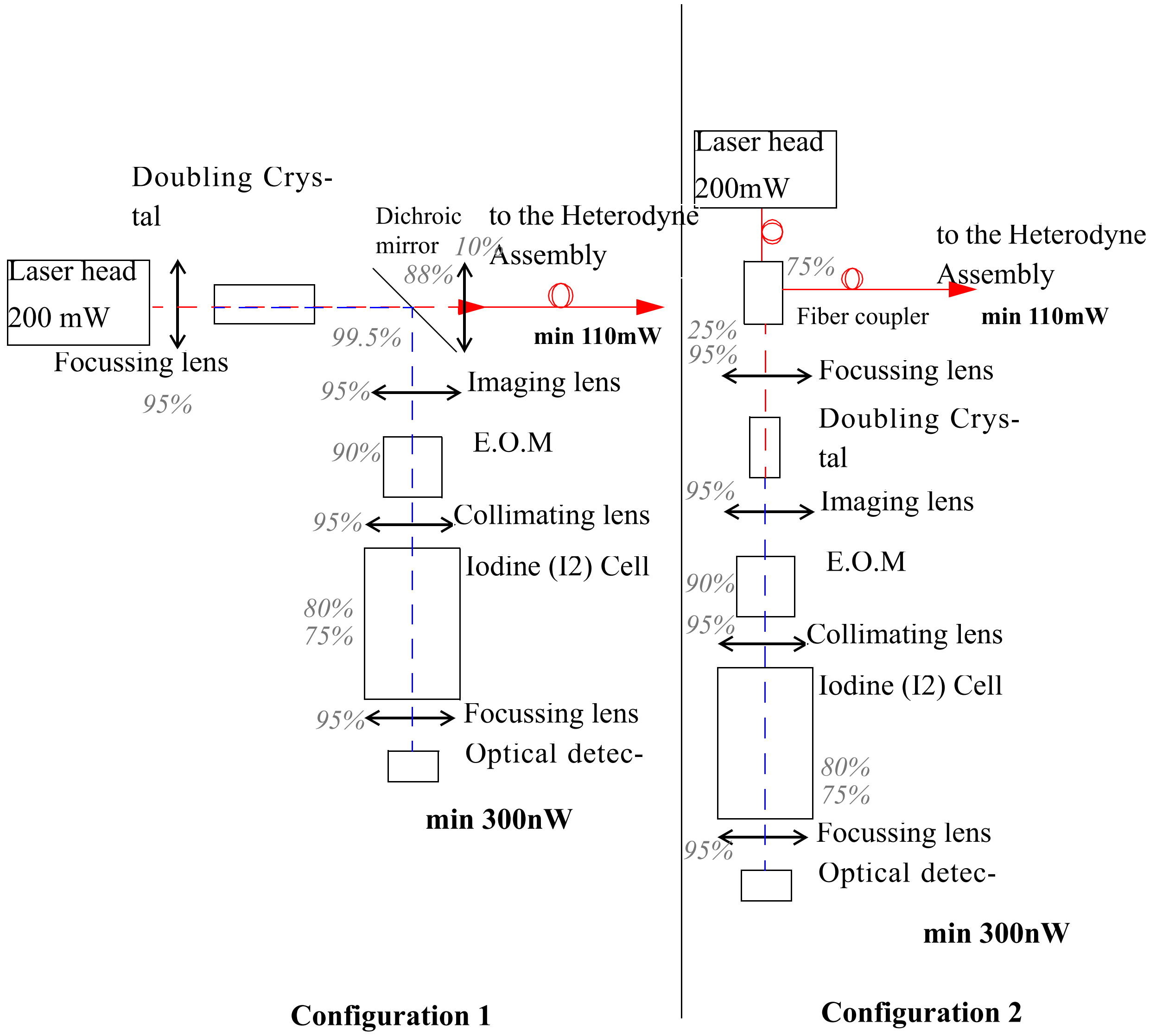

Figure 25 *Two possible hardware configurations for PRIMA laser stabilization. The dash lines represent the optical path.The transmitivity of each element is written in gray.The transmitivity of the EOM are based on the New Focus specifications plus a security margin. The two values of transmitivity for the* I_2 *cell correspond to the loss due to the windows (20%, measured on a cell furnished by ISSI) and to the maximum absorption of the transition (~25%).*

3 Characterization of the iodine transitions around 659.5nm

As explained in 1.3, the stabilization sheme chosen for the PRIMA Metrology System laser is based on the work done by Arie to stabilize a NPRO Nd:YAG laser emitting at 1.319µm [7]. This requires in particular that an I_2 absorption line of tipically 25% depth must be reached within the frequency tuning range of the laser.

The first section will establish the tuning range and the tuning characteristics of the Nd:YAG Lightwave Model 125 (serial number 597).

Then it presents the first results of iodine spectroscopy showing that exploitable transitions can be reached with this laser. The pressure sensitivity of the linedepth is also studied.

Finally specifications for the iodine cells are deduced from the previous results.

3.1 Frequency tuning of the Lihgtwave Model 125

With the NPRO Nd:YAG laser the frequency can be modified either by adjusting the *temperature* of the laser resonator (NPRO crystal) or by applying a *stress* on the laser crystal using a piezo. Both schemes expand or contract the laser cavity but with a different range and a different bandwidth.

The temperature of the laser's crystal can be changed in two ways: by manually tuning the front panel knob of the laser driver or by applying a voltage on the so called "slow input", of the laser power supply. The tuning characteristics of the slow input given by the manufacturer are:

- Tuning coefficient: 3.8 GHz/V (Typical between mode hops)
- Range: 10GHz (continuous range between mode hops); 30GHz (total tuning range)
- maximum input voltage: ±10V
- Bandwidth: 1Hz

The stress is applied to the laser'scrystal is controlled by the voltage send to the *piezo* actuator on the so called "fast input" of the laser driver. The tuning characteristics of the fast input given by the manufacturer are:

- Tuning coefficient: 1.9 MHz/V (Typical)
- Range: 30MHz (for a voltage input range of ±15V)
- Bandwidth: 30kHz

3.1.1 Experimental set-up for the test of frequency tunability

3.1.1.1 Set-up

To test the frequency tuning one need to monitor the emitted wavelength. For this purpose a wavemeter is used (Burleigh WA-1500 WAVEMETER). The only available wavemeter for this experiment was working in the visible which implied that the IR wavelength emitted by the laser could not be directly measured. The SH was first generated to get a beam around 659.5 nm (i.e

1319nm/2). The conversion is done in a PPKTP crystal heated to get a maximal conversion efficiency. The SH beam is refocused after the crystal to enter the wavemeter.

The emitted frequency is tuned by applying a voltage on one of the two inputs of the laser driver.

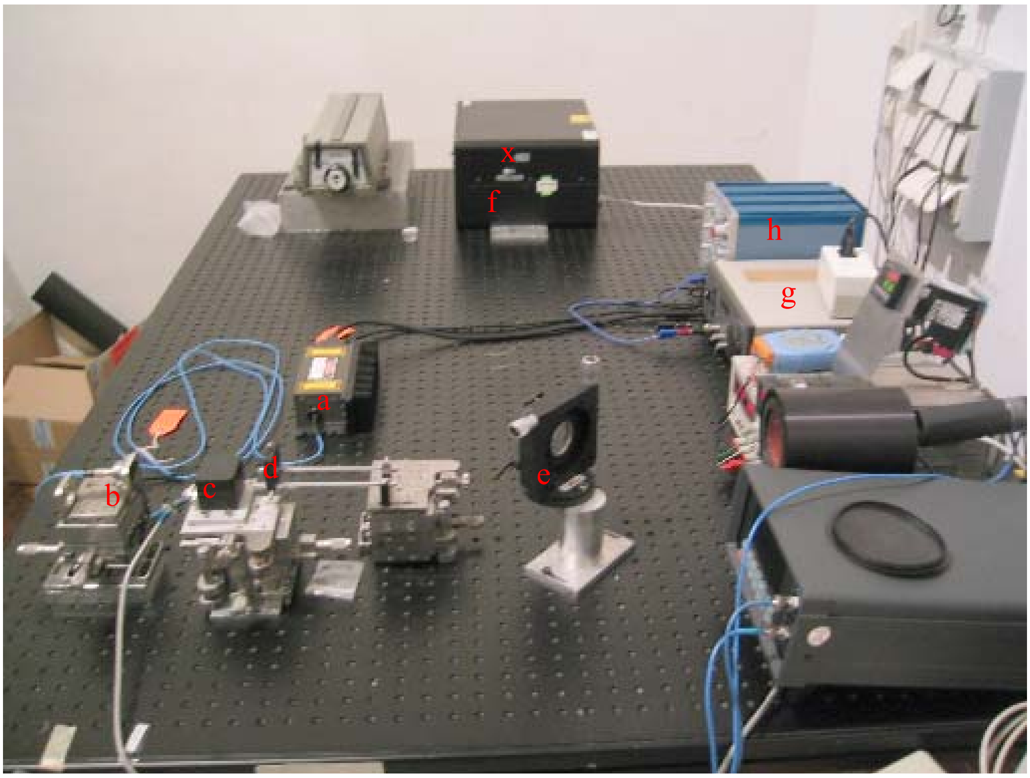

Figure 26 *Experimental set-up for the characterization of the frequency tuning of the Lightwave no 125.(a) NPRO Nd:YAG laser head. (b) fiber port + focusing lens*[1] *(11mm focal length). (c) PPKTP crystal*[2]*+oven*[3]*. (d) 50mm focal length lens. (e) beamsplitter. (f) Wavemeter*[4] *(x marks the free beam input). (g) Laser microprocessor-based power supply. (h) Voltage generator linked to the fast input of the power supply.*

1. OFR PAF-X-11-1319
2. Raicol Crystal (crystal dimensions 10x5x1mm^3)
3. HC Photonics
4. Burleigh WA-1500 wavemeter

3.1.1.2 Burleigh WA-1500 Wavemeter

The wavemeter has an absolute accuracy of $\delta\nu/\nu<10^{-7}$ ($\delta\nu=\pm45$MHz). The measurements are displayed with a resolution of 0.0001 nm which corresponds to about 70 MHz at 659.5 nm. The wavelength value can be displayed in vacuum or in the air. Only the vacuum values were used. The studied beam intensity should be at least 20µW (all our measurements have been done with approximately 40µW).

The wavemeter is described more precisely in APPENDIX F.

3.1.2 Frequency tuning by changing the temperature of the laser's resonator

One way of shifting the frequency is to change the temperature of the laser's crystal to modify the length of the path in the crystal. This is due to the thermal expansion of the crystal and to the increase of the refractive index. On the Lightwave 125 laser this can be done by modifying the target crystal temperature on the power supply controller or by applying a voltage (maximum ±10V) in the “slow” input.

3.1.3 Frequency tuning with a piezo element

With the model 125 microprocessor-based power supply it is possible to chose the temperature of the crystal. It is a simple way of tuning the emitted frequency. The default target temperature of our laser is 50.8 ºC. The target temperature can be selected in a range of ± 30 ºC around the central temperature. This central temperature can be modified by the mean of a potentiometer on the back of the laser head.

The displayed target temperature is not a measured temperature, it is just the temperature selected by the user for the laser crystal. A temperature measured with a low resolution (±0.4 ºC) can be monitored too. The difference between these two temperatures increases with the difference between the default temperature and the target temperature.

The set-up presented previously has been used to determine the range of tuning and the tuning coefficient of the laser head. The target temperature has been shifted from 20.3 ºC to 80.8 ºC with a step of 1 ºC. For each step both the measured temperature and the emitted frequency are recorded. Figure 27 shows the wavelength in function of the target temperature and in function of the measured temperature. It should be noticed that even if the target temperature can be tuned on a total range of 60 ºC, the crystal temperature remains actually in a range of ±15 ºC around the default temperature. *The Target Crystal Temperature is a set point and not a monitor!* Five mode hops can be seen on the graphic. The mode average width is 28GHz. The factory default temperature (50.8 ºC) has been chosen so as the laser begins emitting in the middle of a mode. With the factory settings the laser can be tuned over five modes on 95.5 pm (~66 GHz) between 659.5852 nm and 659.6807 nm.

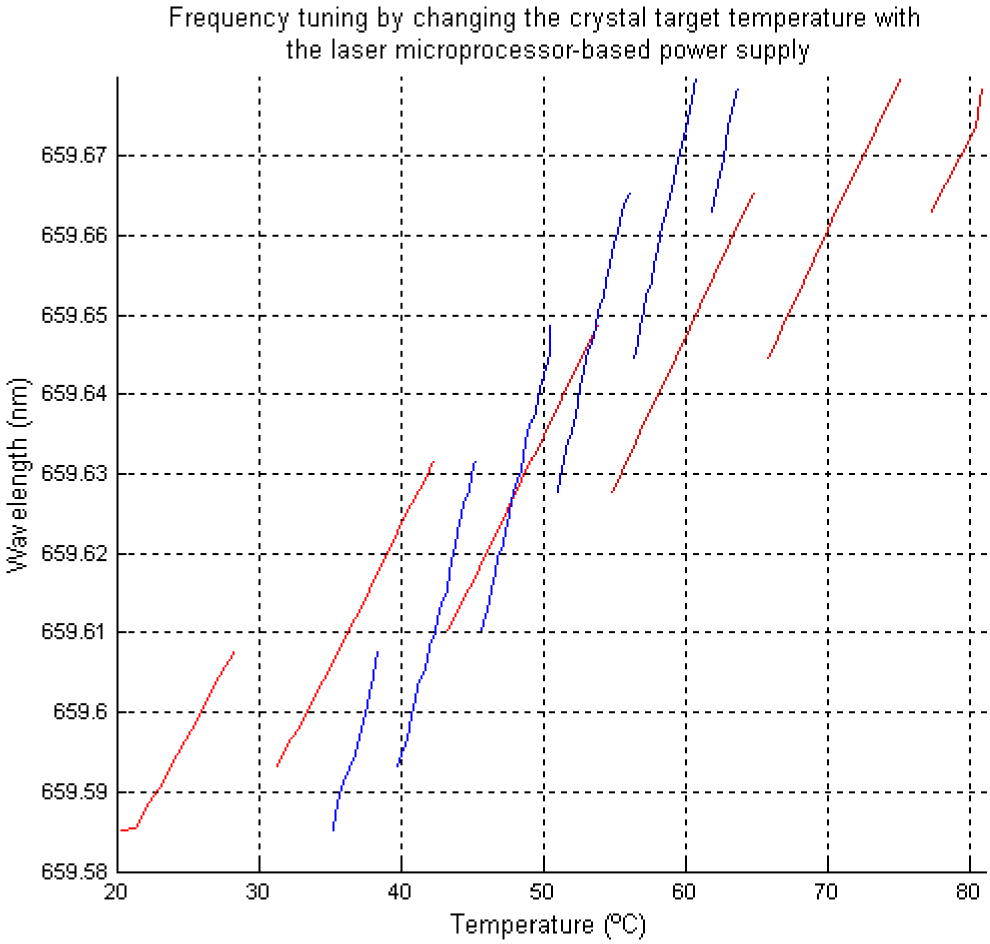

Figure 27 *Emitted wavelength of the laser as a function of the target and measured temperatures of the resonator. With the factory settings the laser frequency can be tuned over 95.5nm and five different longitudinal modes (average width of a mode 28 GHz). In blue the emitted wavelength is plotted versus the crystal measured temperature whereas in red the wavelength is plotted versus the crystal target temperature(selected by the user on the laser power supply, it is only a setpoint and not a monitor!).The blue curve lower quality is due to the poor resolution (0.4°C) of the measured temperature.*

The tuning coefficients deduced from this curve are (only the measured temperature is used):

- 7.80 pm/ºC (~5.4 GHz/ºC) in a mode;
- 3.29 pm/ºC (~2.26 GHz/ºC) over several modes.

3.1.4 Summary of the frequency tuning parameters of the Lightwave 125

Table 7 and Table 8 summarise the characteristics of frequency tuning with the Lightwave 125.

Table 7 *"slow input" tuning (temperature tuning) measured characteristics for the Lightwave 125*

"Slow input" (temperature tuning)	Measured λ=659.5nm	Measured λ=1319nm	Datasheet Lightwave λ=1319nm
within a mode	-5.4 GHz/ºC 5.17 GHz/V	-2.26 GHz/ºC 2.59 GHz/V	-2.4 GHz/ºC
over several modes	2.2 GHz/ºC -3.22 GHz/V	1.1 GHz/ºC -1.61 GHz/V	-1 GHz/ºC
Mode width	27 GHz	13.5 GHz	10 GHz
Total tuning range	66 GHz	33 GHz	30 GHz
Modulation rate			Hertz level

Table 8 *"fast input" (piezo tuning) characteristics given for the Lightwave 125. The frequency shift caused by the piezo is too small to be detected properly with the wavemeter. The characteristics given in the table were measured by Lightwave by generating a beatnote between this laser and an other Lightwave 125 measured with an HP 8591A Spectrum Analyzer.*

"fast input" (piezo tuning)	Lightwave Datasheet
10 V DC	1.9 MHz/V
10 V AC Peak to peak	2.45 MHz/V
Tuning range	until 30 MHz for low modulation rates (<10kHz)
Modulation rate	until 100 kHz for small depth of modulation

3.2 Iodine spectroscopy for the laser stabilization

3.2.1 Exprerimental set-up for iodine spectroscopy

The aim of this study is to determine if exploitable transitions are available in the tuning range of the laser. This is done by measuring the transmission spectrum of I_2. A glass cell (whose temperature is controlled with a precision of ±0.1 ºC) contains a bit of solid iodine. The pressure in the cell can be increased by increasing its temperature.

The first part of the set-up is dedicated to the generation of the SH. The laser fiber is connected to a fiber port on which is mounted a 11mm focal length lens (optimized for a wavelength of 1319nm) to focus the beam in the PPKTP crystal. The crystal is held in an oven whose temperature is controlled with a precision of ±0.1 ºC to get the best conversion rate. Just after the oven is mounted a 50mm focal length lens to refocus the SH beam into the 2mm diameter free beam input of the wavemeter. A beamsplitter is placed after the lens, the one meter long reflected arm goes directly to the wavemeter while the transmitted arm goes through the iodine cell to be finally measured by a photodetector. The iodine cell lent by ISSI is a permanently sealed cell (pressure 0.75 Torr at 43ºC). Arie used another type of cell on which the quantity of iodine in the cell can be increased by the used of a cold finger. Both types of cell are described in APPENDIX H. The whole set-up is presented in Figure 28 and Figure 29.

The absorption spectrum is obtained by scanning the frequency of the laser. The intensity is measured once per mode before the I_2 cell. Then for each step the intensity is measured behind the cell and the ratio of the two measurements gives the transmission of the cell (multiple reflections on the different dioptres) and of the gas.

$$I_{transmited} = t_{cell} \cdot t_{gas} \cdot I_{incident}$$

The gas absorption can then be deduced:

$$t_{gas} = \frac{I_{transmitted}}{I_{incident}} \cdot t_{cell}$$

The loss of energy due to the multiple reflections on the windows of the cell is about 18%.

As the laser intensity is stable enough (amplitude noise 0.022% rms) one can think it is possible to measure only once the incident intensity for every scanned longitudinal mode. Since the photometer has an input for the visible and an input for the IR a dichroic mirror is used to monitor the incident intensity all through the experiment. Indeed, the dichroic splits the beam in an IR beam and in a visible beam. However one knows that the intensity of the generated SH is proportional to the square of the fundamental intensity so that by monitoring the variation of the fundamental beam intensity it is possible to deduce the intensity fluctuation of the SH beam. This has showed that the intensity noise can be neglected and that the most significant cause of noise in the variation of the the measured transmitivity is due to the wavelentgh dependence of the SHG process. This noise can only be suppressed by measuring the intensity of the red beam before the cell more than once per scanned longitudinal mode.

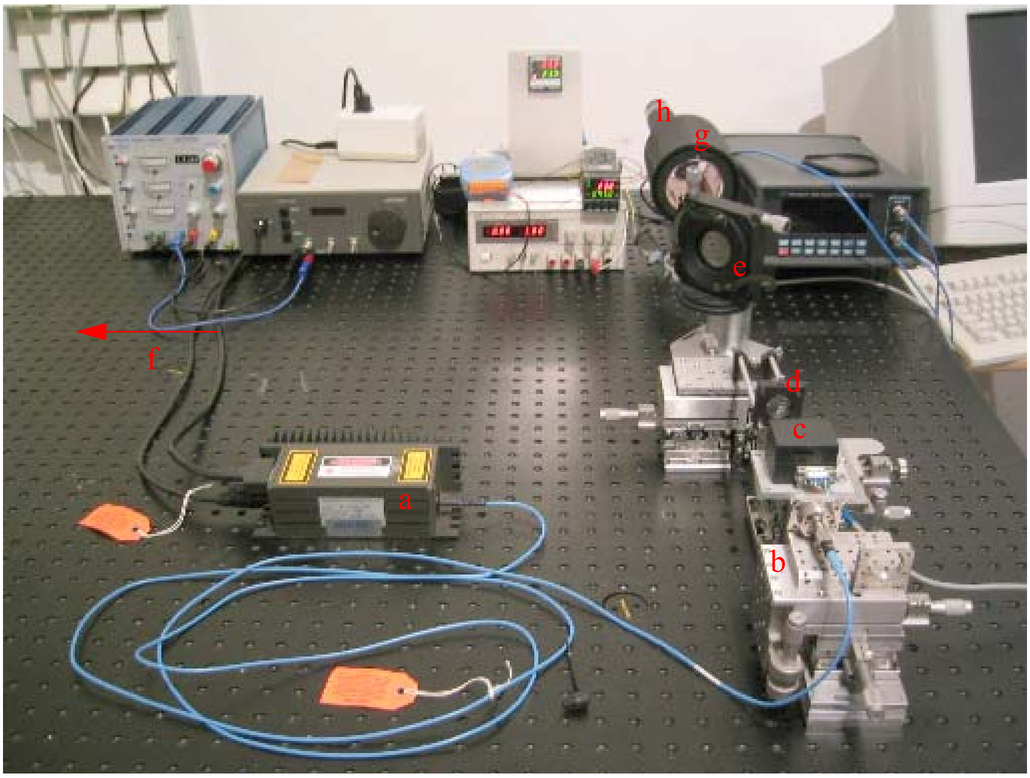

Figure 28 *Set up for the iodine spectroscopy. The NPRO Nd:YAG fiber-coupled laser*[1] *(a) emits an IR beam at 1.319 µm. This beam is focused by an 11mm focal length lens mounted in the fiber port*[2] *(b) to focus the beam in the PPKTP crystal*[3] *hold in the temperature regulated oven*[4] *(c). The generated SH beam is refocused by a 50mm focal length lens just before being separated in two shares by the beam splitter (e). The one meter long reflected arm (f) is superimposed with the probe laser beam coming from the wavemeter*[5] *to ensure a good alignment,i.e a good accuracy. The transmitted beam goes through the* I_2 *cell*[6] *(g) before hitting the photometer sensor (h). On the background can be seen the laser microprocessor-based power supply, the voltage generator used to tune the frequency, both temperature controllers for the PPKTP*[7] *and the* I_2 *cell*[8] *and the photometer.*

1. Innolight Model 125
2. OFR PAF-X-11-1319
3. Raicol (crystal dimensions 10x5x1mm^3)
4. HC Photonics oven
5. Burleigh WA-1500 wavemeter
6. ISSI 5 inches long iodine cell
7. Newport Omega CN77352-C4
8. Newport Omega CN76020

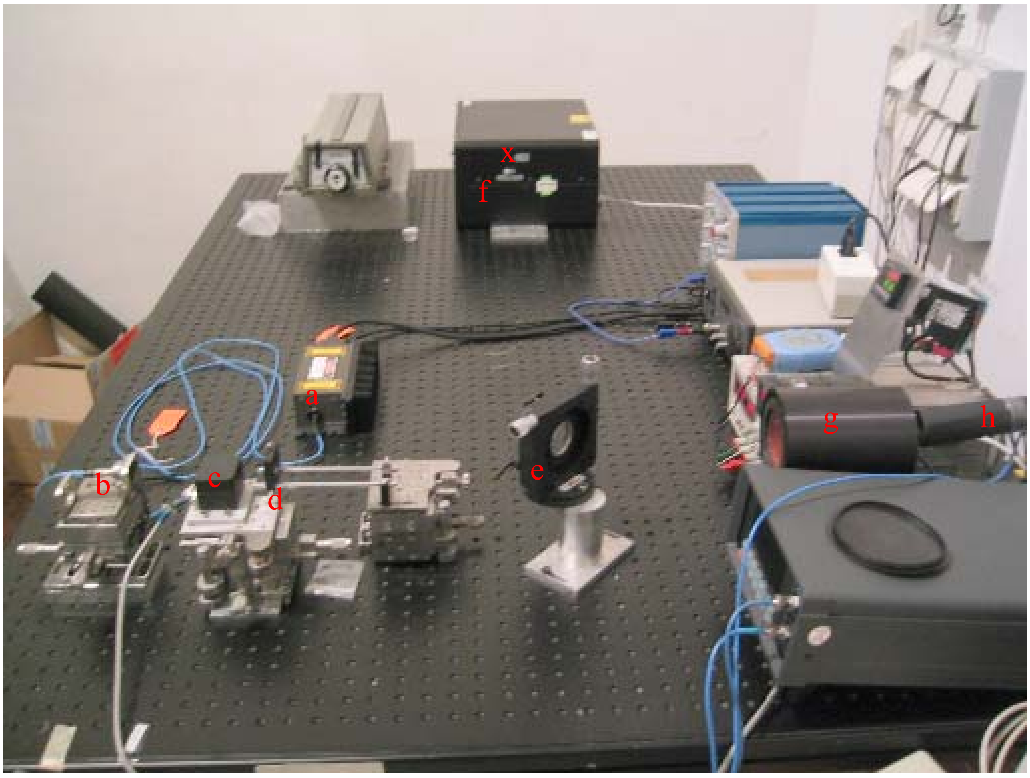

Figure 29 *Set-up for iodine spectroscopy. (a) NPRO Nd:YAG laser head. (b) fiber port + focusing lens (11mm focal length). (c) PPKTP crystal+oven. (d) 50mm focal length lens. (e) beamsplitter. (f) Wavemeter (x marks the free beam input). (g)* I_2 *cell (length:12.7cm). (h) Photometer sensor.*

3.2.2 Iodine spectroscopy

Figure 30 presents the transmission spectrum of I_2 for a cell temperature of 150 ºC and for several laser modes. It can be seen that with the factory settings the transitions described and used by Arie in [7] are not in the laser range. Nevertheless they can be reached by modifying the default crystal temperature (by the mean of a potentiometer located at the back of the laser head). This spectrum has been obtained by scanning different laser longitudinal modes with steps of 0.1V (slow input of the laser driver). For each step the wavelength and the intensity after the I_2 cell are measured. The transmitivity is obtained by dividing the intensity after the cell by the incident intensity measured once for each laser mode. These data are then corrected to take into account the loss due to the cell itself and not to the gas..

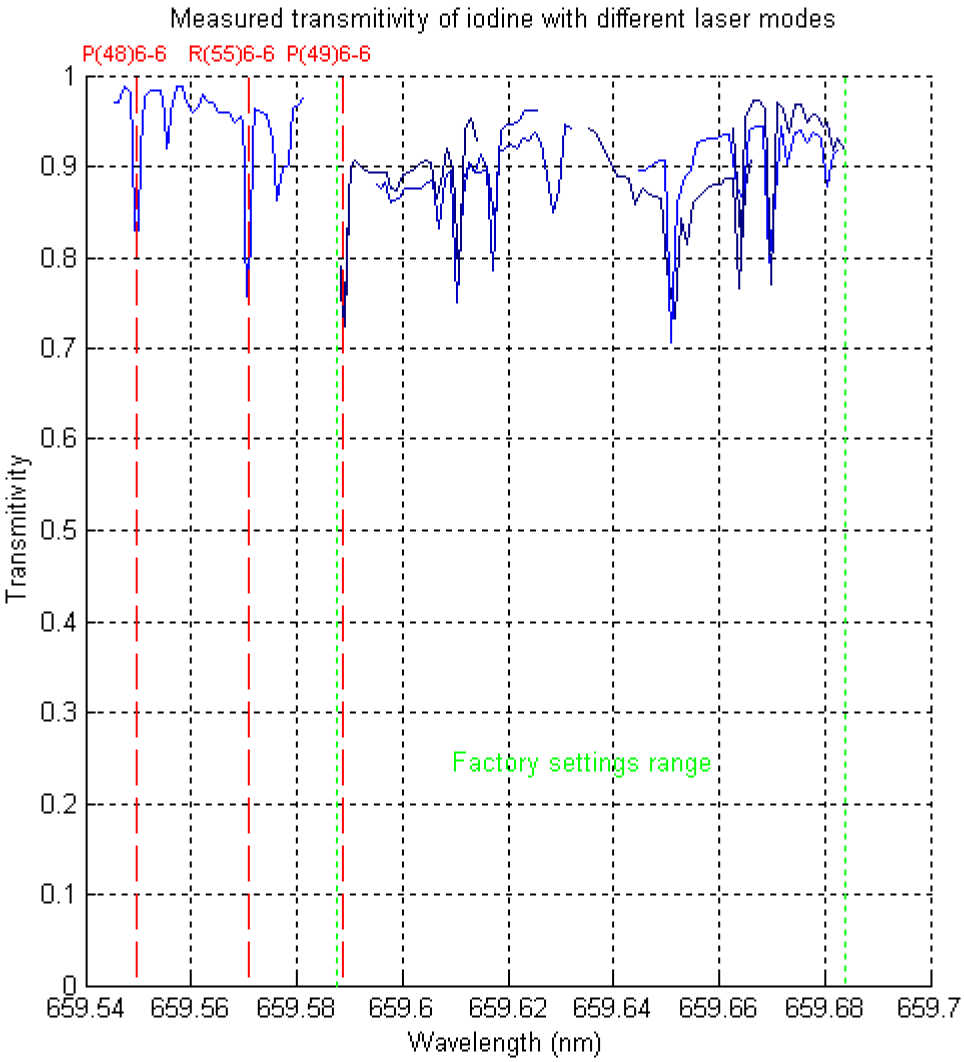

Figure 30 *Transmission spectrum of I_2 around 659.5nm. These data, deduced from the transmitivity of the I_2 cell, present the transmitivity of I_2 for different laser modes. In red are indicated 3 of the transitions studied by Arie [7].The two green lines delimit the tuning range of the laser when it is operated with the factory settings. The left side of the spectrum has been obtained by modifying the default crystal temperature setting of the laser head.Resolution ~820 MHz*

In Figure 30, each curve corresponds to a single longitudinal mode. The curve is not continuous beause during the mode hoping two are emitted at the same time. The global down translation of the spectrum is due to the difficulty of establishing precisely the part of the intensity loss caused by the cell only.

It has been decided to study more precisely the part of the spectrum already used by Arie. As a consequence, the left part of the spectrum of Figure 30 has been scanned more precisely around its transitions. The result is plotted in Figure 31.

The resolution is:

- between transitions: 820MHz (1.2pm, 0.1V in the “slow input”),
- within transitions: 70MHz (~0.1pm, 0.01V in the “slow input”).

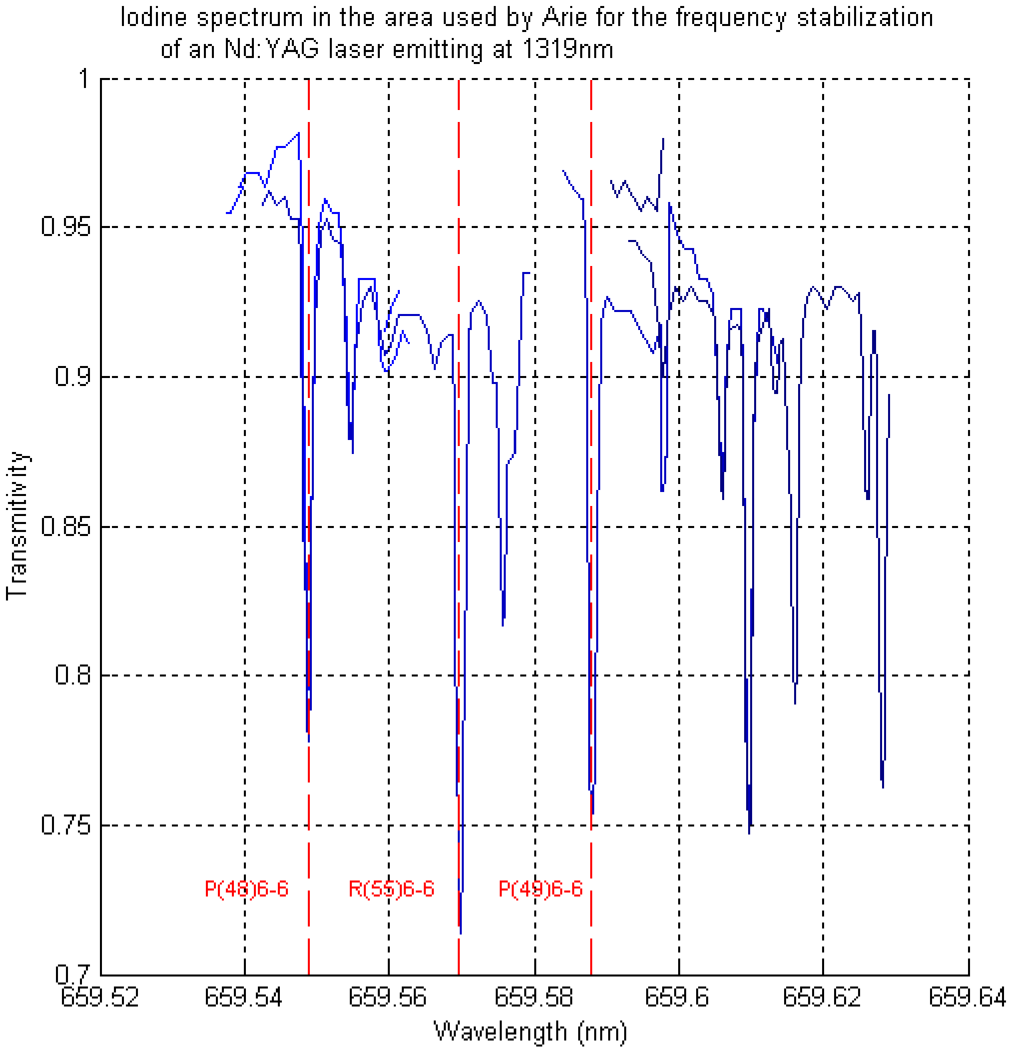

Figure 31 *Iodine spectrum in the area of interest (cell temperature 150°C). Resolution 820MHz between transitions and 70MHz within transitions. In red are indicated the three transitions described by Arie in [7]. Different modes are plotted, one of them could not be measured entirely because the voltage generator could not provide a voltage between -1.5 and +1.5V. The two extreme pieces of it can be seen on the graphic.*

Like in Figure 30 the discontinuities are caused by the mode hoping and the down translation of the spectrum by the reflections on the windows of the cell. Three of the transitions studied by Arie [1][7] can be seen on Figure 31. Nevertheless the spectrum presents a lot of variations of the transmitivity wich prevent from determining precisely the characteristics of the transitions. To get a better spectrum the variations of intensity of the fundamental beam and the wavelength dependence[9] of the SHG have been followed during the scanning of the spectrum. This has showed that if the intensity noise of the fundamental beam is small and can be neglected it is not possible to neglect the wavelength dependence of the SHG. As a consequence the value of the intensity before the I_2 cell has to be measured more than once per mode. The results presented in Figure 32 show a much more flat spectrum from which one can deduce the approximated characteristics of the transitions (Table 9). The other transitions cited in [1] can not be reached with this laser. If one tries to decrease further the temperature of the laser in order to decrease the wavelength the laser stops emitting.

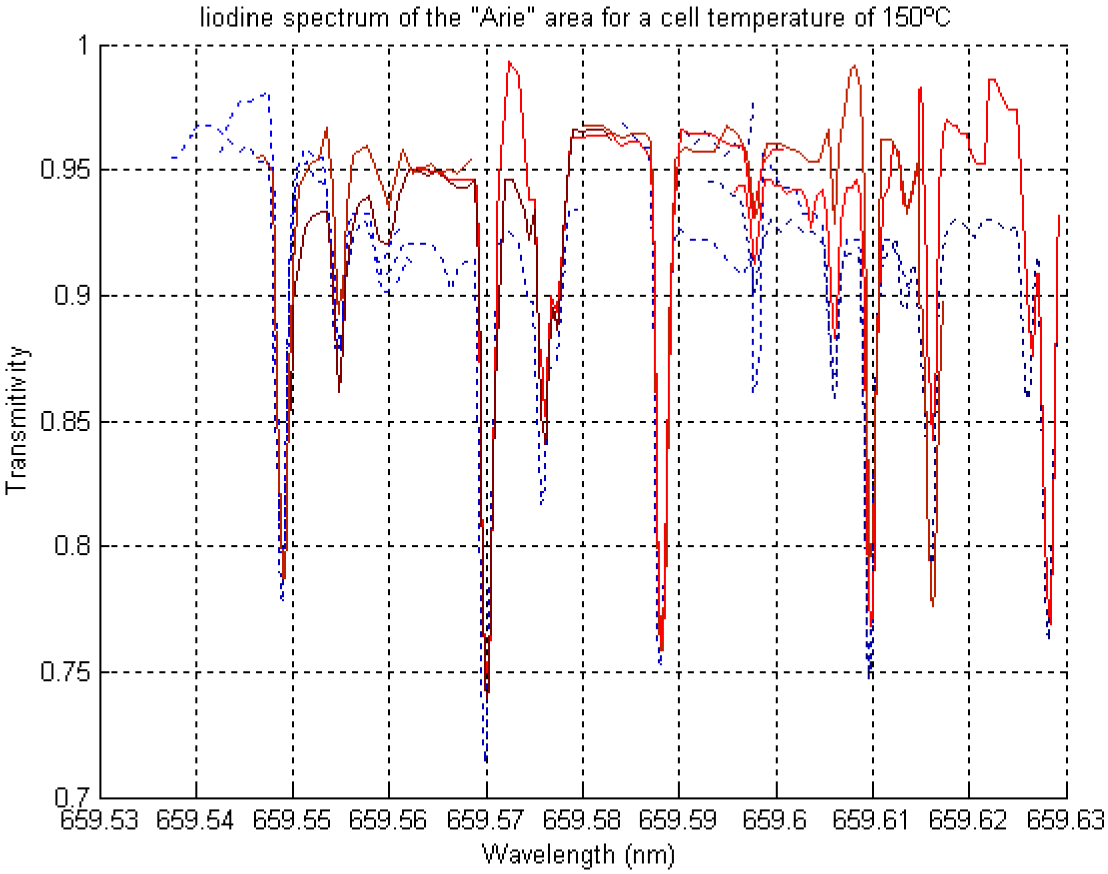

Figure 32 *Iiodine spectrum in the "Arie" area obtained at cell temperature of 150 ºC and taking into account the wavelength dependence of the SHG. The spectrum is more flat and the transitions characteristics are easier to measure. As a comparison the previous spectrum is plotted in blue dashed lines.*

---

9. Indeed, the process of SHG depends on a lot of parameters. In particular for a given set-up with all parameters fixed the variation of wavelength in the fundamental beam causes a variation of the conversion efficiency and so a variation of the SH beam intensity (see 2.1.4.3).

Table 9 *Characteristics of the three main transitions at a temperature of 150°C (~2.81 Torr). The given wavelength is measured. If the transition is not symmetrical the absorption is calculated on the smallest side. The linewidth is given at half the depth of the transition.*

Transition	Wavelength (nm)	Absorption (%)	Linewidth (GHz)
P(48)6-6	659.5489	16.4	~1.5
R(55)6-6	659.5699	19.4	~0.9
P(49)6-6	659.5880	19.8	~0.83

Arie [7] has stabilized his laser on P(48)6-6 at 57ºC and 3.5Torr. In this condition he has measured an absorption of 25.5% and a linewidth of 800MHz. On the spectrum presented Figure 32 R(55)6-6 and P(49)6-6 seem deeper and tighter than P(48)6-6.

With the cell provided by ISSI P(48)6-6 was larger but smaller than what was measured by Arie. As the pressure of iodine is lower the transition is smaller, nevertheless the transition should also be tighter. The width of the transition could be explain by the presence of another gas in the cell increasing the pressure. The linedepth given by the partial pressure od iodine is the same but the increase of the global pressure increases the Doppler effect and thus the linewidth of the transition.

3.2.3 Temperature dependence of linedepth of the transitions

Both the linewidth and the linedepth of the transition are function of the pressure. A transition should get deeper and larger as the pressure increases. The enlargement of the linewidth is due to the Doppler effect and is called Doppler broadening. The same range as in Figure 31 has been scanned at three different cell temperature to evaluate the effect of temperature on the linedepth.

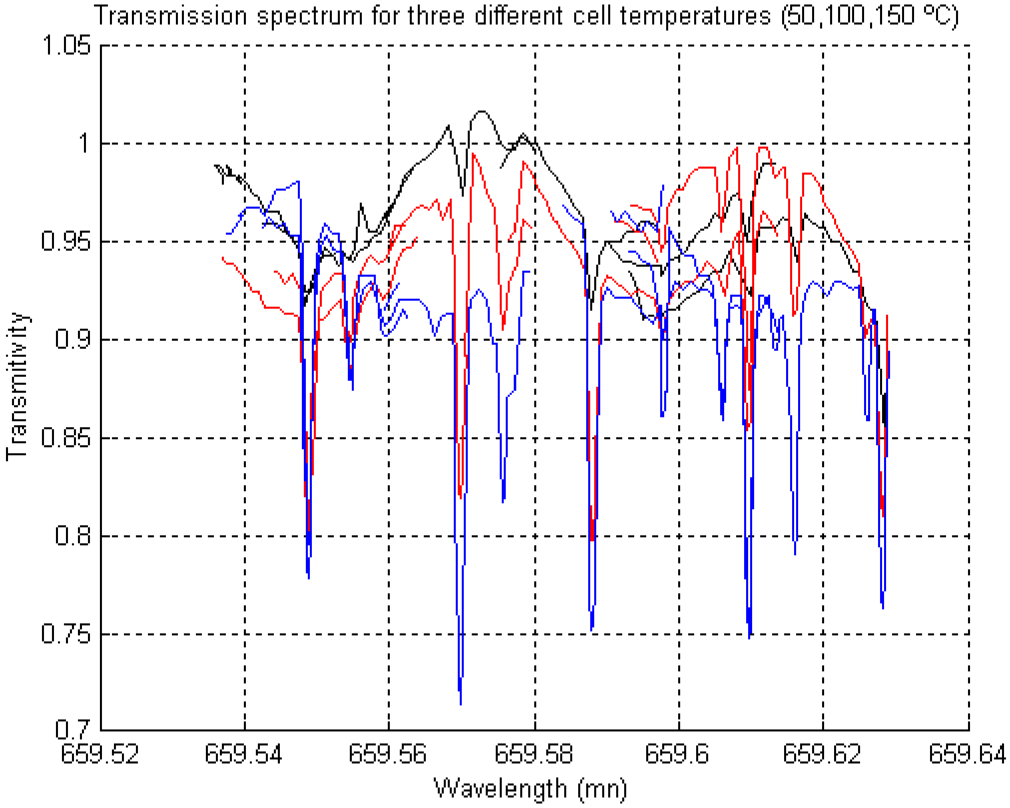

Figure 33 *Transmission spectrum of I_2 for three different temperatures of the cell (in black at 50°C,in red at 100°C and in blue at 150°C).*

Results from linear fit on the absorption versus pressure curve for each of the three transition are given in Table 10.

Table 10 *Absorption depth of the three transitions at 50,100 and 150 °C. The linear fit gives the normalized absorption of the transition in $m^{-1}Torr^{-1}$ around Arie's point (3.5 Torr, 57°C, cell length=13cm).*

Transition	Absorption depth at 50°C ~0.8721 Torr	Absorption depth at 100°C ~1.744 Torr	Absorption depth at 150°C ~2.61 Torr	Linear fit
P(48)6-6	3%	9.3%	17%	0.63xP-0.34
R(55)6-6	3%	12.3%	20%	0.77xP-0.42
P(49)6-6	2.9%	9.3%	17.3%	0.65xP-0.36

Arie has also derived a relation between the abosrption depth of P(48)6-6 and the temperature and the length of the cell from a several measures with a temperature between 40 and 70 (the relation is valid only near Arie functioning point, i.e for a cell not too long and between 1 and 8 Torr). The normalized absorption depth of P(48)6-6 is

$$\text{normalized absorption} = 0.56 \times \text{lenght of the cell (m)} \times \text{pressure of iode (Torr)} \qquad (3.2\text{-}1)$$

Figure 34 presents the curves obtained for the three transitions and the curve obtained with Arie equation.

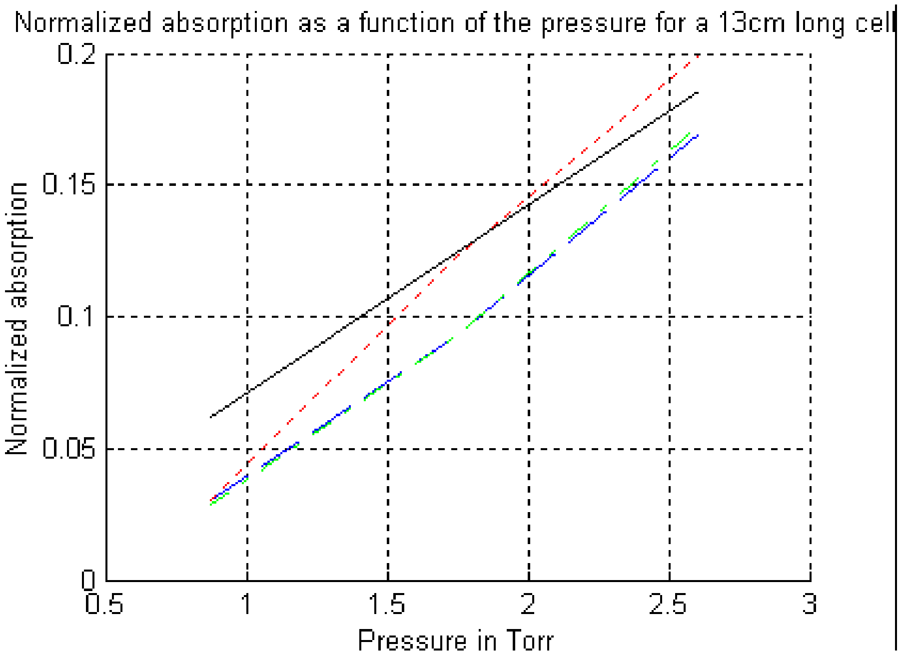

Figure 34 *Normalized absorption as a function of the pressure for a 13cm long cell. The black solid line is Arie's equation. The dash blue line is P(48)6-6, the green dash dot line P(49)6-6 and the red dot line R(55)-6-6.*

Figure 35 presents the expected asborption of P(48)6-6 as a function of the length of the cell.

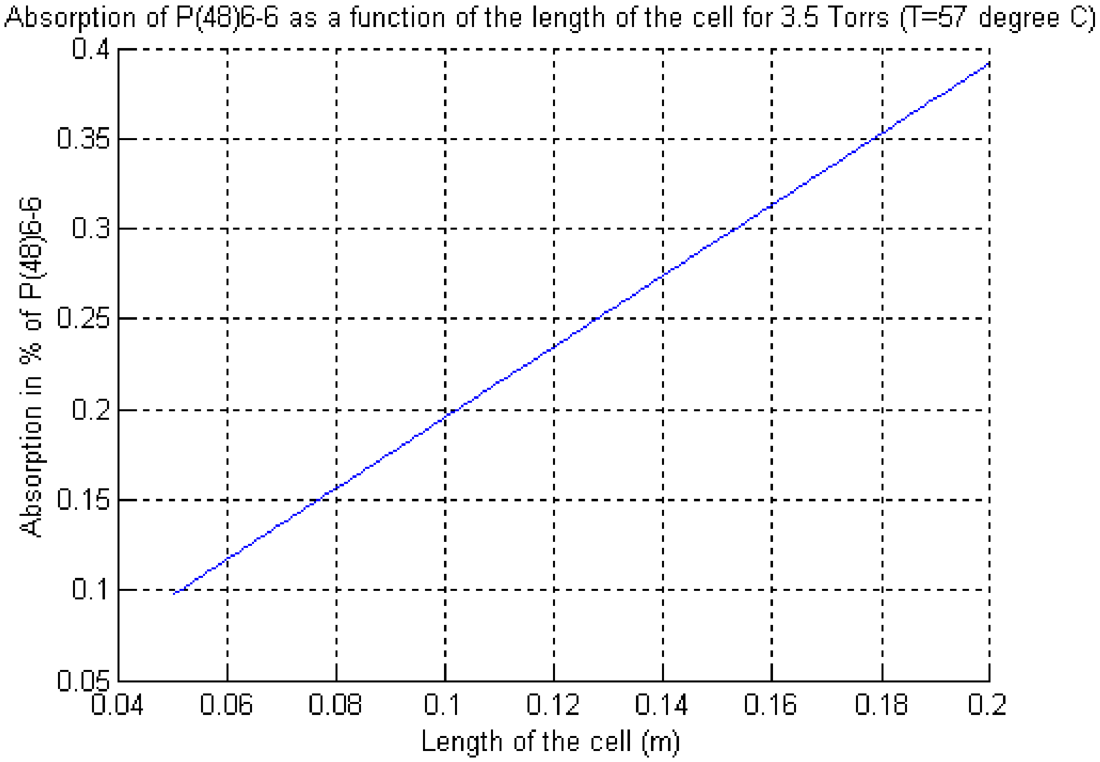

Figure 35 *Expected absorption for P(48)6-6 in an iodine cell with a pressure of 3.5Torr as a function of the cell length. The curve has been drawned using Arie equation.*

3.3 Conclusion on the iodine spectroscopy

Three of the transitions studied by Arie are in the frequency tuning range of the laser and could be used as a frequency reference for the stabilization process. Nevertheless the characteristics of the iodine cell could be improved.

Indeed the loss due to the windows of the cell are too important and can be easily reduced by the use of antireflection coatings and windows at Brewster's angle if possible. Furthermore the goal is to obtain a linedpth of at least 25% for the tightest linewidth possible. As a consequence consequence a long cell should be used because it allows to deepen the linedepth without enlarging the it. No buffer for an additional gas is required since it would only enlarged the transition. Finally a cell with a cold finger would allow to test and find the optimum value for the pressure. The final specifications for the I_2 cell are given in Table 11.

Table 11 Specifications of the iodine cell

Parameters	Specifications	Comments
Application	Laser frequency stabilization at 659.5nm using Pound-Drever-Hall method (FM spectroscopy) on a typically 25% linedepth and 800MHz linewidth	Transitions that may be used: R(55)6-6, P(49)6-6, P(48)6-6
Length	150mm<L<200mm	Goal: D=150mm
Diameter	25mm<D<75mm	Goal: D=50mm
Pressure	4 Torr	to get at least 25% absorption with D=50mm, L=150mm around 55ºC (cold finger temperature), [5]
Transmission λ=659.5nm	T>90%	Contribution of the optical window without gas absorption
AR coating at 659.5nm	yes	
Windows at Brewster angle	yes, if required to reach the transmission requirements	
Optical quality of the windows	λ/10	over a 10mm diameter sub-pupil

Conclusion

PRIMA scientific objectives require the use of a 5nm accuracy metrology system. Based on super-heterodyne interferometry, PRIMA metrology system uses a fiber coupled NPRO Nd:YAG laser, emitting at 1.319µm. Despite its intrinsic frequency stability this laser has to be stabilized by an external system to reach a stability level of $d\nu/\nu=10^{-8}$. Arie's method to stabilize Nd:YAG laser locks the second harmonic of the laser, generated with a nonlinear crystal, on an iodine transition at 659.5nm. The implementation of this technique in the context of PRIMA metrology system required a carefull study of the second harmonic generation as well as of the iodine spectra around 659.5nm.

A theoretical study of the expected conversion efficiency for PPKTP and PPLN crystal has been carried out. It showed that the use of PPKTP should provide enough power in the second harmonic beam. Moreover the study indicated that parameters affecting the conversion efficiency, such as the temperature of the crystal, the angle of incidence or the wavelength of the fundamental beam, are not critical. Both these results have been confirmed by the experimentations with PPKTP. As a consequence two optical configurations for the frequency stabilization sub-system have been proposed and discussed. The chosen configuration separates the laser output with a fiber coupler into two parts of 50 mW and 150mW. The 50 mW beam is used for second harmonic generation and the frequency stabilization while the 150mW beam is sent to the heterodyne assembly. This configuration provides at the same time enough power in the red and in the infrared beam.

The frequency tuning range and the thermal tuning coefficients of the laser have been measured. The frequency tuning range allows to reach convenient transitions for the frequency stabilization. Besides, the iodine spectrometry experimentations were used to specify the iodine cell that will be used for the frequency stabilization of the laser.

The implementation of the whole system, including the correction loop, will be done by IMT and should be delivered to ESO for the end of the first quarter of 2004. During this period ESO will test experimentally a cristal of PPLN to check if the conversion efficiency is increased as much as what is predicted by the theory. The change of cristal would only change the set-up slightly and provide a security margin for the second harmonic power.

The next step for PRIMA metrology system is the study of absolute metrology which would relax some operational constrains by suppressing long calibration process thus allowing more time for the astronomical observations.

More generally, ESO will also benefit from this work while facing the challenge of designing complex metrology systems required for future large telescopes such as ELT or OWL....

Bibliography

[1] Feasibility Study for the Frequency Stabilization of the PRIMA Metrology Laser, VLT-TRE-IMT-15731-2868, Issue 1, 20/07/03

[2] An introduction to stabilized lasers, M. W. Hamilton, Contemporary Physics, Vol. 30, No. 1, 1989, pages 21-33

[3] An introduction to Pound-Drever-Hall laser frequency stabilization, E. D. Black, Am. J. Phys. 69 (1), January 2001

[4] Frequency-modulation spectroscopy: a new method for measuring weak absorptions and dispersions, G. C. Bjorklund, Optics Letters, Vol. 5, No. 1, January 1980

[5] Absolute frequency stabilization of diode-laser-pumped Nd:YAG lasers to hyperfine transitions in molecular iodine, A. Arie, S. Schuller, E. K. Gustafson, R. L. Byer, Optics letters, Vol. 17, No. 17, 1 Septenber 1992

[6] Frequency stabilization of the 1064-nm Nd:YAG lasers to Doppler-broadened lines of iodine, A. Arie, R. L. Byer, Applied optics, Vol. 32, No. 36, 20 December 1993

[7] Iodine Spectroscopy and Absolute Frequency Stabilization with the Second Harmonic of the 1319-nm Nd:YAG Laser, A. Arie, M. L. Bortz, M. M. Fejer, R.L. Byer, Optics Letters, Vol. 18, No. 20, 15 October 1993

[8] Analysis of second harmonic generation in KTP, VLT-TRE-IMT-15731-3006,01/03/03

[9] Characterization of iodine transitions around 659.5nm, VLT-TRE-ESO-15731-3064, 23/05/03

[10] Photonics, Linear and nonlinear interactions of laser light and matter, R. Menzel, Springer Verlag, 2001

[11] Fundamentals of photonics, B. E. A. Saleh, M. C. Teich, Wiley-interscience, 1991

[12] Parametric Interaction of Focused Gaussian Light Beams, G. D. Boyd, D. A. Kleinmann, Journal of Applied Physics, Vol. 39, No. 8, July 1968

[13] Quasi-Phase-Matched Second Harmonic Generation: Tuning and Tolerances, M. M. Fejer, IEEE Journal of Quantum Electronics, Vol. 28, No. 11, November 1992

[14] Refractive-index temperature derivatives of potassium titanyl phosphate, W. Wiechmann, S. Kubota, T. Fukui, H. Masuda, Optics Letters, Vol. 18, No. 15, August 1993

[15] Second-harmonic generation and photons bunching in multimode laser beams, Y. Qu, S. Singh, Physical Review A, Vol. 47, No. 4, April 1993

[16] Technical Specifications for the laser assembly of PRIMA Metrology System, VLT-SPE-ESO-15731-2852, issue 1

[17] A study of contamination in $^{127}I_2$ cells using laser-induced fluorescence, S. Picard-Fredin, Metrologia, 26, 1989, pages 235-244

[18] Two-wavelength laser interferometry using superheterodyne detection, R. Dändliker, R. Thalmann, D. Prongué, Optics Letters, Vol. 13, No. 15, May 1998, pages 339-341

APPENDIX A : The European Southern Observatory, ESO

General

ESO, the European Southern Observatory, is an intergovernmental scientific organisation in which ten European countries participate. They are: Belgium, Denmark, Germany, France, Italy, the Netherlands, Portugal, Sweden, the United Kingdom and Switzerland. The ESO Convention was signed on 5th October 1962 and has provided the basic framework for the organisation. According to the convention, ESO was founded because the member country governments were "desirous of jointly creating an observatory equipped with powerful instruments in the southern hemisphere and accordingly promoting and organising co-operation in asronomical research". Emphasis was placed on the southern hemisphere because the southern sky was relatively unexplored. ESO is financed by contributions from its member states. The Council is the main organ which lays down the general policies. The Council is supported by committees such as the Finance Committee, the Scientific/Technical Committee and the Observing Programmes Committe.

Geographical establishements

The Organisation is subdivised in two geographical establishements (Figure 36).

The European Headquarters

The scientific-technical centre of ESO in europe has three main functions: the development of new telescopes and instruments, the processing of data obtained at La Silla and Paranal and the fostering of European Coordinating Facility (ST-ECF) which carries out its activities on the ESO premises in Garching.

The Chile establishment

The La Silla Observatory

The observatory at La Silla (2400m) situated in the Atacama desert at about 600 km north of Santiago is one of the largest observatories in the world, with 14 functionning optical telescopes with diameters up to 3.6m, including the 3.5m NTT and one 15m sub-millimeter radio telescope.

The Paranal Observatory

The Paranal Observatory (2635m) situated in the Atacam desert, 120km south of the town of Antofagasta and 12km inland from the Pacific coast in one of the world's driest areas. ESO started there the construction in 1991 of the VLT: four 8.2m telescopes (named[10] Antu, Kueyen, Melipal and Yepun). The Observatory will become the largest optical telescope in the world.

Santiago

ESO Office in Santiago Vitacura serves as main operational base for ESO in Chile. It houses a computer centre, a scientific library and offices for the scientific and administrative Staff. It is the focal point for activities involving ESO staff astrnomers, Chilean scientists and visiting astronomers from Europe. Staff arriving in Santiago will be taken care by this office and are usually accommodated in the ESO Gesthouse before continuing to the Observatories.

---

[10] In March 1999, at the time of the Paranal Inauguration, four meaningful names of objects in the sky in the Mapuche (Mapudungun) language were chosen. This indigeneous people lives mostly in the area south of the Bio-Bio river, some 500 km south of Santiago de Chile. Antu is “The Sun”, Kueyen “The Moon”, Melipal “The Southern Cross” and Yepun “Venus” as “The evening Star”.

Figure 36 *Geographical establishements. Top left: headquarters in Garching beï München (Germany). Top right:offices in Vitacura (Chile). Bottom left: La Silla observatory (Chile). Bottom right: Cerro Paranal observatory (Chile).*

Internal structure of ESO

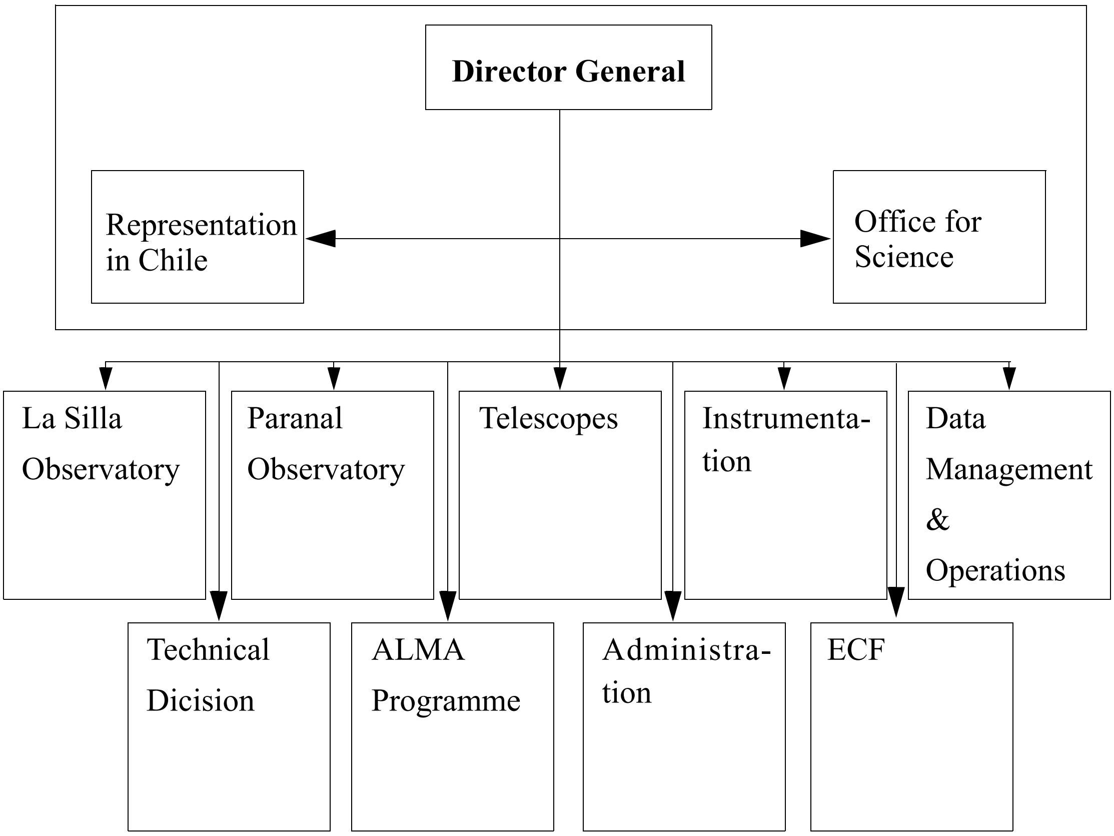

Figure 37 Internal structure of ESO. The office of the Director General and the 9 divisions.

Some divisions and their sub-groups:

- Office of the Director Genreal: Director Genreal Secretariat, The Programme Office, The Education and Public Relations, The Representation In Chile, The Office for Science, the Telescope Time Allocation and the VLT Programme Scientist;
- Telescope Division: Division Office, the VLT Programme including the VLTI group and the VST Project;
- Instrumentation Division: Division Office, the Department of the Infrared Instruments and Detectors, the Optical Instruments, the Optical Detectors, the Integration Laboratory;
- Data Management and Operations Division: USER Support, the Data Flow Systems, the Data Flow Operations;
- The Space Telescope-European Co-ordinating facility (ECF): European Coordinating Facility Office, the Instrument Physical Modeling, the Science Data and Software and the Instrument Information;

In total there are approximately 240 International Staff in Europe and Chile and about 170 Local Staff in Chile. In addition approximately 46 Fellows, Associates and visiting scientists work at ESO for fixed periods up to a maximum of 3 years.

APPENDIX B : The Very Large Telescope Interferometer (VLTI) and PRIMA

Very Large Telescope Interferometer

The Very Large Telescope Interferometer is born from the Very Large Telescope project. The initial idea was the construction of a 16m diameter telescope. Through the years the project has shifted to a linear array of four 8m telescopes to finaly include the possibility to use interferometry for astrometry and imaging.

Build on the top of Cerro Paranal in Chile, the observatory and its first generation instruments is organised as in Figure 38.

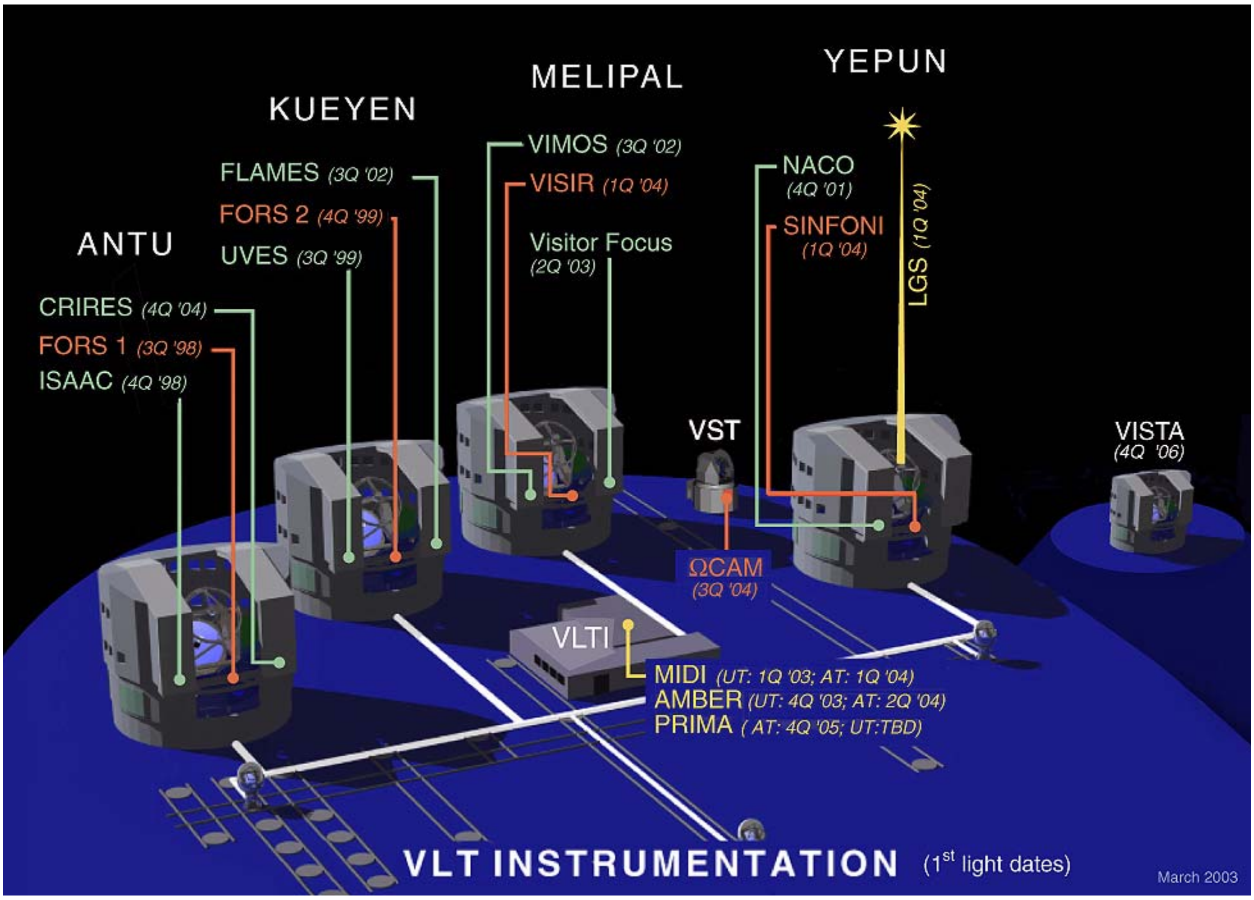

Figure 38 The Very Large Telescope Interferometer and its first generation instruments.

Once finished the observatory will be composed of a total of eight telescopes. Seven of them may be used in the interferometric mode.

The Unit Telescopes, UTs

There are four main telescopes called UT (Kueyen, Melipal, Antu and Yepun). The light is collected by a monolithic 8.2m diameter mirror and can be focused in three different points (Cassegrain, Nasmyth or Coude) or sent to the interferometric laboratory through the tunnels via the relay optics.

The Auxilliaries Telescopes, ATs

The three ATs, 1.8m diameter, can be located in 22 different stations to access several baselines and thus improve the u-v plane coverage or the resolution in the interferometric mode. The light is directed through the tunnels to the interferometric laboratory. The maximum baseline is 128m with UTs and 200m with the ATs.

Phase-Referenced Imaging and Micro-arcsecond Astrometry, PRIMA

The "Phase-Referenced Imaging and Micro-arcsecond Astrometry" (PRIMA) facility of the VLTI is based on the simultaneous coherent observation of two celestial objects in which the two interferometric signals are tied together by an internal metrology system. The role of this metrology system is to monitor the PRIMA instrumental optical path errors to possibly reach a final instrumental phase accuracy limited by atmospheric piston anisoplanatism.

Overall description and principle

The general principle of an observation with PRIMA is illustrated in Figure 39.

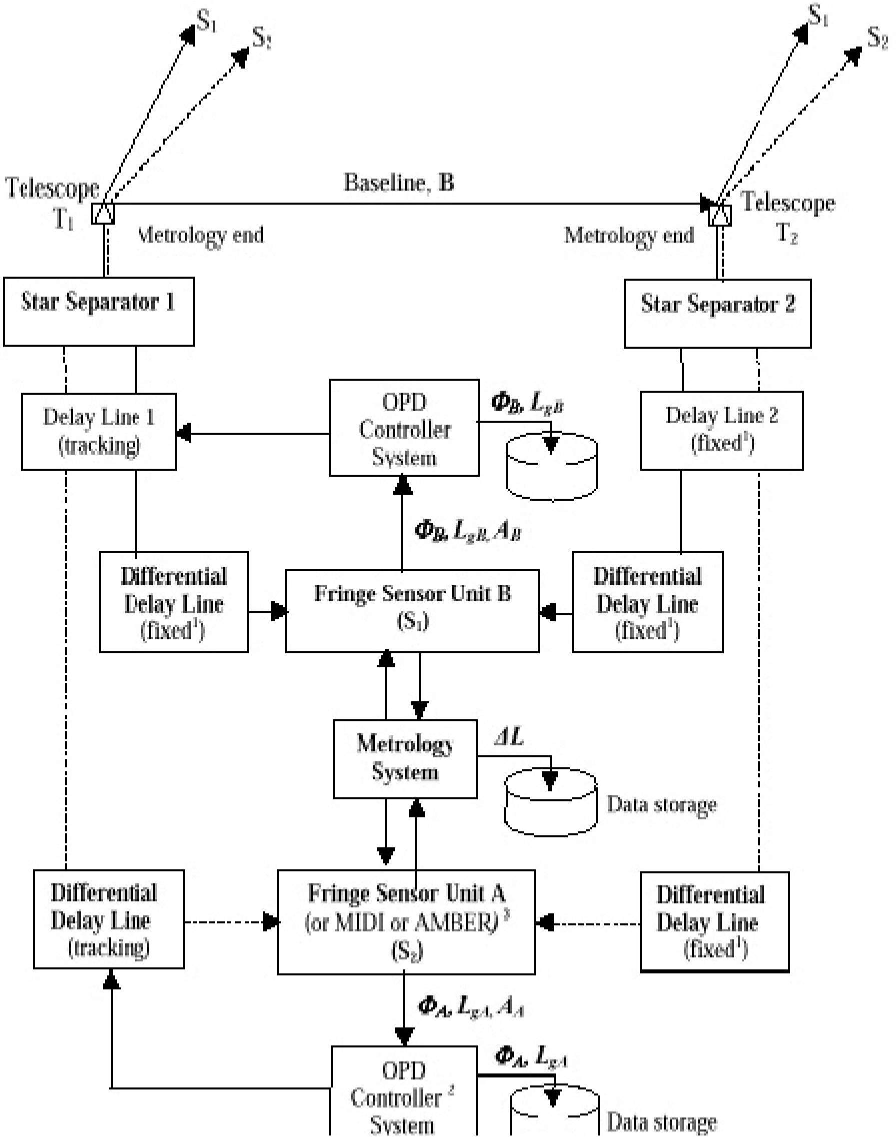

Figure 39 General principle of PRIMA.

The selected object and reference star are observed by a pair of telescopes (either UT-8m or AT-1.8m). The selection of the reference star is made within the anisoplanetic angle at the selected wavelength. For Paranal the anisoplanetic angle varies between 10 arcsec in H band and 60 arcsec in N band. The two field separation will be performed by the Star Separator System (STS) located at Coudé focus of each telescope. The STS will collimate the two beams and send them to the delay lines tunnel. The main Delay Lines will compensate for both beams the optical path difference introduced by Earth rotation. They will also transfer the pupil from the telescope to the selected instrument. Before the instruments, both beams will be directed to the Differential Delay Lines. Those DDL have for function to compensate the relative Optical Path Difference introduced between both beams coming from the same telescope. This optical path difference is related to the angular separation between the object and the reference. There will be one DDL per beam and per telescope for a total of 4 systems to keep the optical symmetry. After the DDL, the reference beams will be directed to the Fringe Sensor Unit B. The FSU –B- will generate the interference and analyse the fringe pattern in order to determine the Optical Path Difference to be compensated by the main DL and the DDL. The FSU B is used as a fringe tracker for both reference and object. The two beams coming from the scientific object will be directed either to the instruments (VINCI, MIDI, or AMBER) in imaging mode or to the Fringe Sensor Unit A in case of astrometry mode. At the level of the FSU A/B and Instrument, the metrology will be introduced in the optical path. The metrology will measure in real time the relative optical path difference between the reference and the object beams. The fringe patterns of both objects combined with metrology measurement will be analysed to determine either the angular separation of both objects in the sky (astrometry) or the complex visibility of the science object (imaging Mode).

In order to place the metrology sytem in the context of PRIMA, let us consider two celestial objects of vector coordinates S_1 and S_2, simultaneously observed on two independent beam combiners, i.e. using a dual-feed configuration. By stabilizing the interference fringes on the so-called reference object S_1, the residual Optical Path Difference, ΔOPD, seen by S_2 is given by:

$$\Delta OPD = B \cdot (S_2 - S_1) + \frac{\Phi}{k} + dA + \Delta L$$

where:

- B is the vector baseline of the interferometer
- Φ is a phase factor inherent to the nature of the observed objects and is the observable for phased-referenced imaging, k being the wave number
- dA represents the OPD (or piston) anisoplanatism which contributes to the residual fringe motion seen by S_2. For the maximum angular separation S_2-S_1 of PRIMA of 1 arcmin, the standard deviation of dA is about 10 times lower than the open-loop atmospheric fringe motion imposed on S_1. dA has a zero mean and can be averaged-out by successive measurements of ΔOPD in a typical 30 minute time frame for a 10 arcsec star separation and a 10marcsec astrometric accuracy.
- L_2-L_1 represents the difference between the internal OPD's of each object. ΔL can thus be seen as the instrumental contribution to ΔOPD.

Knowing the baseline vector B and by measuring independently ΔOPD and ΔL, Equation () shows that one can estimate either the factor Φ for a known star separation (Phase-referenced Imaging mode), or inversely the star separation for a known Φ (Astrometric mode). The bottom line being that the implementation of PRIMA is intimately linked with the ability to trace back the "differential" internal OPD between the two objects, ΔL.

The accuracy requirement on ΔL is driven by the astrometric mode but it can be relaxed by a factor 50 to 100 in the imaging mode, and depending on the observing parameters. For an astrometric accuracy goal of $d\Theta=10\mu$arcsec, and a baseline of B=100m, ΔL must be known with a $B.d\Theta$=5nm accuracy or $\lambda/200$ for $\lambda=1$ µm. It is important to recall that this astrometric accuracy also assumes an object separation of 10 arcsec and a 30 min observation to average out the OPD anisoplanatism.

Therefore, any quasi-stationary random errors on ΔL, with a zero mean over 30 min, will also be averaged out. On the other hand, care must be taken to minimize any drift of the metrology within this time scale.

PRIMA metrology system

The concept of the PRIMA metrology system developed by ESO in collaboration with the Institute of Microtechnology of Neuchatel (IMT) is based on super-heterodyne laser interferometry [18], where two heterodyne Michelson interferometers are operating simultaneously and have a common optical path with both observed stars through the VLTI optical train. The two interferometers use different heterodyne frequencies (650 kHz and 450 kHz) generated using four fiber coupled acousto-optics modulators connected to a single Nd-YAG laser emitting at 1319 nm (selected for its power 200mW, its linewidth 5kHz providing the required coherence length, its emitted wavelength, its intrinsic frequency stability). After photodetection and filtering, the individual heterodyne signals are mixed such that the disturbance to be monitored is directly coded in the phase of a 200 kHz carrier signal (i.e. 650 kHz -450 kHz). Finally, the phase of the 200 kHz carrier is measured with a digital phasemeter.

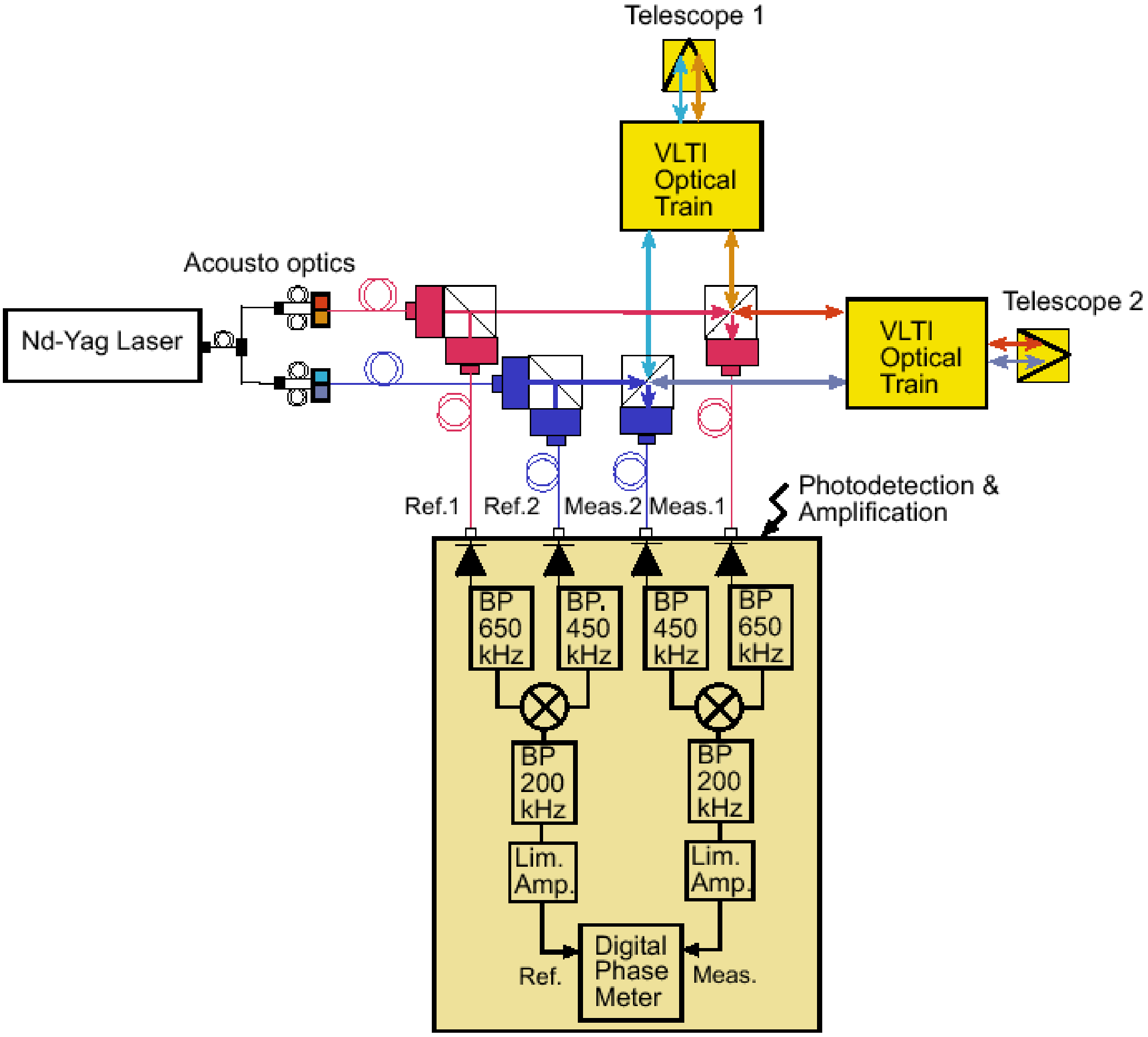

Figure 40 *PRIMA Metrology system. On this schematic the stabilization part of the system is not showed.*

APPENDIX C : KTP Physical properties

Values from http://www.mt-berlin.com/charts/chart_01.htm#IND6 (Molecular Technology GmbH), except the refractive-index temperature derivatives from [14].

Table 12 Physical properties of KTP.

Parameters	**Value**
Physical Properties	
Crystal structures	orthorhombic
Space group	$Pna2_1$
Lattice constants:	a=12.814 Å; b=6.404 Å; c=10.616 Å
Density	$3.0 g/cm^3$
Melting point	1150 ºC
Transition temperature:	936 ºC
Mohs hardness	5
Thermal expansion coefficient:	$a_1=11\times10^{-6}\,^{\circ}C^{-1}a_2=9\times10^{-6}\,^{\circ}C^{-1;}a_3=0.6\times10^{-6}\,^{\circ}C^{-1}$
Thermal conductivity:	$k_1=2.0\times10^{-2}W/cm\,^{\circ}C$; $k_2=3.0\times10^{-2}W/cm\,^{\circ}C$ $k_3=3.3\times10^{-2}W/cm\,^{\circ}C$
Optical Properties	
Transparency:	350nm-4400nm
refractive index	$n_x^2=2.1146+0.89188/(1-(0.20861/\lambda)^2)-0.01320\times\lambda^2$ $n_y^2=2.1518+0.87862/(1-(0.21801/\lambda)^2)-0.01327\times\lambda^2$ $n_z^2=2.3136+1.00012/(1-(0.23831/\lambda)^2)-0.01679\times\lambda^2$
Refractive-index temperature derivatives	$\partial n_x/\partial T=(1.427\lambda^{-3}-4.735\lambda^{-2}+8.711\lambda^{-1}+0.952)(10^{-6}/^{\circ}C)$ $\partial n_y/\partial T=(4.269\lambda^{-3}-14.761\lambda^{-2}+21.232\lambda^{-1}-2.113)(10^{-6}/^{\circ}C)$ $\partial n_z/\partial T=(12.415\lambda^{-3}-44.414\lambda^{-2}+59.129\lambda^{-1}-12.101)(10^{-6}/^{\circ}C)$
Nonlinear Properties	
Nonlinear coefficients:	$d_{31}=\pm6.5pm/V$ $d_{32}=\pm5pm/V$ $d_{33}=\pm13.7pm/V$ $d_{24}=\pm7.6pm/V$ $d_{15}=\pm6.1pm/V$

APPENDIX D : LN Physical properties

Values from http://www.inrad.com/pdf/Inrad_datasheet_LNB.pdf.

Table 13 Physical properties of LN ($LiNbO_3$).

Parameters	**Value**
Physical Properties	
Crystal structures	trigonal, R3c
Space group	3m
Lattice constants:	a=5.15052 Å; c=13.86496 Å
Density	$4.648 g/cm^3$
Melting point	1240 ºC
Transition temperature:	1145 ºC
Mohs hardness	5
Thermal expansion coefficient:	$\alpha_a=14.1\times10^{-6}\,^{\circ}C^{-1}$; $\alpha_c=4.1\times10^{-6}\,^{\circ}C^{-1}$
Thermal conductivity:	$k_1=4W^{\circ}C^{-1}m^{-1}$
Optical Properties	
Transparency:	400nm-5000nm
refractive index	$n_o^2=4.9048+0.11768/(1-(0.0475/\lambda)^2)-0.027169\times\lambda^2$ $n_e^2=4.582+99169/(1-(044432/\lambda)^2)-0.02195\times\lambda^2$
Refractive-index temperature derivatives	$\partial n_o/\partial T=3.3\ (10^{-6}/^{\circ}C)$ $\partial n_e/\partial T=37\ (10^{-6}/^{\circ}C)$
Nonlinear Properties	
Nonlinear coefficients:	$d_{31}=\pm4.52 pm/V$ $d_{33}=\pm31.5 pm/V$ $d_{22}=\pm2.4 pm/V$

APPENDIX E : Set-up and wiring for the oven and the temperature controller

The connection to the oven is made with a SubD9 male connector. Only 4 pins out of 9 are used, 2 for the pt100/RTD sensor (R=110 Ω±5%) and 2 for the heating wire resistance (200 Ω<R<250 Ω). HC Photonics has provided a 5m long cable. The configuration of each extremity of the cable are described in Table 14 and can be controlled with an ohmmeter.

Table 14 Cable connector configuration for the HC Photonics OV03 oven

Pin number	Oven (male)	Controller (female)
1	pt100/RTD	-
2	pt100/RTD	-
3	-	pt100/RTD
4	Heating	-
5	Heating	pt100/RTD
6	-	Heating
7	-	-
8	-	-
9	-	Heating

The back panel of the CN77352-C4 is presented in Figure 41. The wiring for a 2wires pt100/RTD is showed on Figure 42.

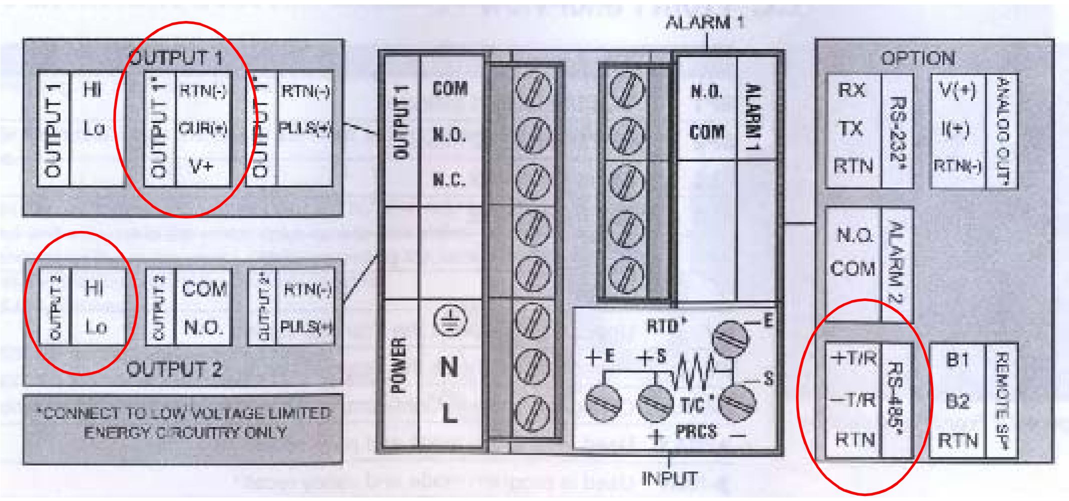

Figure 41 Rearpanel of a CN77XXX controller. The configuration of the CN77352-C4 is highlighted in red.

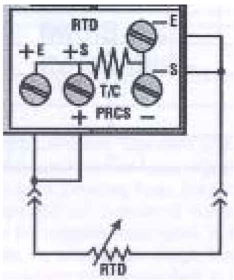

Figure 42 Wiring for a 2wires pt100/RTD.

Instead of being configured via the 4 front panel buttons the CN77352-C4 can be configured from a PC using a software provided by Newport Omega (Micro-infinity® ICN7700 & Micromega® CN77000 configuration 1.1, http://www.newportus.com/software/MISC.htm) and a RS-232 RS-485 convertor (ICP CON 7520). The convertor uses a 10~30V DC generator. The convertor is connected to the serial port of the PC with a DB9 cable and its two outputs *Data-* and *Data+* are connected respectively to the *-T/R* and *+T/R* inputs of the controller. *No ground should be used between the convertor and the controller!* The software should be configured for the right model of controller CN77352-C4 which is done in the hardware menu by selecting the options as shown in Table 15. Finally the controller should be manually configured for the communication with the parameters as shown in Table 16. Once this is done the controller can be configured for the type of input, the mode of regulation, the regulation parameters, the type of ouputs, the setpoints, the mode of display...

Table 15 Hardware menu configuration in Micro-infinity (configuration 1.1) for setting-up the comuni-

cation between the PC and the CN77352-C4 controller.

Parameters	**Value**
Model#	CN77[case]52-C4
Output 1	VI
Output 2	SSR
Options	RS-485
RS-485 address	0001 (default)

Table 16 CN77352-C4 configuration for setting up the communication between the PC and the controller.

Parameters	**Value**
Data bits	7
Stop bits	1
parity	odd
Baud	9600
Echo	on
Line feed	no
Mode	Command

APPENDIX F : Burleigh WA-1500 Wavemeter

The wavelength is measured by an interferometric method. The laser beam to be studied is introduced in a Michelson interferometer as in Fig. 43. The intensity reaching the input photodetector depends on the relative lengths of the two paths which govern whether constructive or destructive interference occurs at the beamsplitter. As the retro-reflectors move back and forth the detected intensity follows a sinusoidal function.

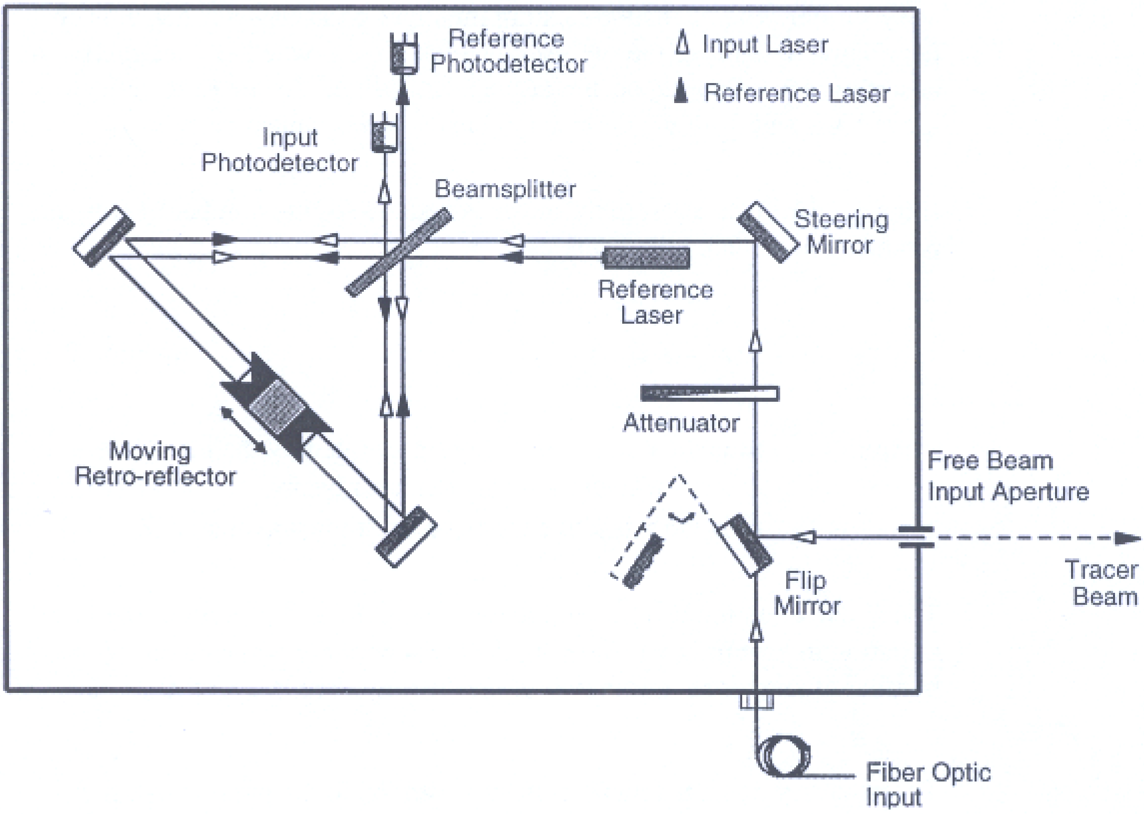

Figure 43 Burleigh WA-1500 wavemeter optical schematic.

The number m of fringes detected by the sensor for a displacement d of the retro-reflector is given by

$$m\lambda = 4n_\lambda d$$

where:

- m is the number of detected fringes
- n_λ is the refractive index of air
- λ is the wavelength of the input laser.

If d is known with enough accuracy λ can be obtained by substituting the refraction index of air by its value. To get a precise value for d a He:Ne laser is build in the wavemeter and its beam follows the same path as the measured one. For the reference beam one has the same relation as before:

$$m_0 \lambda_0 = 4n_0 d$$

And then combining the two equations one gets:

$$\lambda = \frac{m_0}{m} \cdot \frac{n_\lambda}{n_0} \cdot \lambda_0$$

The value of the measured wavelength is proportional to the ratio of the number of fringes detected, to a term depending on the refractive index of air and to the reference wavelength of the He-Ne laser. The accuracy depends on all the three terms of the previous equation. The refractive index of air is calculated from the revised Edlen equation from Birch and Downs (Metrologia,30,155(1993)). This takes into account temperature and pressure measured by sensors in the wavemeter and humidity (entered manually by the user).

The wavemeter has an absolute accuracy of $\delta\nu/\nu<10^{-7}$ ($\delta\nu=\pm 45$MHz). The measurements are displayed with a resolution of 0.0001 nm which corresponds to about 70 MHz at 659.5 nm. The wavelength value can be displayed in vacuum or in the air. Only the vacuum values were used. The studied beam intensity should be at least 20µW.

APPENDIX G : Characteristics of the Dichroic mirror

After SHG the fundamental beam (1.319µm) and the SH beam (659.5nm) are spatially superimposed. Configuration 1 presented in Section 2.4 requires to separate both components of the output beam using a dichroic mirror.

This dichroics should be optimized to reflect the visible, i.e optimize the flux reflected for frequency stabilisation, and transmit the IR. Furthermore, it should not affect the linear polarization state of the IR laser whose extinction ratio is -20dB.

The characteristics of the dichroic mirror purchased at Laser Components GmbH are the following:

- reflectivity at 659.5nm>99.5%;
- transmitivity at 1319nm~88%;
- extinction ratio[11]: -25.6dB.

The extinction ratio of the dichroic mirror has been measured using a linear polarizer[12] before the mirror and another one after. The measured curves are plotted in Figure 44.

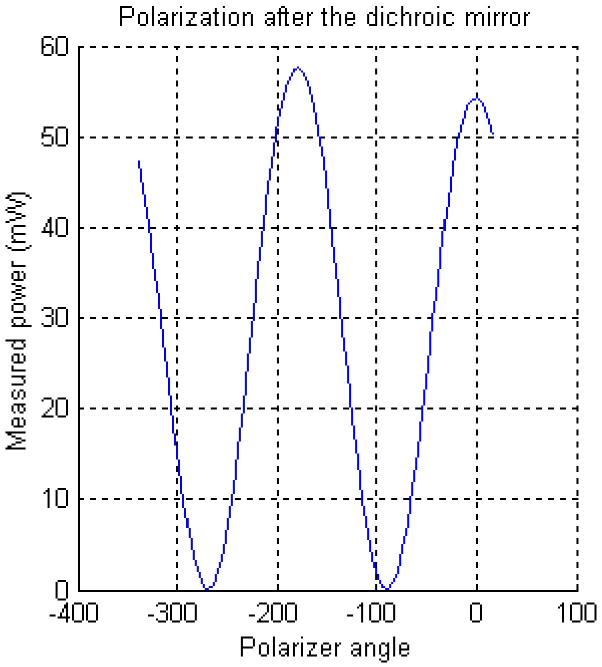

Figure 44 *Polarization after the dichroic mirror of an linearly polarized incident beam at 1.319µm. The measured extinction ratio is approximately 25.5dB.*

---

[11] The extinction ratio, ER, is defined by the ratio between maximum and minimum intensities recorded while a linear polarizer is rotated by 360 degrees. The extinction ratio in dB is given by $ER_{db}=-10\times\log_{10}[ER]$.

[12] the extinction ratio of the linear polarizor is better than -30dB

APPENDIX H : Iodine cells

Iodine cells are usually used in spectroscopy and can be used as frequency references for the stabilization of lasers (He:Ne and Nd:YAG doubled in frequency).

Two types of cells are available:

- permanently cealed cells;
- cells equipped with a cold finger.

Permanently cealed cells (also known as gas cells)

These cells are manufactured with a prescribed iodine partial pressure. The housing is connected to a cold finger with iodine and the partial pressure of iodine is set before the cell is sealed with a torch. In addition, the transistions can be pressure broadened with nitrogen partial pressure.

In this case once the cell is sealed the partial pressure of iodine is given by the temperature of the cell. The relation between temperature and pressure can be approximated by the law of the perfect gas.

Cells with a cold finger (also known as vapor cells)

These cells are permanently connected to a cold finger which contains a bit of iodine (typically a fraction of a gram). In this case the partial pressure of iodine is given by the temperature of iodine.

The pressure of iodine in the cell can be deduced from the temperature of the cold finger using the following equation [17]

$$\log P = -\frac{3512.83}{T} - 2.013\log T + 13.374$$

where P is expressed in atmospheres and T in kelvins.

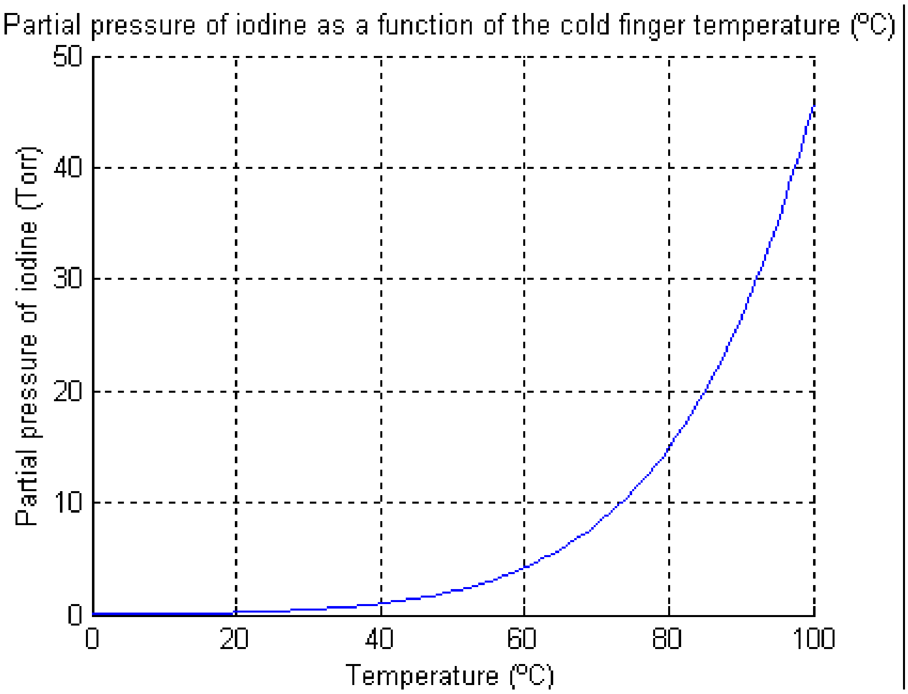

Figure 45 *Partial pressure of iodine (Torr) as a function of the cold finger temperature (ºC)*